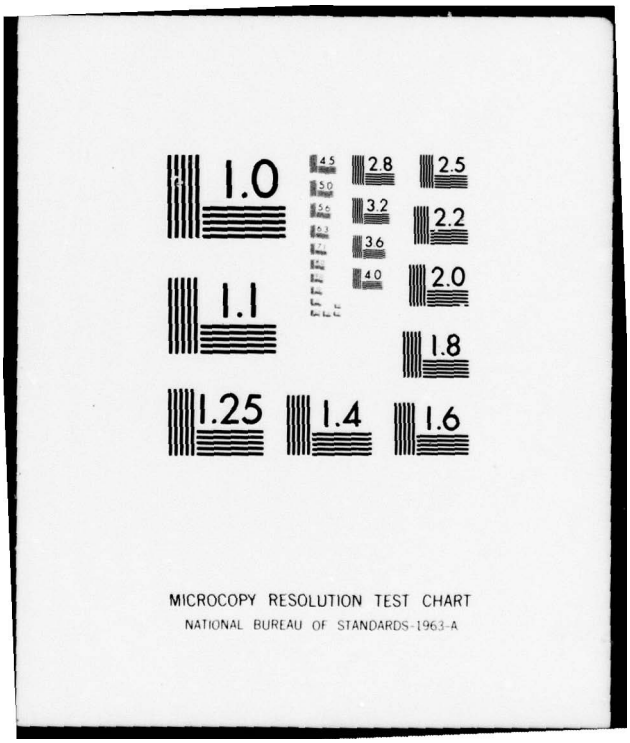
AD-A036 213 MCDONNELL AIRCRAFT CO ST LOUIS MO F/G 20/4
NUMERICAL SOLUTION OF SUBSONIC VISCOUS-INVISCID INTERACTING FLO--ETC(U)
JUL 76 A VERHOFF F33615-73-C-4062
UNCLASSIFIED AFFDL-TR-76-64 NL

1 OF 2
AD
A036213




1.0
1.1
1.25
1.4
1.6
1.8
2.0
2.2
2.5
2.8
3.2
3.6
4.0
4.5
5.0
MICROCOPY RESOLUTION TEST CHART
NATIONAL BUREAU OF STANDARDS-1963-A

AD A036213

AFFDL-TR-76-64

(2) NW

NUMERICAL SOLUTION OF SUBSONIC VISCOUS - INVISCID INTERACTING FLOWS

MCDONNELL AIRCRAFT COMPANY
MCDONNELL DOUGLAS CORPORATION
P.O. BOX 516
ST. LOUIS, MISSOURI 63166

DDC
RECEIVED
MAR 2 1977
C

JULY 1976

TECHNICAL REPORT AFFDL-TR-76-64
FINAL REPORT FOR PERIOD 16 APRIL 1973 - 31 DECEMBER 1975

Approved for public release; distribution unlimited

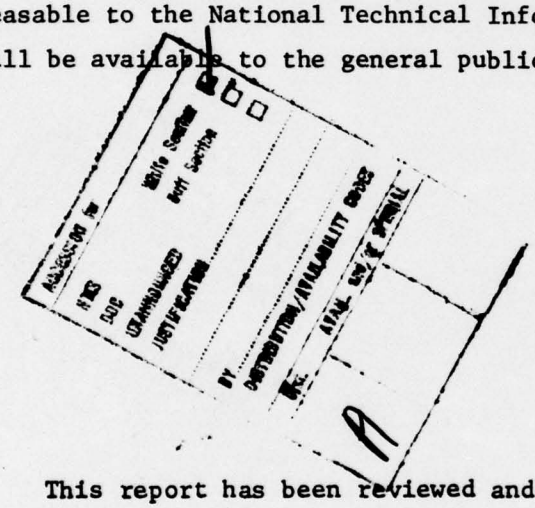
COPY AVAILABLE TO DDC DOES NOT
PERMIT FULLY LEGIBLE PRODUCTION

AIR FORCE FLIGHT DYNAMICS LABORATORY
AIR FORCE WRIGHT AERONAUTICAL LABORATORIES
AIR FORCE SYSTEMS COMMAND
WRIGHT-PATTERSON AIR FORCE BASE, OHIO 45433

NOTICES

When Government drawings, specifications, or other data are used for any purpose other than in connection with a definitely related Government procurement operation, the United States Government thereby incurs no responsibility nor any obligation whatsoever; and the fact that the government may have formulated, furnished, or in any way supplied the said drawings, specifications, or other data, is not to be regarded by implication or otherwise as in any manner licensing the holder or any other person or corporation, or conveying any rights or permission to manufacture, use, or sell any patented invention that may in any way be related thereto.

This report has been reviewed by the Information Office (IO) and is releasable to the National Technical Information Service (NTIS). At NTIS, it will be available to the general public, including foreign nations.



This report has been reviewed and is approved for publication.

Alfred C. Draper

ALFRED C. DRAPER
Asst. for Research & Technology
Aeromechanics Division

Copies of this report should not be returned unless return is required by security considerations, contractual obligations, or notice on a specific document.

UNCLASSIFIED

SECURITY CLASSIFICATION OF THIS PAGE (When Data Entered)

REPORT DOCUMENTATION PAGE	READ INSTRUCTIONS BEFORE COMPLETING FORM
1. REPORT NUMBER: AFFDL-TR-76-64	2. GOVT ACCESSION NO. / 3. RECIPIENT'S CATALOG NUMBER
4. TITLE (and Subtitle): NUMERICAL SOLUTION OF SUBSONIC VISCOUS-INVISCID INTERACTING FLOWS	5. TYPE OF REPORT & PERIOD COVERED: Final, 16 Apr 73 - Dec 75
	6. PERFORMING ORG. REPORT NUMBER
7. AUTHOR(s): August Verhoff	8. CONTRACT OR GRANT NUMBER(s): F33615-73-C-4062 new
9. PERFORMING ORGANIZATION NAME AND ADDRESS: McDonnell Aircraft Company, McDonnell Douglas Corporation, P.O. Box 516, St. Louis, Mo. 63166	10. PROGRAM ELEMENT, PROJECT, TASK AREA & WORK UNIT NUMBERS: Project: 1929, Task: 04, Work Unit: 22
11. CONTROLLING OFFICE NAME AND ADDRESS: Air Force Flight Dynamics Laboratory, AFFDL/FXM, Wright-Patterson AFB, Ohio 45433	12. REPORT DATE: July 1976
	13. NUMBER OF PAGES: 104
14. MONITORING AGENCY NAME & ADDRESS (if different from Controlling Office) 112 p.	15. SECURITY CLASS. (of this report): Unclassified
	15a. DECLASSIFICATION/DOWNGRADING SCHEDULE

16. DISTRIBUTION STATEMENT (of this Report)

Approved for public release, distribution unlimited.

A.P.D.C. RECEIVED MAR 2 1977

17. DISTRIBUTION STATEMENT (of the abstract entered in Block 20, if different from Report)

Final rept. 16 Apr 73 - 31 Dec 75,

18. SUPPLEMENTARY NOTES

19. KEY WORDS (Continue on reverse side if necessary and identify by block number)

Numerical Aerodynamics
Subsonic Flow
Unsteady Flow
Turbulent Boundary Layer
Turbulence Model

61102F

20. ABSTRACT (Continue on reverse side if necessary and identify by block number)

A numerical procedure has been developed which determines steady state solutions of the turbulent two-dimensional Navier-Stokes equations as the asymptotic large-time limit of the full unsteady equations. The formulation is presented for inviscid flow, laminar flow and turbulent flow using an analytic transformation from the physical space around the body to a computational space. Accurate boundary conditions are derived for inviscid and laminar flow. Inviscid flow calculations for several body shapes show convergence to the steady state solution. The formulation for turbulent flow incorporates → next page

DD FORM 1 JAN 73 1473 EDITION OF 1 NOV 65 IS OBSOLETE

UNCLASSIFIED

SECURITY CLASSIFICATION OF THIS PAGE (When Data Entered)

403 111

equations for turbulence energy and dissipation, and uses a "law-of-the-wall" boundary condition to avoid the need for fine mesh spacing in the laminar sublayer. Results are presented for a symmetric Joukowsky airfoil for completely laminar flow and for laminar flow with transition to turbulence.

FOREWORD

This report summarizes results of research carried out under Contract No. F33615-73-C-4062, Project 1929, Task 04, during the period beginning 16 April 1973 and ending 31 December 1975. The work was supported by the Aerospace Research Laboratories, Air Force Systems Command, United States Air Force; the Air Force program monitor was Maj. David S. McRae of the Theoretical Aerodynamics Research Laboratory (ARL/LH). This report was submitted by the author in March 1976.

The program at McDonnell Aircraft Company, St. Louis, Missouri 63166, was conducted by the Aerodynamics Department under the supervision of Mr. J. Pavelka, Branch Manager. Dr. August Verhoff was Principal Investigator. Major contributors to the program were Messrs. G. G. Grose, Program Manager, H. J. Fivel of McDonnell Douglas Astronautics Company, and Prof. Gino Moretti of Polytechnic Institute of New York as Consultant.

TABLE OF CONTENTS

Section			Page
1.	INTRODUCTION AND SUMMARY		1
2.	TIME DEPENDENT COMPUTATION (TDC) PROGRAM DESCRIPTION		2
	2.1	Navier-Stokes Equations	2
	2.2	Transformation Onto the Computational Plane	5
	2.3	Boundary Conditions	9
		2.3.1 Initial Conditions	9
		2.3.2 Wave Front Conditions	11
		2.3.3 Body Surface Conditions	20
		2.3.3.1 Inviscid Flow	20
		2.3.3.2 Laminar Viscous Flow	31
		2.3.4 Symmetry or Identity Conditions	37
	2.4	TDC Computer Program Organization	38
3.	EXTENSION OF TDC PROGRAM FORMULATION TO TURBULENT FLOW		40
	3.1	Spalding k-ε Turbulence Model	40
	3.2	Equations of Motion	41
	3.3	Boundary Conditions	44
4.	INVISCID SAMPLE CASES		49
	4.1	Non-Lifting Flow Past a Circular Cylinder	49
	4.2	Lifting Flow Past a Circular Cylinder	55
	4.3	Non-Lifting Flow Past an Ellipse	62
	4.4	Non-Lifting Flow Past a Symmetric Joukowsky Airfoil	64
5.	VISCOUS SAMPLE CASES		82
	5.1	Laminar Flow	94
	5.2	Turbulent Flow	98
6.	CONCLUSIONS AND RECOMMENDATIONS		101
	REFERENCES		103

PRECEDING PAGE BLANK-NOT FILMED

LIST OF ILLUSTRATIONS

Figure	Title	Page
1	Coordinate Transformation	3
2	Coordinate System About Airfoil in Physical Space	7
3	Coordinate System Image in Circle Plane	7
4	Fixed Outer Boundary Geometry for $t \leq t_o$	10
5	Relation Between Normal-Tangential Coordinates (ξ,η) and Radial-Angular Coordinates (r,n) at Outer Wave	12
6	Relation Between Normal-Tangential Coordinates (ξ,η) and Radial-Angular Coordinates (r,n) at Body Surface	20
7	Organization of Time Dependent Computation (TDC) Computer Program	39
8	"Law-of-the-Wall" Boundary Conditions	46
9	Grid Geometry for Cylinder Flow	50
10	Cylinder: Surface Pressure Distribution	51
11	Cylinder: Near-Field Pressure Distribution	51
12	Cylinder: Surface Pressure Distribution	52
13	Cylinder: Near-Field Pressure Distribution	52
14	Cylinder: Time Variation of Stagnation Pressure	53
15	Cylinder: Surface Pressure Distribution	53
16	Circular Cylinder with Circulation (Inviscid) Surface Pressure Distribution	56
17	Circular Cylinder with Circulation (Inviscid) Near-Field Pressure Distribution	57
18	Circular Cylinder with Circulation (Inviscid) Time Variation of Lift and Drag	58
19	Circular Cylinder with Circulation (Inviscid) Surface Pressure Distribution	59
20	Circular Cylinder with Circulation (Inviscid) Near-Field Pressure Distribution	60
21	Circular Cylinder with Circulation (Inviscid) Time Variation of Lift and Drag	61
22	Ellipse: Surface Pressure Distribution	63
23	Ellipse: Near-Field Pressure Distribution	63
24	Joukowsky Airfoil: Surface Pressure Distribution (Inviscid)	65
25	Joukowsky Airfoil: Surface Velocity Distribution (Inviscid)	66
26	Joukowsky Airfoil: Time Variation of Stagnation, Minimum and Trailing Edge Pressures (Inviscid)	67
27	Joukowsky Airfoil: Surface Pressure Distribution (Inviscid)	68

LIST OF ILLUSTRATIONS (Continued)

Figure	Title	Page
28	Joukowsky Airfoil: Surface Velocity Distribution (Inviscid) . .	69
29	Joukowsky Airfoil: Time Variation of Stagnation, Minimum and Trailing Edge Pressures (Inviscid)	70
30	Joukowsky Airfoil: Surface Pressure Distribution (Inviscid) .	71
31	Joukowsky Airfoil: Surface Velocity Distribution (Inviscid) .	72
32	Joukowsky Airfoil: Time Variation of Stagnation, Minimum and Trailing Edge Pressures (Inviscid)	73
33	Effect of Transformation Parameter τ on Angular Distribution of Body Grid Points	75
34	Viscous Effect on Pressure Distribution: 11.8% Joukowsky Airfoil	83
35	Comparison of Boundary Layers on Joukowsky Airfoil: Shape Factor	84
36	Comparison of Boundary Layers on Joukowsky Airfoil: Momentum Thickness	84
37	Comparison of Boundary Layers on Joukowsky Airfoil: Displacement Thickness	85
38	Comparison of Boundary Layers on Joukowsky Airfoil: Boundary Layer Thickness	85
39	Joukowsky Airfoil: Grid Boundary of Viscous Calculations . . .	88
40	Joukowsky Airfoil: Boundary Layer Velocity Profiles in "Law-of-the-Wall" Coordinates.	90
41	Joukowsky Airfoil: Shear Variation Across Turbulent Boundary Layer	92
42	Junction Between "Law-of-the-Wall" and "Velocity Defect" Regions	93
43	Joukowsky Airfoil: Time Variation of Stagnation, Minimum and Trailing Edge Pressures (Viscous)	95
44	Joukowsky Airfoil: Surface Pressure Distribution (Laminar). . .	96
45	Joukowsky Airfoil: Velocity Variation with Distance from Wall at Mid-Chord	97
46	Joukowsky Airfoil: Surface Pressure Distribution (Turbulent) .	99

1. INTRODUCTION AND SUMMARY

A numerical procedure, known as the Time Dependent Computation (TDC) computer program is being developed which determines steady state solutions of the turbulent, two-dimensional Navier-Stokes equations as the asymptotic large-time limit of the full unsteady equations. The hyperbolic character of the unsteady equations offers the advantage of solving an initial and boundary value problem which is well suited for a digital computer. In addition to providing steady state solutions, accurate transient results are also obtained thus adding to the program's versatility.

In Section 2, the formulation is presented for time dependent calculations of inviscid and laminar flow using an analytic coordinate transformation which maps the space between the body and the initial outgoing wave front onto a computational plane. A coordinate transformation is developed for a symmetrical Joukowsky airfoil as an example. Accurate boundary conditions are derived for the general case; a special treatment of the singularities induced by the example transformation at the cusped trailing edge is also presented.

In Section 3, the formulation is extended to time dependent calculation of turbulent, viscous flow by incorporating the Extended Energy-Dissipation turbulence model of Spalding into the equations of motion. The fine mesh spacings required to compute flow properties across the laminar sublayer are avoided by developing approximate surface boundary conditions based on the "law-of-the-wall" relations.

Results for inviscid, subcritical calculations demonstrating convergence to the steady state solution are presented in Section 4. Some results for completely laminar flow and laminar flow with transition to turbulence are presented in Section 5 for the case of a symmetric Joukowsky airfoil.

2. TIME DEPENDENT COMPUTATION (TDC) PROGRAM DESCRIPTION

The TDC program formulation is modeled after the approach first proposed by Moretti (Reference 1), with particular emphasis placed upon proper physical representation of the flow field. The flow is produced by accelerating any arbitrary body smoothly from rest to a constant velocity in a fluid whose motion may be arbitrarily prescribed. The numerical compucations are performed within the region (physical plane) bounded by the body and the surrounding initial perturbation wave which propagates outward from the body at the start of its motion. This allows initial conditions consistent with the physical situation to be properly imposed along with the enforcement of correct far-field boundary conditions as the solution develops with time. Correct representation of both initial and boundary conditions is necessary to ensure convergence to the correct steady state solution.

The annular shaped physical plane surrounding the body is mapped onto a rectangular computational plane by means of a series of coordinate mappings and stretching transformations. This is illustrated simply in Figure 1. These transformations are chosen such that uniform grid spacing in the computational plane corresponds to a highly non-uniform grid arrangement in the physical plane. This provides for fine coordinate mesh spacing in those regions where gradients are large, such as boundary layers, wake regions, and separated layers and coarse mesh spacing where gradients are small. As a result, economic computation times are achieved by reducing the total number of points required to adequately describe a given flow field.

A steady flow solution is first realized in a narrow region immediately surrounding the body at some time after the body has accelerated to uniform velocity. The size of this region continuously grows with subsequent computations until a steady state region of acceptable size is attained, at which point the calculations may be terminated.

2.1 Navier-Stokes Equations

For two-dimensional problems, the Navier-Stokes equations are most efficiently solved in polar coordinates r and θ, as can be seen by examining Figure 1. Specifically, for a perfect gas with constant viscosity and thermal conductivity,

$$\frac{\partial R}{\partial t} + U\frac{\partial R}{\partial r} + \frac{V}{r}\frac{\partial R}{\partial \theta} + \frac{\partial U}{\partial r} + \frac{U}{r} + \frac{1}{r}\frac{\partial V}{\partial \theta} = 0 \tag{1}$$

$$\frac{\partial U}{\partial t} + U\frac{\partial U}{\partial r} + \frac{V}{r}\frac{\partial U}{\partial \theta} - \frac{V^2}{r} = -Q\frac{\partial P}{\partial r} + \frac{\sqrt{\gamma}M_\infty}{Re}e^{-R}\left[\frac{4}{3}\left(\frac{\partial^2 U}{\partial r^2} + \frac{1}{r}\frac{\partial U}{\partial r} - \frac{U}{r^2}\right)\right.$$
$$\left. + \frac{1}{r^2}\frac{\partial^2 U}{\partial \theta^2} - \frac{7}{3}\frac{1}{r^2}\frac{\partial V}{\partial \theta} + \frac{1}{3}\frac{1}{r}\frac{\partial^2 V}{\partial r \partial \theta}\right] + \frac{dU_\infty}{dt}\cos\theta + \frac{dV_\infty}{dt}\sin\theta \tag{2}$$

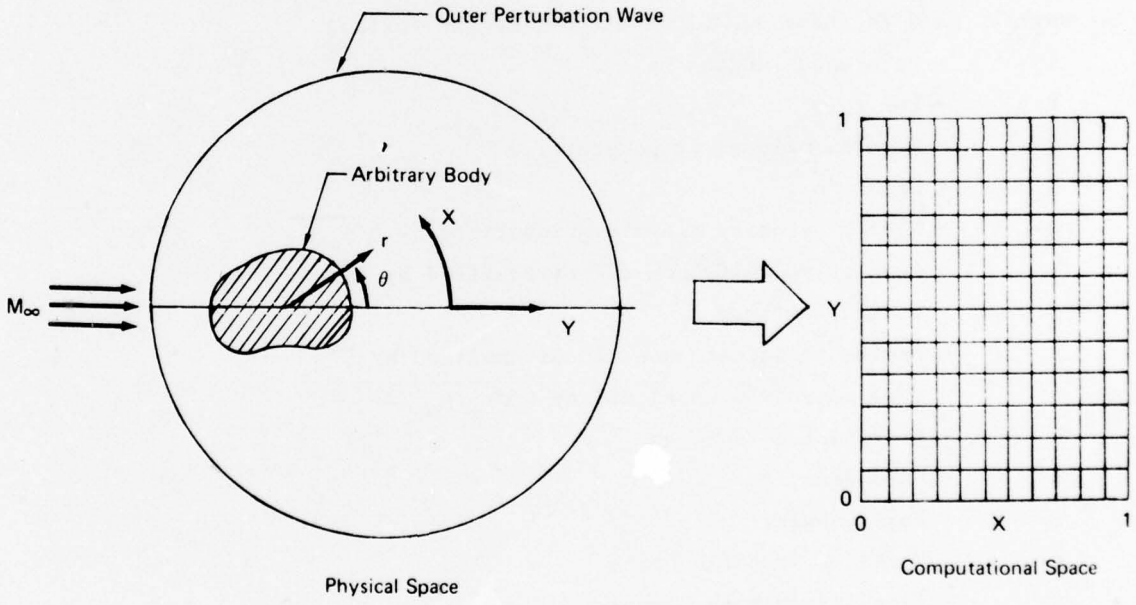


FIGURE 1. COORDINATE TRANSFORMATION

$$\frac{\partial V}{\partial t} + U\frac{\partial V}{\partial r} + \frac{V}{r}\frac{\partial V}{\partial \theta} + \frac{UV}{r} = -\frac{Q}{r}\frac{\partial P}{\partial \theta} + \frac{\sqrt{\gamma}M_\infty}{Re}e^{-R}\left[\frac{\partial^2 V}{\partial r^2} + \frac{1}{r}\frac{\partial V}{\partial r} - \frac{V}{r^2}\right.$$
$$\left. + \frac{4}{3}\frac{1}{r^2}\frac{\partial^2 V}{\partial \theta^2} + \frac{7}{3}\frac{1}{r^2}\frac{\partial U}{\partial \theta} + \frac{1}{3}\frac{1}{r}\frac{\partial^2 U}{\partial r \partial \theta}\right] - \frac{dU_\infty}{dt}\sin\theta + \frac{dV_\infty}{dt}\cos\theta \tag{3}$$

$$\frac{\partial P}{\partial t} + U\frac{\partial P}{\partial r} + \frac{V}{r}\frac{\partial P}{\partial \theta} = e^{-P}\Phi + \frac{\gamma^{3/2}M_\infty}{Pr\ Re}e^{-R}\left\{\frac{1}{r}\left(\frac{\partial P}{\partial r} - \frac{\partial R}{\partial r}\right) + \left(\frac{\partial P}{\partial r} - \frac{\partial R}{\partial r}\right)^2\right.$$
$$\left. + \frac{\partial^2 P}{\partial r^2} - \frac{\partial^2 R}{\partial r^2} + \frac{1}{r^2}\left[\left(\frac{\partial P}{\partial \theta} - \frac{\partial R}{\partial \theta}\right)^2 + \frac{\partial^2 P}{\partial \theta^2} - \frac{\partial^2 R}{\partial \theta^2}\right]\right\} - \gamma\left(\frac{\partial U}{\partial r} + \frac{U}{r} + \frac{1}{r}\frac{\partial V}{\partial \theta}\right) \tag{4}$$

and

$$\Phi = (\gamma - 1)\frac{\sqrt{\gamma}M_\infty}{Re}\left\{2\left[\left(\frac{\partial U}{\partial r}\right)^2 + \left(\frac{1}{r}\frac{\partial V}{\partial \theta} + \frac{U}{r}\right)^2 + \frac{1}{2}\left(\frac{1}{r}\frac{\partial U}{\partial \theta} + \frac{\partial V}{\partial r} - \frac{V}{r}\right)^2\right]\right.$$
$$\left. - \frac{2}{3}\left(\frac{\partial U}{\partial r} + \frac{U}{r} + \frac{1}{r}\frac{\partial V}{\partial \theta}\right)^2\right\} \tag{5}$$

The symbols used in these equations are defined as follows:

- L - Reference length
- P - Log (p/p_∞)
- Q - Non-dimensional temperature, e^{P-R}
- R - Log (ρ/ρ_∞)
- U - Radial velocity non-dimensionalized by $\sqrt{p_\infty/\rho_\infty}$
- V - Angular velocity non-dimensionalized by $\sqrt{p_\infty/\rho_\infty}$
- p - Static pressure
- r - Radial coordinate non-dimensionalized by L
- t - Time non-dimensionalized by $L\sqrt{\rho_\infty/p_\infty}$
- Φ - Dissipation function
- ρ - Mass density
- θ - Polar angle
- γ - Ratio of specific heats
- M_∞ - Free stream Mach number
- Re - Free stream Reynolds number
- Pr - Prandtl number
- p_∞ - Free stream static pressure
- ρ_∞ - Free stream mass density
- U_∞ - Longitudinal free stream velocity component
- V_∞ - Vertical free stream velocity component

2.2 Transformation Onto the Computational Plane

The transformation mapping the physical plane (r,θ) onto the computational plane (X,Y) has the form

$$t \rightarrow T$$

$$r \rightarrow Y(t,r,\theta) \qquad (0 \leq Y \leq 1)$$

$$\theta \rightarrow X(t,r,\theta)$$

$$F(t,r,\theta) \rightarrow F(T,X,Y)$$

where F represents any dependent variable, P, R, U, or V. Derivatives of F are obtained in a straightforward manner from the above transformation functions. For example,

$$\frac{\partial F}{\partial t} = \frac{\partial F}{\partial T} + \frac{\partial F}{\partial X}\frac{\partial X}{\partial t} + \frac{\partial F}{\partial Y}\frac{\partial Y}{\partial t}$$

$$\frac{\partial F}{\partial r} = \frac{\partial F}{\partial X}\frac{\partial X}{\partial r} + \frac{\partial F}{\partial Y}\frac{\partial Y}{\partial r} \tag{6}$$

$$\frac{\partial F}{\partial \theta} = \frac{\partial F}{\partial X}\frac{\partial X}{\partial \theta} + \frac{\partial F}{\partial Y}\frac{\partial Y}{\partial \theta}$$

The transformation functions X and Y for any given problem are constructed analytically to provide the desired non-uniform mesh spacing in the physical plane. That is, nodal points are heavily distributed in regions of large gradients with wider spacing elsewhere. In general, X and Y are chosen such that the magnitude of third derivatives of the dependent variables in the computational plane does not become large. Since X and Y are analytic functions, their derivatives which appear as coefficients in the transformed equations of motion via Equations (6) are also analytic, thereby eliminating any approximation error due to the transformation of coordinates.

At each interior point, (X,Y) of the computational plane, the dependent flow field variables P, R, U and V are updated at each time step by means of a second-order accurate numerical scheme developed by MacCormack (Reference 2). This scheme is of the predictor-corrector type with the allowable time step-size for stable computations determined by the Courant-Friederichs-Lewy criterion (Reference 3).

Construction details for the functions X and Y can be illustrated quite simply for the case of a symmetric Joukowsky airfoil section of arbitrary thickness h. Conceptually, the transformation proceeds in several steps. First, the airfoil section denoted by $b(\theta)$ and the surrounding outer perturbation wave

$s(\theta,t)$ sketched in Figure 2 are mapped from the physical (r,θ) plane to an intermediate (ρ,ϕ) plane by means of the Joukowsky transformation

$$z = \zeta + \varepsilon + \frac{a^2}{\zeta+\varepsilon} \tag{7}$$

where

$$\begin{aligned} z &= re^{i\theta} \\ \zeta &= \rho e^{i\phi} \\ \varepsilon &= \varepsilon_r + i\varepsilon_i \end{aligned} \tag{8}$$

and $\varepsilon_i = 0$ for the symmetric airfoil case. This mapping produces a smooth image of the outer perturbation wave denoted by $S(\phi,t)$ in the ζ-plane as shown in Figure 3 and maps the airfoil onto a circle of radius c provided $a = c + \varepsilon_r$. Many of the necessary resolution features for computing complex airfoil flow fields are incorporated in this transformation. Note that the two overlapped rows of nodal points AB and CD behind the airfoil in the physical z-plane facilitate satisfying boundary conditions at the X = 0 and X = 1 boundaries of the computational plane.

Next a normalizing function Z is defined in the ζ-plane by

$$Z = \frac{\rho - c}{S - c} \tag{9}$$

The mapping to the computational plane is completed by constructing functions of the form

$$\begin{aligned} X &= X(\rho,\phi,\alpha_i) \\ Y &= Y(Z,\beta_i) \end{aligned} \tag{10}$$

where $\alpha_i(r,\theta,t)$ and $\beta_i(r,\theta,t)$ $(i = 1,2,\ldots)$ are arbitrary functions chosen to produce a grid network in the physical plane having the desired nodal point distribution. That is, points should be heavily concentrated near the body and its wake where viscous gradients are large, near the outer perturbation wave where pressure gradients may be steep, and in the vicinity of dividing streamlines when flow separation occurs for good resolution of viscous shear layers. Moretti (Reference 4) has successfully computed laminar boundary layer development for supersonic blunt body flows with fewer than ten points distributed across the layer using these basic concepts. The number of points required to accurately predict viscous layer development will be studied and determined by making comparisons of the TDC program results with the results of other viscous layer calculations such as Cebeci (Reference 5).

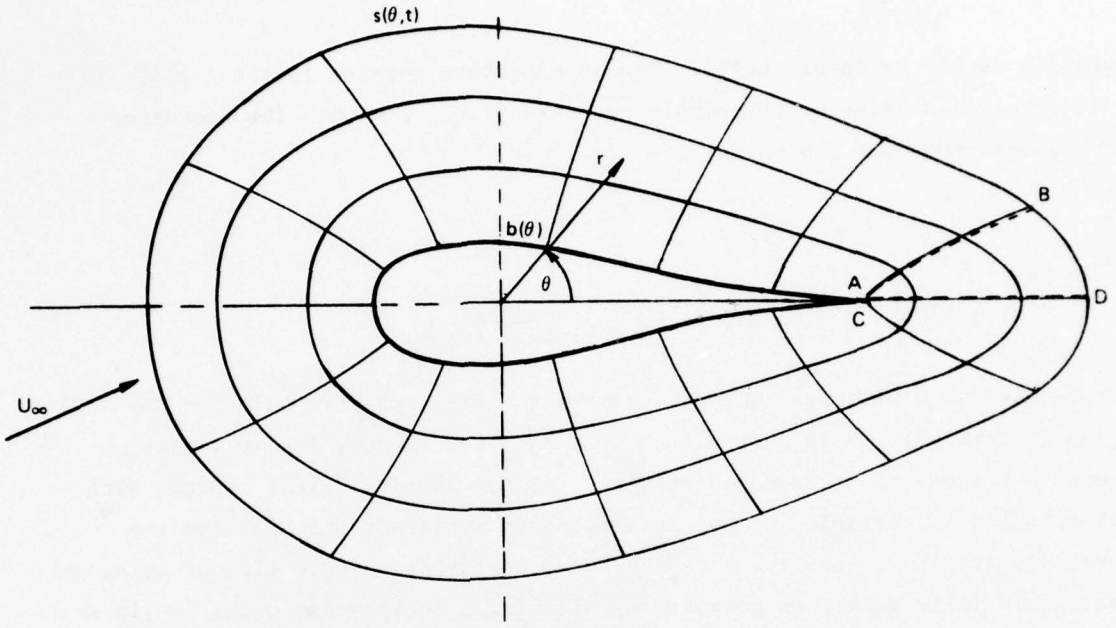


FIGURE 2. COORDINATE SYSTEM ABOUT AIRFOIL IN PHYSICAL SPACE

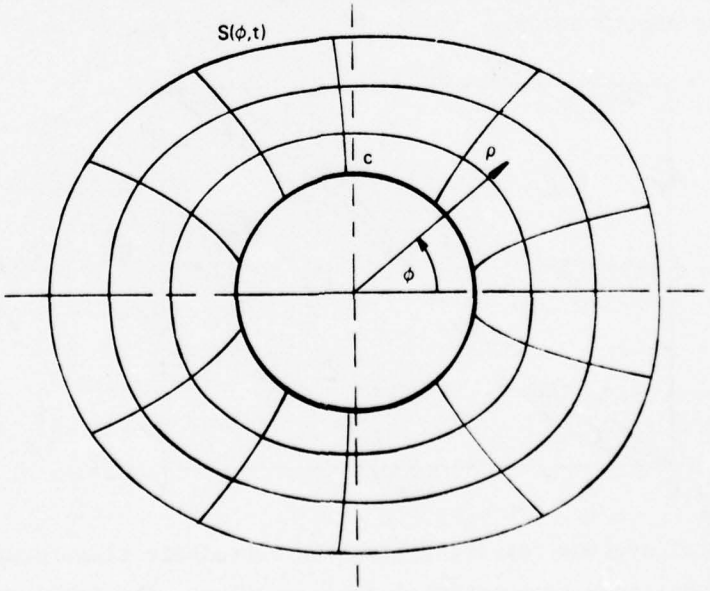


FIGURE 3. COORDINATE SYSTEM IMAGE IN CIRCLE PLANE

A simple transformation example is given in Reference 1 for the case of inviscid flow past a circular cylinder. The normalizing function is defined as

$$Z = \frac{r - b}{s - b}$$

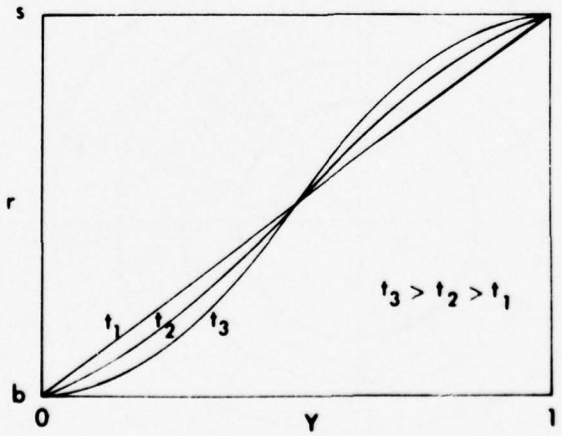
where b is the cylinder radius. The intermediate mapping to the ζ-plane is not required because of the simple geometry (i.e., $a \equiv 0$). The coordinate transformations are chosen as

$$X = \frac{\theta}{\pi}$$

and

$$Y = 1/2 \left\{ 1 + \frac{1}{\alpha} \log \left[\frac{1 + (2Z - 1)\tanh(\alpha/2)}{1 - (2Z - 1)\tanh(\alpha/2)} \right] \right\}$$

where $\alpha(t)$ is arbitrary. Lines of constant X are simply rays in the physical plane. Initially, α is chosen such that an approximately linear variation between r and Y along each ray results. As the physical plane expands with time, a linear variation is not sufficient to satisfactorily resolve the pressure gradients near the body and outer perturbation wave without using an extremely large number of points. By allowing α to increase with time in such a manner that a constant minimum spacing is maintained between the first interior point and the body along the forward stagnation streamline, fewer points are needed. The variation in mesh point distribution at various times is shown qualitatively in the sketch below.



Although the grid systems resulting from the coordinate transformations described above present many computational logic problems, the resulting smaller number of grid points required to adequately resolve the flow field offers a

considerable saving in computer storage requirements and actual computation time.

2.3 Boundary Conditions

2.3.1 Initial Conditions - Initially the body is at rest followed by a smooth acceleration during $0 \leq t \leq t_s$ to the steady velocity $\sqrt{\gamma}\, M_\infty$. Hence, at time zero values of the dependent variables, P, R, U and V are zero at all points of the flow field. The motion of the body (r,θ) origin relative to the initial location is described by

$$\dot{x}_o = -\sqrt{\gamma}\, M_\infty \sin\omega t$$

$$x_o = \frac{\sqrt{\gamma}\, M_\infty}{\omega} (\cos\omega t - 1)$$

for

$$0 \leq t \leq t_s = \pi/2\omega$$

where t_s is arbitrarily chosen.

At the start of motion, a disturbance wave propagates outward from the initial body surface location at the speed of sound. Up to a time t_o, which is small compared to the acceleration time t_s, the physical plane grid geometry is held stationary with respect to the moving body origin with the outer boundary location coincident with the location this wave front will have at time t_o. This is done to provide a finite size physical space with which to initiate the computations. Beyond time t_o, when the initial perturbation wave just reaches the initial grid outer boundary, the outer grid boundary moves along with the wave front. This scheme provides for better definition of the possibly strong gradients which may occur along portions of the wave and allows exact far-field boundary conditions to be imposed.

At the start of the body acceleration ($t < t_o$), the velocities and pressure disturbances are small and the wave speed can be assumed constant and equal to the non-dimensional free stream speed of sound, $\sqrt{\gamma}$. Points on the wave front at time t_o will lie at a distance $\sqrt{\gamma}\, t_o$ on the outward normals from points on the initial body surface location (Figure 4).

Given a point on the body surface at t = 0 located at (b_o,δ) relative to the origin of motion (Figure 4), let the corresponding point on the outward normal at the wave front at time t_o be at $(s_o,\theta_{s,o})$ relative to the origin of motion and be located at (s,θ_s) relative to the coordinate origin at time t_o. The angle

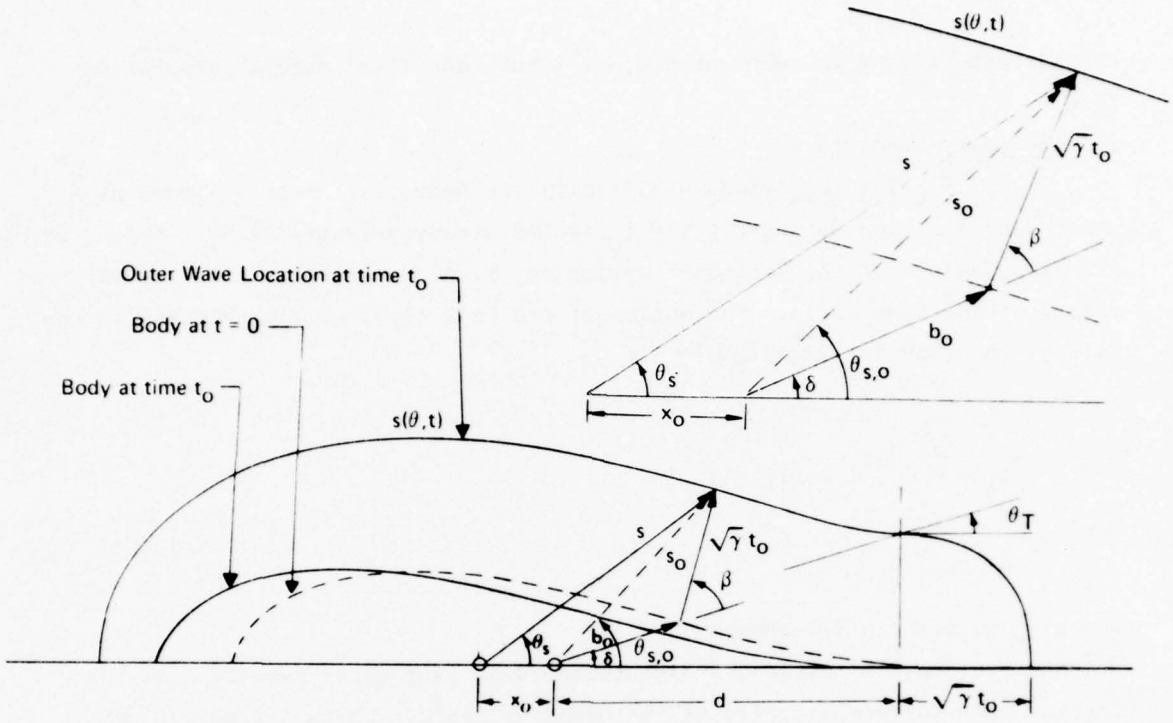


FIGURE 4. FIXED OUTER BOUNDARY GEOMETRY FOR $t \leq t_o$

between the outward normal and the radial direction at (b_o, δ) is denoted by β. For a given value of δ, the point $(s_o, \theta_{s,o})$ is calculated from the body geometry by

$$s_o^2 = b_o^2 + \gamma t_o^2 + 2\, b_o \sqrt{\gamma}\, t_o \cos\beta \tag{11}$$

and

$$\sin(\theta_{s,o} - \delta) = \frac{\sqrt{\gamma}\, t_o}{s_o} \sin\beta \tag{12}$$

where

$$\cos\beta = \left[1 + \left(\frac{b_o'}{b_o}\right)^2\right]^{-1/2}$$

$$\sin\beta = -\frac{b_o'}{b_o} \cos\beta$$

and primes denote differentiation with respect to δ. Likewise, for a given value of θ_s

$$s^2 = s_o^2 + x_o^2 + 2\, s_o\, x_o \cos\theta_{s,o} \tag{13}$$

$$\sin(\theta_{s,o} - \theta_s) = \frac{x_o \sin\theta_{s,o}}{s} \tag{14}$$

A Newton-Raphson iteration on δ for a given value of θ_s yields a solution of Equations (11) through (14) for the unknowns δ, $\theta_{s,o}$, s_o and s.

An additional level of iteration may be required depending on the nature of the transformation linking the physical (r,θ) plane to the computational (X,Y) plane. That is, a given point $(X,1)$ corresponding to a point on the outer boundary may be related to the point (s,θ_s) by relationships such as those given by Equations (7) through (10).

The derivative $\frac{\partial s}{\partial \theta}$ required in the course of the flow field computation for $0 \le t \le t_o$ may be obtained from the above relationships as

$$\frac{\partial s}{\partial \theta} = \frac{s\left[\sin(\theta_{s,o} - \theta_s) - F\cos(\theta_s - \delta)\right]}{F\sin(\theta_s - \delta) - \cos(\theta_{s,o} - \theta_s)}$$

where

$$F = \frac{b_o b_o' + \sqrt{\gamma} t_o\,(b_o' \cos\beta - b_o\,\beta' \sin\beta)}{s_o\left[\sqrt{\gamma} t_o\,\beta' \cos\beta + s_o \cos(\theta_{s,o} - \delta)\right]}$$

Also required is the derivative $\frac{\partial s}{\partial t}$ which is zero for $0 \le t \le t_o$.

The preceding analysis applies to that part of the outer boundary ahead of the outward normal from the initial trailing edge location, $(x_o + d)$, or for $\theta \ge \theta_T$ (Figure 4). For $\theta < \theta_T$ the boundary is a circular wave of radius $\sqrt{\gamma} t_o$ centered at the trailing edge location. The outer boundary geometry and derivative for a given value of θ_s is determined as

$$s = (x_o + d)\cos\theta_s + \sqrt{\gamma t_o^2 - (x_o + d)^2 \sin^2\theta_s}$$

$$\frac{\partial s}{\partial \theta} = \frac{-s\,(x_o + d)\sin\theta_s}{\sqrt{\gamma t_o^2 - (x_o + d)^2 \sin^2\theta_s}}$$

2.3.2 Wave Front Conditions - The outer perturbation wave (Y = 1) surrounding the body is compressive upstream and expansive downstream of the body

and can be assumed essentially free of viscous effects. Gradients over the expansion portion tend not to be large and the wave moves outward at the free stream speed of sound. Values of P and R at points on this portion of the wave are zero while the velocity components U and V are determined by the local free stream velocity components. Over the compression portion, pressure waves due to the body's motion tend to coalesce and form steep gradients, especially if the free stream Mach number is not small. This portion of the wave is handled most efficiently by allowing the pressure gradient to steepen and form a sharp discontinuity. Jump conditions across the moving discontinuity are then computed in conjunction with the Rankine-Hugoniot shock relations coupled with a characteristics relation to determine the local shock velocity relative to the (r,θ) origin.

Flow property calculations at the outer wave nodal points are most efficiently carried out with respect to a local normal-tangential coordinate system denoted by (ξ,η) in Figure 5. The orientation of this system is related to the wave geometry by

$$\cos\beta = -(1 + \sigma^2)^{-1/2}$$
$$\sin\beta = \sigma\,(1 + \sigma^2)^{-1/2} \qquad (15)$$

where

$$\sigma \equiv \frac{1}{s}\frac{\partial s}{\partial \theta}$$

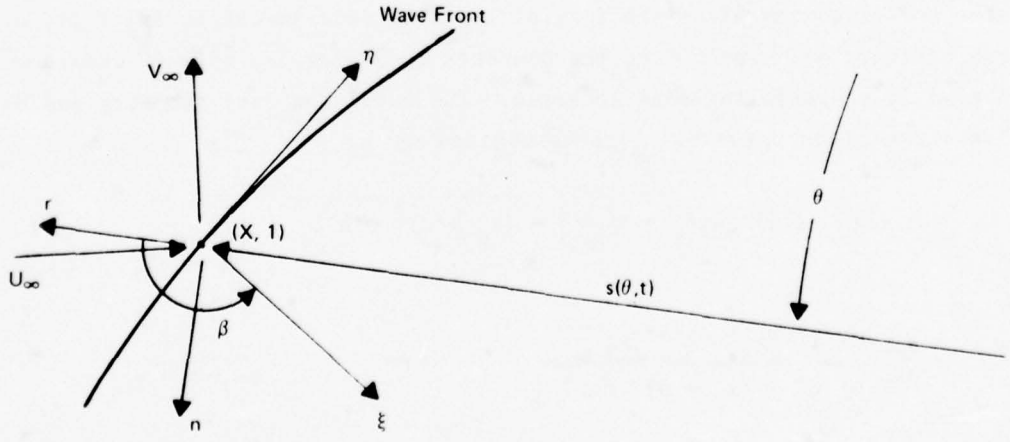


FIGURE 5. RELATION BETWEEN NORMAL-TANGENTIAL COORDINATES (ξ, η) AND RADIAL-ANGULAR COORDINATES (r, n) AT OUTER WAVE

The free stream velocity components (U_∞, V_∞) can be resolved into wave oriented components by

$$V_\xi = (U_\infty \cos\theta + V_\infty \sin\theta)\cos\beta - (U_\infty \sin\theta - V_\infty \cos\theta)\sin\beta \tag{16}$$

and

$$V_\eta = -(U_\infty \cos\theta + V_\infty \sin\theta)\sin\beta - (U_\infty \sin\theta - V_\infty \cos\theta)\cos\beta \tag{17}$$

Since tangential velocity across the wave front is conserved whether or not the wave has become a discontinuity

$$V_\eta = V \cos\beta - U \sin\beta \tag{18}$$

where U and V are the radial and angular components of velocity immediately behind the wave front. Likewise, the normal velocity U_ξ immediately behind the wave front is

$$U_\xi = U \cos\beta + V \sin\beta = \cos\beta(U - \sigma V) \tag{19}$$

where both U_ξ and V_η are measured relative to the (r,θ) origin fixed in the body.

Measured relative to the wave motion, the normal velocity in front of the wave is

$$u_1 = V_\xi - W \tag{20}$$

while behind the wave the normal velocity is

$$u_2 = U_\xi - W \tag{21}$$

where W is the normal wave velocity measured relative to the (r,θ) origin and is given by

$$W = \cos\beta \frac{\partial s}{\partial t} \tag{22}$$

If the wave is compressive, the velocities u_1 and u_2 are related by the Rankine-Hugoniot relation

$$u_2 = \frac{2\gamma + (\gamma-1)\, u_1^2}{(\gamma+1)\, u_1} \tag{23}$$

Likewise, the pressure and density behind the wave are given by

$$\frac{p}{p_\infty} = \frac{(\gamma+1)u_1 - (\gamma-1)u_2}{(\gamma+1)u_2 - (\gamma-1)u_1} \tag{24}$$

and

$$\frac{\rho}{\rho_\infty} = \frac{u_1}{u_2} \tag{25}$$

If the wave is expansive, $u_1 = u_2$ so that

$$U_\xi = V_\xi$$
$$p = p_\infty$$
$$\rho = \rho_\infty$$

and

$$W = V_\xi - \sqrt{\frac{\gamma p_\infty}{\rho_\infty}} \tag{26}$$

Differentiating Equations (23), (24) and (25) with respect to T

$$\frac{\partial u_2}{\partial T} = \left[\frac{\gamma-1}{\gamma+1} - \frac{2\gamma}{(\gamma+1)u_1^2}\right] \frac{\partial u_1}{\partial T}$$

$$\frac{\partial P}{\partial T} = \frac{2u_1}{u_1^2 - \frac{\gamma-1}{2}} \frac{\partial u_1}{\partial T} \tag{27}$$

and

$$\frac{\partial R}{\partial T} = \frac{4\gamma(\gamma+1)u_2}{\left[2\gamma + (\gamma-1)u_1^2\right]^2} \frac{\partial u_1}{\partial T} = \frac{4\gamma}{(\gamma+1)u_1^2 u_2} \frac{\partial u_1}{\partial T}$$

Differentiating Equations (20) and (21) and making use of Equations (27)

$$\frac{\partial u_1}{\partial T} = \frac{\partial V_\xi}{\partial T} - \frac{\partial W}{\partial T}$$

and

$$\frac{\partial u_2}{\partial T} = \frac{\partial U_\xi}{\partial T} - \frac{\partial W}{\partial T} = \left[\frac{\gamma-1}{\gamma+1} - \frac{2\gamma}{(\gamma+1)u_1^2}\right] \frac{\partial u_1}{\partial T}$$

so that

$$\frac{\partial P}{\partial T} = \frac{2u_1}{u_1^2 - \frac{\gamma-1}{2}} \left[\frac{\partial V_\xi}{\partial T} - \frac{\partial W}{\partial T}\right] \tag{28}$$

$$\frac{\partial R}{\partial T} = \frac{4\gamma}{(\gamma+1)u_1^2 u_2}\left[\frac{\partial V_\xi}{\partial T} - \frac{\partial W}{\partial T}\right] \tag{29}$$

and

$$\frac{\partial U_\xi}{\partial T} = \frac{2(\gamma+u_1^2)}{(\gamma+1)u_1^2}\frac{\partial W}{\partial T} + \left[\frac{\gamma-1}{\gamma+1} - \frac{2\gamma}{(\gamma+1)u_1^2}\right]\frac{\partial V_\xi}{\partial T} \tag{30}$$

The derivative $\frac{\partial V_\xi}{\partial T}$ appearing in these expressions may be evaluated from Equation (16) as

$$\begin{aligned}\frac{\partial V_\xi}{\partial T} = \cos\theta\Bigg[&\cos\beta\left(\frac{dU_\infty}{dT} + V_\infty\frac{\partial\theta}{\partial T}\right) + \sin\beta\left(\frac{dV_\infty}{dT} - U_\infty\frac{\partial\theta}{\partial T}\right)\\ &+ (\sigma U_\infty + V_\infty)\frac{\partial}{\partial T}(\sin\beta)\Bigg] + \sin\theta\Bigg[\cos\beta\left(\frac{dV_\infty}{dT} - U_\infty\frac{\partial\theta}{\partial T}\right)\\ &- \sin\beta\left(\frac{dU_\infty}{dT} + V_\infty\frac{\partial\theta}{\partial T}\right) + (\sigma V_\infty - U_\infty)\frac{\partial}{\partial T}(\sin\beta)\Bigg]\end{aligned} \tag{31}$$

where, from Equations (15),

$$\frac{\partial}{\partial T}(\sin\beta) = -\cos^3\beta\frac{\partial\sigma}{\partial T}$$

$$\frac{\partial\sigma}{\partial T} = \frac{1}{s}\left[\frac{\partial}{\partial T}\left(\frac{\partial s}{\partial\theta}\right) - \sigma\frac{\partial s}{\partial T}\right]$$

$$\frac{\partial}{\partial T}\left(\frac{\partial s}{\partial\theta}\right) = \frac{\partial^2 s}{\partial t\partial\theta} + \frac{\partial^2 s}{\partial\theta^2}\frac{\partial\theta}{\partial T}$$

The unknown shock acceleration $\frac{\partial W}{\partial T}$ appearing in Equations (28), (29) and (30) can be determined from the inviscid equations of motion by forming a characteristic relation valid immediately behind the wave front (Reference 6). Since $dY \equiv 0$ along the wave

$$\frac{1}{r}\frac{\partial Y}{\partial \theta} = -\sigma\frac{\partial Y}{\partial r}$$

and

$$\frac{\partial Y}{\partial t} = -\frac{\partial s}{\partial t}\frac{\partial Y}{\partial r}$$

Making use of these expressions, the equations of motion, in transformed computational space coordinates, are (see Equations (1) through (6))

$$\frac{\partial P}{\partial T} + \frac{DX}{Dt}\frac{\partial P}{\partial X} + \frac{DY}{Dt}\frac{\partial P}{\partial Y} + \gamma\left[\frac{\partial Y}{\partial r}\left(\frac{\partial U}{\partial Y} - \sigma\frac{\partial V}{\partial Y}\right) + \frac{\partial X}{\partial r}\frac{\partial U}{\partial X}\right.$$

$$\left. + \frac{U}{s} + \frac{1}{s}\frac{\partial X}{\partial \theta}\frac{\partial V}{\partial X}\right] = 0 \tag{32}$$

$$\frac{\partial R}{\partial T} + \frac{DX}{Dt}\frac{\partial R}{\partial X} + \frac{DY}{Dt}\frac{\partial R}{\partial Y} + \frac{\partial Y}{\partial r}\left(\frac{\partial U}{\partial Y} - \sigma\frac{\partial V}{\partial Y}\right) + \frac{\partial X}{\partial r}\frac{\partial U}{\partial X}$$

$$+ \frac{U}{s} + \frac{1}{s}\frac{\partial X}{\partial \theta}\frac{\partial V}{\partial X} = 0 \tag{33}$$

$$\frac{\partial U}{\partial T} + \frac{DX}{Dt}\frac{\partial U}{\partial X} + \frac{DY}{Dt}\frac{\partial U}{\partial Y} - \frac{V^2}{s} + Q\left(\frac{\partial Y}{\partial r}\frac{\partial P}{\partial Y} + \frac{\partial X}{\partial r}\frac{\partial P}{\partial X}\right)$$

$$= \cos\theta\frac{dU_\infty}{dT} + \sin\theta\frac{dV_\infty}{dT} \tag{34}$$

$$\frac{\partial V}{\partial T} + \frac{DX}{Dt}\frac{\partial V}{\partial X} + \frac{DY}{Dt}\frac{\partial V}{\partial Y} + \frac{UV}{s} + Q\left(\frac{1}{s}\frac{\partial X}{\partial \theta}\frac{\partial P}{\partial X} - \sigma\frac{\partial Y}{\partial r}\frac{\partial P}{\partial Y}\right)$$

$$= \cos\theta\frac{dV_\infty}{dT} - \sin\theta\frac{dU_\infty}{dT} \tag{35}$$

where

$$\frac{DX}{Dt} \equiv \frac{\partial X}{\partial t} + U\frac{\partial X}{\partial r} + \frac{V}{s}\frac{\partial X}{\partial \theta}$$

and

$$\frac{DY}{Dt} \equiv \frac{\partial Y}{\partial r}\left(U - \sigma V - \frac{\partial s}{\partial t}\right)$$

By means of Equations (15), (19) and (22)

$$\frac{DY}{Dt} = \frac{1}{\cos\beta}\frac{\partial Y}{\partial r}(U_\zeta - W)$$

Differentiating Equation (19) with respect to T

$$\frac{\partial U_\xi}{\partial T} = \cos\beta \left(\frac{\partial U}{\partial T} - \sigma \frac{\partial V}{\partial T} \right) - \cos^3\beta \frac{\partial \sigma}{\partial T} (\sigma U + V)$$

Combining Equations (34) and (35) according to this relation gives

$$\frac{\partial U_\xi}{\partial T} + \frac{D\gamma}{Dt} \frac{\partial U_\xi}{\partial Y} + \frac{Q}{\cos\beta} \frac{\partial \gamma}{\partial r} \frac{\partial P}{\partial Y} = A \tag{36}$$

where

$$A = \cos\beta \left[(\cos\theta + \sigma\sin\theta) \frac{dU_\infty}{dT} + (\sin\theta - \sigma\cos\theta) \frac{dV_\infty}{dT} \right.$$

$$\left. - \cos^2\beta \, V_\eta \frac{\partial \sigma}{\partial T} - \frac{DX}{Dt} \left(\frac{\partial U}{\partial X} - \sigma \frac{\partial V}{\partial X} \right) - Q \frac{\partial P}{\partial X} \left(\frac{\partial X}{\partial r} - \frac{\sigma}{s} \frac{\partial X}{\partial \theta} \right) \right] + \frac{VV_\eta}{s}$$

Equation (32) may be written

$$\frac{\partial P}{\partial T} + \frac{D\gamma}{Dt} \frac{\partial P}{\partial Y} + \frac{\gamma}{\cos\beta} \frac{\partial \gamma}{\partial r} \frac{\partial U_\xi}{\partial Y} = B \tag{37}$$

where

$$B = - \frac{DX}{Dt} \frac{\partial P}{\partial X} - \gamma \left[\frac{\partial X}{\partial r} \frac{\partial U}{\partial X} + \frac{U}{s} + \frac{1}{s} \frac{\partial X}{\partial \theta} \frac{\partial V}{\partial X} \right]$$

Forming a characteristic equation from Equations (36) and (37),

$$\frac{\partial P}{\partial T} - \frac{\gamma}{a} \frac{\partial U_\xi}{\partial T} + \frac{1}{\cos\beta} \frac{\partial \gamma}{\partial r} (U_\xi - W - a) \left[\frac{\partial P}{\partial Y} - \frac{\gamma}{a} \cos\beta \left(\frac{\partial U}{\partial Y} - \sigma \frac{\partial V}{\partial Y} \right) \right]$$

$$= B - \frac{\gamma}{a} A$$

where a is the local speed of sound. Eliminating the term $\left(\frac{\partial U}{\partial Y} - \sigma \frac{\partial V}{\partial Y} \right)$ by means of Equation (33) and employing Equations (28), (29) and (30), this characteristic equation reduces to

$$\frac{\partial W}{\partial T} = D \left[E \frac{\partial V_\xi}{\partial T} + F \right] \tag{38}$$

where

$$D = \left[\frac{2u_1}{u_1^2 - \frac{\gamma-1}{2}} + \frac{2\gamma(\gamma+u_1^2)}{(\gamma+1)au_1^2} + \frac{4\gamma^2(u_2 - a)}{(\gamma+1)au_1^2 u_2} \right]^{-1}$$

$$E = \frac{2u_1}{u_1^2 - \frac{\gamma-1}{2}} - \frac{\gamma}{a} \left[\frac{\gamma-1}{\gamma+1} - \frac{2\gamma}{(\gamma+1)u_1^2} \right] + \frac{4\gamma^2(u_2 - a)}{(\gamma+1)au_1^2 u_2}$$

$$F = \frac{u_2 - a}{\cos\beta} \frac{\partial Y}{\partial r}\left[\frac{\partial P}{\partial Y} + \frac{\gamma u_2}{a}\frac{\partial R}{\partial Y}\right] + \frac{\gamma}{a} A - B$$

and $\frac{\partial V_\xi}{\partial T}$ is obtained from Equation (31).

Having determined the shock acceleration $\frac{\partial W}{\partial T}$ at a given node point, the shock velocity is updated by a predictor-corrector scheme using the first-order Taylor approximation

$$W(T+\Delta T) = W(T) + \Delta T \frac{\partial W}{\partial T}$$

With the updated wave velocity $W(T+\Delta T)$, updated values of P, R and U_ξ immediately behind the wave may be determined from Equations (20) through (25). For the expansion portion of the wave, $\frac{\partial W}{\partial T}$ is obtained by simply differentiating Equation (26) giving

$$\frac{\partial W}{\partial T} = \frac{\partial V_\xi}{\partial T}$$

while

$$W(T+\Delta T) = V_\xi(T+\Delta T) - a_\omega$$

$$U_\xi(T+\Delta T) = V_\xi(T+\Delta T)$$

and

$$P = R = 0$$

At each nodal point along the outer wave, the physical plane boundary position can then be updated by means of the second-order Taylor expansion

$$s(\theta, t+\Delta T) = s(\theta,t) + \Delta T \frac{\partial s}{\partial T} + \frac{1}{2}\Delta T^2 \frac{\partial^2 s}{\partial T^2} \tag{39}$$

where

$$\frac{\partial s}{\partial T} = \frac{\partial s}{\partial t} + \frac{\partial s}{\partial \theta}\frac{\partial \theta}{\partial T} \tag{40}$$

and

$$\frac{\partial^2 s}{\partial T^2} = \frac{\partial^2 s}{\partial t^2} + 2\frac{\partial^2 s}{\partial t \partial \theta}\frac{\partial \theta}{\partial T} + \frac{\partial^2 s}{\partial \theta^2}\left(\frac{\partial \theta}{\partial T}\right)^2 + \frac{\partial s}{\partial \theta}\frac{\partial^2 \theta}{\partial T^2} \tag{41}$$

Since $\frac{dX}{dT} \equiv 0$ for a fixed nodal point,

$$\frac{\partial \theta}{\partial T} = -\left[\frac{\partial X}{\partial t} + \frac{\partial X}{\partial r}\frac{\partial s}{\partial T}\right]\left(\frac{\partial X}{\partial \theta}\right)^{-1}$$

and

$$\frac{\partial^2\theta}{\partial T^2} = -\left[\frac{\partial X}{\partial r}\frac{\partial^2 s}{\partial T^2} + F\right]\left(\frac{\partial X}{\partial \theta}\right)^{-1}$$

where

$$F = \frac{\partial^2 X}{\partial t^2} + 2\frac{\partial^2 X}{\partial t \partial r}\frac{\partial s}{\partial T} + 2\frac{\partial^2 X}{\partial t \partial \theta}\frac{\partial \theta}{\partial T} + \frac{\partial^2 X}{\partial r^2}\left(\frac{\partial s}{\partial T}\right)^2 + 2\frac{\partial^2 X}{\partial r \partial \theta}\frac{\partial s}{\partial T}\frac{\partial \theta}{\partial T} + \frac{\partial^2 X}{\partial \theta^2}\left(\frac{\partial \theta}{\partial T}\right)^2$$

Therefore, Equations (40) and (41) become

$$\frac{\partial s}{\partial T} = \left[\frac{\partial s}{\partial t}\frac{\partial X}{\partial \theta} - \frac{\partial s}{\partial \theta}\frac{\partial X}{\partial t}\right]\left[\frac{\partial X}{\partial \theta} + \frac{\partial s}{\partial \theta}\frac{\partial X}{\partial r}\right]^{-1}$$

and

$$\frac{\partial^2 s}{\partial T^2} = \left\{\frac{\partial X}{\partial \theta}\left[\frac{\partial^2 s}{\partial t^2} + 2\frac{\partial^2 s}{\partial t \partial \theta}\frac{\partial \theta}{\partial T} + \frac{\partial^2 s}{\partial \theta^2}\left(\frac{\partial \theta}{\partial T}\right)^2\right] - \frac{\partial s}{\partial \theta}F\right\}\left[\frac{\partial X}{\partial \theta} + \frac{\partial s}{\partial \theta}\frac{\partial X}{\partial r}\right]^{-1}$$

The θ derivatives appearing in these expressions are determined by

$$\frac{\partial s}{\partial \theta} = \frac{\partial X}{\partial \theta}\frac{\partial s}{\partial X}\left[1 - \frac{\partial X}{\partial r}\frac{\partial s}{\partial X}\right]^{-1} \tag{42}$$

$$\frac{\partial^2 s}{\partial \theta^2} = \frac{\partial}{\partial X}\left(\frac{\partial s}{\partial \theta}\right)\left[\frac{\partial X}{\partial \theta} + \frac{\partial s}{\partial \theta}\frac{\partial X}{\partial r}\right]$$

and

$$\frac{\partial^2 s}{\partial t \partial \theta} = \frac{\partial}{\partial X}\left(\frac{\partial s}{\partial t}\right)\left[\frac{\partial X}{\partial \theta} + \frac{\partial s}{\partial \theta}\frac{\partial X}{\partial r}\right]$$

The derivatives $\frac{\partial s}{\partial t}$ and $\frac{\partial^2 s}{\partial t^2}$ are related to the local propagation velocity of the outer wave W by Equation (22) and its derivative giving

$$\frac{\partial^2 s}{\partial t^2} = \frac{1}{\cos\beta}\frac{\partial W}{\partial T} + \frac{\sigma}{s}\cos^2\beta\frac{\partial s}{\partial t}\left[\frac{\partial^2 s}{\partial t \partial \theta} + \frac{\partial^2 s}{\partial \theta^2}\frac{\partial \theta}{\partial T} - \sigma\frac{\partial s}{\partial T}\right] - \frac{\partial^2 s}{\partial t \partial \theta}\frac{\partial \theta}{\partial T}$$

Finally, from Equations (18) and (19),

$$U = U_\xi \cos\beta - V_\eta \sin\beta$$
$$V = U_\xi \sin\beta + V_\eta \cos\beta$$

from which updated values of U and V may be determined using updated values of $\sin\beta$ and $\cos\beta$ computed from Equations (15), (39) and (42).

2.3.3 Body Surface Conditions - Boundary conditions at the body surface may be determined in a manner quite similar to that for the outer wave conditions. That is, a characteristics relationship reflecting the fact that the normal velocity vanishes at the surface is used to compute surface pressure. Hence, a local normal-tangential coordinate system denoted by (ξ,η) in Figure 6

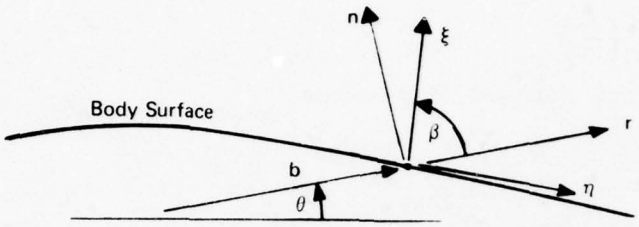


FIGURE 6. RELATION BETWEEN NORMAL-TANGENTIAL COORDINATES (ξ, η) AND RADIAL-ANGULAR COORDINATES (r, n) AT BODY SURFACE

is the most efficient system with which to carry out the computations. The orientation of this system is related to the body geometry by

$$\cos\beta = (1 + \sigma^2)^{-1/2}$$
$$\sin\beta = -\sigma(1 + \sigma^2)^{-1/2} \tag{43}$$

where

$$\sigma \equiv \frac{1}{b}\frac{db}{d\theta}$$

Also, since $dY \equiv 0$ along the body surface

$$\frac{1}{b}\frac{\partial Y}{\partial \theta} = -\sigma\frac{\partial Y}{\partial r} \tag{44}$$

2.3.3.1 Inviscid Flow - Making use of Equations (43) and (44), the normal and tangential velocities at the body surface measured relative to the (r,θ) origin fixed in the body are

$$v = \cos\beta\,(U - \sigma V) = 0$$

and (45)

$$u = \cos\beta\,(\sigma U + V)$$

Likewise, the inviscid equations of motion, in transformed computational space coordinates, are

$$\frac{\partial P}{\partial T} + \frac{DX}{Dt}\frac{\partial P}{\partial X} + \gamma\left[\frac{\partial Y}{\partial r}\left(\frac{\partial U}{\partial Y} - \sigma\frac{\partial V}{\partial Y}\right) + \frac{\partial X}{\partial r}\frac{\partial U}{\partial X} + \frac{U}{b} + \frac{1}{b}\frac{\partial X}{\partial \theta}\frac{\partial V}{\partial X}\right] = 0 \tag{46}$$

$$\frac{\partial R}{\partial T} + \frac{DX}{Dt}\frac{\partial R}{\partial X} + \frac{\partial Y}{\partial r}\left(\frac{\partial U}{\partial Y} - \sigma\frac{\partial V}{\partial Y}\right) + \frac{\partial X}{\partial r}\frac{\partial U}{\partial X} + \frac{U}{b} + \frac{1}{b}\frac{\partial X}{\partial \theta}\frac{\partial V}{\partial X} = 0 \tag{47}$$

$$\frac{\partial U}{\partial T} + \frac{DX}{Dt}\frac{\partial U}{\partial X} - \frac{V^2}{b} + Q\left(\frac{\partial X}{\partial r}\frac{\partial P}{\partial X} + \frac{\partial Y}{\partial r}\frac{\partial P}{\partial Y}\right) = -\frac{dU_\infty}{dT}\cos\theta + \frac{dV_\infty}{dT}\sin\theta \tag{48}$$

$$\frac{\partial V}{\partial T} + \frac{DX}{Dt}\frac{\partial V}{\partial X} + \frac{UV}{b} + Q\left(\frac{1}{b}\frac{\partial X}{\partial \theta}\frac{\partial P}{\partial X} - \sigma\frac{\partial Y}{\partial r}\frac{\partial P}{\partial Y}\right) = \frac{dV_\infty}{dT}\cos\theta - \frac{dU_\infty}{dT}\sin\theta \tag{49}$$

where

$$\frac{DX}{Dt} \equiv U\frac{\partial X}{\partial r} + \frac{V}{b}\frac{\partial X}{\partial \theta}$$

Differentiating the above tangential velocity expression with respect to T and using the fact that $U = \sigma V$ on the body surface

$$\frac{\partial u}{\partial T} = \cos\beta\left(\sigma\frac{\partial U}{\partial T} + \frac{\partial V}{\partial T}\right) = \frac{1}{\cos\beta}\frac{\partial V}{\partial T}$$

Combining Equations (48) and (49) according to this relation gives a tangential momentum equation of the form

$$\frac{\partial V}{\partial T} = \cos^2\beta\left[\frac{dU_\infty}{dT}(\sigma\cos\theta - \sin\theta) + \frac{dV_\infty}{dT}(\sigma\sin\theta + \cos\theta) - \frac{DX}{Dt}\left(\sigma\frac{\partial U}{\partial X} + \frac{\partial V}{\partial X}\right) - Q\left(\sigma\frac{\partial X}{\partial r} + \frac{1}{b}\frac{\partial X}{\partial \theta}\right)\frac{\partial P}{\partial X}\right] \tag{50}$$

with

$$U = \sigma V$$

Differentiating the normal velocity relation with respect to T gives

$$\frac{\partial v}{\partial T} = \cos\beta\left(\frac{\partial U}{\partial T} - \sigma\frac{\partial V}{\partial T}\right) = 0$$

Combining Equations (48) and (49) according to this relation gives a normal momentum equation of the form

$$\frac{\partial v}{\partial T} + \frac{Q}{\cos\beta}\frac{\partial Y}{\partial r}\frac{\partial P}{\partial Y} = \cos\beta\left[\frac{dU_\infty}{dT}(\cos\theta + \sigma\sin\theta) + \frac{dV_\infty}{dT}(\sin\theta - \sigma\cos\theta) + \frac{V^2}{b\cos^2\beta} - \frac{DX}{Dt}\left(\frac{\partial U}{\partial X} - \sigma\frac{\partial V}{\partial X}\right) - Q\left(\frac{\partial X}{\partial r} - \frac{\sigma}{b}\frac{\partial X}{\partial \theta}\right)\frac{\partial P}{\partial X}\right]$$

Forming a characteristic equation with this result and Equation (46),

$$\frac{\partial P}{\partial T} = \frac{\partial Y}{\partial r}\left[\frac{a}{\cos\beta}\frac{\partial P}{\partial Y} - \gamma\left(\frac{\partial U}{\partial Y} - \sigma\frac{\partial V}{\partial Y}\right)\right] - \frac{DX}{Dt}\frac{\partial P}{\partial X} - \gamma\left[\frac{\partial X}{\partial r}\frac{\partial U}{\partial X} + \frac{U}{b} + \frac{1}{b}\frac{\partial X}{\partial\theta}\frac{\partial V}{\partial X}\right] - \frac{\gamma}{a}\cos\beta\left[\frac{dU_\infty}{dT}(\cos\theta + \sigma\sin\theta) + \frac{dV_\infty}{dT}(\sin\theta - \sigma\cos\theta) + \frac{V^2}{b\cos^2\beta} - \frac{DX}{Dt}\left(\frac{\partial U}{\partial X} - \sigma\frac{\partial V}{\partial X}\right) - Q\left(\frac{\partial X}{\partial r} - \frac{\sigma}{b}\frac{\partial X}{\partial\theta}\right)\frac{\partial P}{\partial X}\right] \tag{51}$$

where a is the local sonic velocity. Finally, Equations (46) and (47) may be combined to give

$$\frac{\partial R}{\partial T} = \frac{1}{\gamma}\left[\frac{\partial P}{\partial T} + \frac{DX}{Dt}\left(\frac{\partial P}{\partial X} - \gamma\frac{\partial R}{\partial X}\right)\right] \tag{52}$$

which reflects the fact that entropy is convected along streamlines.

Updated values of P, R, U and V at points on the body surface can be determined by means of Equations (50), (51) and (52). However, special consideration must be given to points of surface discontinuity such as sharp trailing edges. This will be illustrated below for the case of a non-lifting, symmetric Joukowsky airfoil.

The Joukowsky transformation defined by Equations (7) and (8) gives rise to a geometric singularity at the cusped trailing edge which in turn induces singular behavior in the spatial derivatives of the flow variables P, R, U and V. This is evident by expanding in terms of body surface polar angle θ near the trailing edge the quantity σ defined by Equations (43). That is,

$$\sigma = K_1\,\theta^{-1/3} + K_2\,\theta^{1/3} + K_3\,\theta + \cdots$$

where

$$K_1 = -\frac{K}{3}\left(\frac{c}{c+\epsilon_r}\right)^2$$

$$K_2 = -\frac{5}{6}KK_1\left(\frac{\epsilon_r}{c+\epsilon_r}\right)^2$$

and

$$k = (c+\epsilon_r)^2\left(\frac{4}{\epsilon_r^2 c^4}\right)^{1/3}$$

Since, from Equations (50), $U = \sigma V$ along the body surface, in order that the trailing edge velocity remain finite, V must possess an expansion of the form

$$V = A_1 \theta^{1/3} + A_2 \theta + A_3 \theta^{5/3} + \cdots \tag{53}$$

so that

$$U = A_1K_1 + (A_1K_2 + A_2K_1)\theta^{2/3} + (A_1K_3 + A_2K_2 + A_3K_1)\theta^{4/3} + \cdots \tag{54}$$

This implies

$$A_1 = \frac{U_{TE}}{K_1}$$

where U_{TE} denotes the trailing edge velocity. Analogous expansions may be assumed for P and R having the form

$$P + P_{TE} + B_1 \theta^{2/3} + B_2 \theta^{4/3} + \cdots \tag{55}$$

and

$$R = R_{TE} + C_1 \theta^{2/3} + C_2 \theta^{4/3} + \cdots \tag{56}$$

Along the body surface

$$\frac{1}{b}\frac{d}{d\theta} = \sigma \frac{\partial}{\partial r} + \frac{1}{b}\frac{\partial}{\partial \theta} \tag{57}$$

so that the inviscid equations of motion may be written

$$\frac{\partial P}{\partial t} + \frac{V}{b}\frac{dP}{d\theta} + \gamma\left(\frac{\partial U}{\partial r} + \frac{U}{b} + \frac{1}{b}\frac{\partial V}{\partial \theta}\right) = 0 \tag{58}$$

$$\frac{\partial R}{\partial t} + \frac{V}{b}\frac{dR}{d\theta} + \frac{\partial U}{\partial r} + \frac{U}{b} + \frac{1}{b}\frac{\partial V}{\partial \theta} = 0 \tag{59}$$

$$\frac{\partial U}{\partial t} + \frac{V}{b}\frac{dU}{d\theta} - \frac{V^2}{b} + Q\frac{\partial P}{\partial r} = \frac{dU_\infty}{dt}\cos\theta \tag{60}$$

$$\frac{\partial V}{\partial t} + \frac{V}{b}\frac{dV}{d\theta} + \frac{UV}{b} + \frac{Q}{b}\frac{\partial P}{\partial \theta} = -\frac{dU_\infty}{dt}\sin\theta \tag{61}$$

Since $\frac{\partial V}{\partial t} \equiv 0$ at the trailing edge for the non-lifting, symmetrical airfoil section, Equations (53) and (61) imply

$$\frac{1}{b}\frac{\partial P}{\partial \theta} = -\frac{A_1^2}{3bQ}\theta^{-1/3} + \cdots$$

$$= -\frac{U_{TE}^2}{3bQK_1^2}\theta^{-1/3} + \cdots$$

and therefore, by Equations (55) and (57),

$$\frac{\partial P}{\partial r} = \frac{1}{3bK_1}\left(2\,B_1 + \frac{U_{TE}^{\,2}}{QK_1^{\,2}}\right) + \cdots \tag{62}$$

Equations (58), (59) and (60) are not amenable to finite difference computation at the trailing edge since the derivatives $\frac{dP}{d\theta}$, $\frac{dR}{d\theta}$ and $\frac{dU}{d\theta}$ are singular at this point although the terms $V\frac{dP}{d\theta}$, $V\frac{dR}{d\theta}$ and $V\frac{dU}{d\theta}$ remain finite. This difficulty can be circumvented by considering instead the derivatives

$$\frac{d}{d\theta}\left[V\,(P - P_{TE})\right] = A_1B_1 + \frac{5}{3}\,(A_1B_2 + B_1A_2)\,\theta^{2/3} + \cdots$$

$$\frac{d}{d\theta}\left[V\,(R - R_{TE})\right] = A_1C_1 + \frac{5}{3}\,(A_1C_2 + C_1A_2)\,\theta^{2/3} + \cdots$$

and

$$\frac{d}{d\theta}\left[V\,(U - U_{TE})\right] = A_1\,(A_1K_2 + A_2K_1) + \frac{5}{3}\,(A_1^{\,2}K_3 + 2\,A_1A_2K_2 + A_1\,A_3K_1 + A_2^{\,2}K_1)\,\theta^{2/3} + \cdots$$

obtained from Equations (53) through (56). The problem terms appearing in the equations of motion may be written

$$V\frac{dP}{d\theta} = \frac{2}{3}\,A_1B_1 + \frac{2}{3}\,(B_1A_2 + 2\,B_2A_1)\,\theta^{2/3} + \cdots$$

$$V\frac{dR}{d\theta} = \frac{2}{3}\,A_1C_1 + \frac{2}{3}\,(C_1A_2 + 2\,C_2A_1)\,\theta^{2/3} + \cdots$$

and

$$V\frac{dU}{d\theta} = \frac{2}{3}\,A_1\,(A_1K_2 + A_2K_1) + \frac{2}{3}\,(3\,A_1A_2K_2 + A_2^{\,2}K_1 + 2\,A_1^{\,2}K_3 + 2\,A_1A_3K_1)\,\theta^{2/3} + \cdots$$

so that at the trailing edge where $\theta = 0$,

$$V\frac{dP}{d\theta} = \frac{2}{3}\frac{d}{d\theta}\left[V\,(P - P_{TE})\right]$$

$$V\frac{dR}{d\theta} = \frac{2}{3}\frac{d}{d\theta}\left[V\,(R - R_{TE})\right] \tag{63}$$

$$V\frac{dU}{d\theta} = \frac{2}{3}\frac{d}{d\theta}\left[V\,(U - U_{TE})\right]$$

and from Equation (62),

$$\frac{\partial P}{\partial r} = \frac{2}{3bU_{TE}} \frac{d}{d\theta} \left[V \left(P - P_{TE} \right) \right] + \frac{U_{TE}^2}{3bQ_{TE} K_1^3}$$

The term $\frac{\partial U}{\partial r}$ in Equations (58) and (59) may be written in computational space coordinates as

$$\frac{\partial U}{\partial r} = \frac{\partial U}{\partial X} \frac{\partial X}{\partial r} + \frac{\partial U}{\partial Y} \frac{\partial Y}{\partial r} \tag{64}$$

From Equations (10),

$$\frac{\partial X}{\partial r} = \frac{\partial X}{\partial \rho} \frac{\partial \rho}{\partial r} + \frac{\partial X}{\partial \phi} \frac{\partial \phi}{\partial r}$$

and

$$\frac{\partial Y}{\partial r} = \frac{\partial Y}{\partial \rho} \frac{\partial \rho}{\partial r}$$

where $\frac{\partial Y}{\partial \phi} = 0$ has been assumed since body surface points are being considered. Since the Joukowsky transformation defined by Equation (7) is analytic, the Cauchy-Riemann conditions

$$\frac{\partial \phi}{\partial r} = \frac{-1}{bc} \frac{\partial \rho}{\partial \theta}$$

and

$$\frac{\partial \phi}{\partial \theta} = \frac{b}{c} \frac{\partial \rho}{\partial r} \tag{65}$$

must be satisfied. Equation (44) is equivalent to

$$\frac{1}{b} \frac{\partial \rho}{\partial \theta} = - \sigma \frac{\partial \rho}{\partial r} \tag{66}$$

since $\rho \equiv c$ along the body surface. Therefore,

$$\frac{\partial \phi}{\partial r} = \frac{\sigma}{c} \frac{\partial \rho}{\partial r} \tag{67}$$

and, from Equations (57), (65), (66) and (67),

$$\frac{1}{b} \frac{dX}{d\theta} = \sigma \frac{\partial X}{\partial r} + \frac{1}{b} \frac{\partial X}{\partial \theta} = \frac{(1 + \sigma^2)}{c} \frac{\partial X}{\partial \phi} \frac{\partial \rho}{\partial r} \tag{68}$$

Equation (64) may now be written

$$\frac{\partial U}{\partial r} = \left[\frac{\partial U}{\partial X}\left(\frac{\partial X}{\partial \rho} + \frac{\sigma}{c}\frac{\partial X}{\partial \phi}\right) + \frac{\partial U}{\partial Y}\frac{\partial Y}{\partial \rho}\right]\frac{\partial \rho}{\partial r} \tag{69}$$

Analysis of the Joukowsky transformation yields the result, valid on the airfoil surface,

$$\lim_{\theta \to 0}\left(\frac{\partial \rho}{\partial r}\right) = -\frac{3}{4}\frac{\epsilon_r}{c} \tag{70}$$

The limiting value of the term $\sigma \frac{\partial U}{\partial X}$ in Equation (69) can be determined by L'Hospital's rule. That is, using Equation (68),

$$\lim_{\theta \to 0}\left(\sigma \frac{\partial U}{\partial X}\right) = 3 K_1 \frac{\partial^2 U}{\partial X^2} \lim_{\theta \to 0}\left(\theta^{2/3}\frac{dX}{d\theta}\right) \tag{71}$$

$$= 3 K_1^3 \frac{b}{c}\frac{\partial^2 U}{\partial X^2}\frac{\partial X}{\partial \phi}\frac{\partial \rho}{\partial r}$$

Therefore, the limiting value of Equation (69) becomes

$$\lim_{\theta \to 0}\left(\frac{\partial U}{\partial r}\right) = \frac{3}{4}\frac{\epsilon_r}{c}\left[\frac{9}{4}\frac{\epsilon_r b}{c^3} K_1^3 \left(\frac{\partial X}{\partial \phi}\right)^2 \frac{\partial^2 U}{\partial X^2} - \frac{\partial U}{\partial Y}\frac{\partial Y}{\partial \rho}\right] \tag{72}$$

where $\frac{\partial X}{\partial \rho} = 0$ has been assumed because of symmetry.

In a similar manner, the term $\frac{1}{b}\frac{\partial V}{\partial \theta}$ in Equations (58) and (59) may be written

$$\frac{1}{b}\frac{\partial V}{\partial \theta} = \frac{1}{b}\left(\frac{\partial V}{\partial X}\frac{\partial X}{\partial \theta} + \frac{\partial V}{\partial Y}\frac{\partial Y}{\partial \theta}\right) \tag{73}$$

where

$$\frac{\partial X}{\partial \theta} = \frac{\partial X}{\partial \rho}\frac{\partial \rho}{\partial \theta} + \frac{\partial X}{\partial \phi}\frac{\partial \phi}{\partial \theta}$$

and

$$\frac{\partial Y}{\partial \theta} = \frac{\partial Y}{\partial \rho}\frac{\partial \rho}{\partial \theta}$$

By means of Equations (65) and (66),

$$\frac{1}{b}\frac{\partial V}{\partial \theta} = \frac{\partial \rho}{\partial r}\left[\frac{\partial V}{\partial X}\left(\frac{1}{c}\frac{\partial X}{\partial \phi} - \sigma\frac{\partial X}{\partial \rho}\right) - \sigma\frac{\partial V}{\partial Y}\frac{\partial Y}{\partial \rho}\right] \tag{74}$$

Again using L'Hospital's rule (refer to Equation (71)),

$$\lim_{\theta \to 0}\left(\sigma\frac{\partial X}{\partial \rho}\right) = K_1^3\frac{b}{c}\frac{\partial X}{\partial \phi}\frac{\partial}{\partial X}\left(\frac{\partial X}{\partial \rho}\right)\frac{\partial \rho}{\partial r}$$

and

$$\lim_{\theta \to 0}\left(\sigma\frac{\partial V}{\partial Y}\right) = 3K_1^3\frac{b}{c}\frac{\partial^2 V}{\partial X \partial Y}\frac{\partial X}{\partial \phi}\frac{\partial \rho}{\partial r}$$

Therefore, the limiting value of Equation (74) becomes

$$\lim_{\theta \to 0}\left(\frac{1}{b}\frac{\partial V}{\partial \theta}\right) = -\frac{3}{4}\frac{\varepsilon_r}{c^2}\frac{\partial X}{\partial \phi}\left\{\frac{\partial V}{\partial X} + \frac{3}{4}\frac{\varepsilon_r b}{c}K_1^3\left[3\frac{\partial Y}{\partial \rho}\frac{\partial^2 V}{\partial X \partial Y} + \frac{\partial}{\partial X}\left(\frac{\partial X}{\partial \rho}\right)\frac{\partial V}{\partial X}\right]\right\} \tag{75}$$

Making use of Equations (63), (72) and (75), the equations governing the flow properties at the trailing edge are

$$\frac{\partial P}{\partial t} = \gamma F - \frac{2}{3b}\frac{d}{d\theta}\left[V\,(P - P_{TE})\right]$$

$$\frac{\partial R}{\partial t} = F - \frac{2}{3b}\frac{d}{d\theta}\left[V\,(R - R_{TE})\right] \tag{76}$$

and

$$\frac{\partial U}{\partial t} = \frac{dU_\infty}{dt} - \frac{2}{3b}\left\{\frac{d}{d\theta}\left[V\,(U - U_{TE})\right] + \frac{Q_{TE}}{U_{TE}}\frac{d}{d\theta}\left[V\,(P - P_{TE})\right]\right\} - \frac{U_{TE}^2}{3bK_1^3}$$

where

$$F = \frac{3}{4}\frac{\varepsilon_r}{c}\left\{\frac{\partial Y}{\partial \rho}\frac{\partial U}{\partial Y} + \frac{1}{c}\frac{\partial X}{\partial \phi}\frac{\partial V}{\partial X} + \frac{9}{4}\frac{\varepsilon_r}{c^2}bK_1^3\frac{\partial X}{\partial \phi}\left[\frac{\partial Y}{\partial \rho}\frac{\partial^2 V}{\partial X \partial Y} + \frac{1}{3}\frac{\partial}{\partial X}\left(\frac{\partial X}{\partial \rho}\right)\frac{\partial V}{\partial X}\right.\right.$$

$$\left.\left. - \frac{1}{c}\frac{\partial X}{\partial \phi}\frac{\partial^2 U}{\partial X^2}\right]\right\} - \frac{U_{TE}}{b}$$

All terms in these expressions can be evaluated at the trailing edge in a straightforward manner.

Since MacCormack's scheme makes use of both forward and backward spatial differencing, it is consistent to develop relations analogous to the above Equations (76) based on an analysis of flow conditions immediately downstream of the trailing edge. For flow along the trailing edge streamline, the equations of motion reduce to

$$\frac{\partial P}{\partial t} + U \frac{\partial P}{\partial r} + \gamma\left(\frac{\partial U}{\partial r} + \frac{U}{r} + \frac{1}{r}\frac{\partial V}{\partial \theta}\right) = 0 \tag{77}$$

$$\frac{\partial R}{\partial t} + U \frac{\partial R}{\partial r} + \frac{\partial U}{\partial r} + \frac{U}{r} + \frac{1}{r}\frac{\partial V}{\partial \theta} = 0 \tag{78}$$

$$\frac{\partial U}{\partial t} + U \frac{\partial U}{\partial r} + Q \frac{\partial P}{\partial r} = \frac{dU_\infty}{dt} \tag{79}$$

$$V = 0$$

The singular nature of the trailing edge geometry again induces singular behavior in the derivatives of the flow variables P, R and U appearing in these equations.

From the Joukowsky transformation, it can be shown that

$$\rho = \frac{r}{2} - \varepsilon_r + \frac{1}{2}(r^2 - b^2)^{1/2}$$

and (80)

$$\frac{\partial \rho}{\partial r} = \frac{1}{2} + \frac{r}{2}(r^2 - b^2)^{-1/2}$$

along the trailing edge streamline, where b denotes the value of r at the trailing edge. This latter result suggests expansions of the form

$$U = U_{TE} + A_1\left(\frac{r-b}{b}\right)^{1/2} + A_2\frac{r-b}{b} + \ldots$$

$$P = P_{TE} + B_1\left(\frac{r-b}{b}\right)^{1/2} + B_2\frac{r-b}{b} + \ldots$$

$$R = R_{TE} + C_1\left(\frac{r-b}{b}\right)^{1/2} + C_2\frac{r-b}{b} + \ldots$$

$$\frac{1}{r}\frac{\partial V}{\partial \theta} = \frac{D_1}{2b}\left(\frac{r-b}{b}\right)^{-1/2} + \frac{D_2}{b} + \ldots \tag{81}$$

and

$$Q = \exp\left[P_{TE} - R_{TE} + (B_1 - C_1)\left(\frac{r-b}{b}\right)^{1/2} + \ldots\right]$$

$$= Q_{TE}\left[1 + (B_1 - C_1)\left(\frac{r-b}{b}\right)^{1/2} + \ldots\right]$$

Equations (77) and (78) may be combined to give

$$\frac{\partial P}{\partial t} - \gamma\frac{\partial R}{\partial t} + U\left(\frac{\partial P}{\partial r} - \gamma\frac{\partial R}{\partial r}\right) = 0$$

If this result is to be well-behaved at the trailing edge, then the above expansions lead to

$$C_1 = \frac{B_1}{\gamma} \tag{82}$$

Likewise, if Equations (77) and (79) are to be non-singular at the trailing edge,

$$A_1 U_{TE} + B_1 Q_{TE} = 0$$

and (83)

$$B_1 U_{TE} + \gamma (A_1 + D_1) = 0$$

With these results, the governing equations at the trailing edge become

$$\frac{\partial P}{\partial t} = \frac{U_{TE}}{b}\left(\frac{A_1^2}{2Q_{TE}} - B_2\right) - \frac{\gamma}{b}(A_2 + U_{TE} + D_2)$$

$$\frac{\partial R}{\partial t} = \frac{U_{TE}}{b}\left(\frac{A_1^2}{2\gamma Q_{TE}} - C_2\right) - \frac{1}{b}(A_2 + U_{TE} + D_2) \tag{84}$$

and

$$\frac{\partial U}{\partial t} = \frac{dU_\infty}{dt} - \frac{U_{TE}}{b}A_2 - \frac{Q_{TE}}{b}B_2 - \frac{A_1^2}{2b}\left(1 + \frac{\gamma-1}{\gamma}\frac{U_{TE}^2}{Q_{TE}}\right)$$

From Equations (81) and (83) evaluated at r = b,

$$\frac{\partial}{\partial r}\left[U_{TE}(U - U_{TE}) + Q_{TE}(P - P_{TE})\right] = \frac{U_{TE}}{b}A_2 + \frac{Q_{TE}}{b}B_2$$

$$\frac{\partial}{\partial r}\left[U_{TE}(P - P_{TE}) + \gamma(U - U_{TE})\right] = \frac{U_{TE}}{b}B_2 + \frac{\gamma}{b}A_2 \tag{85}$$

and

$$\frac{\partial}{\partial r}\left[U_{TE}\ (R - R_{TE}) + U - U_{TE}\right] = \frac{U_{TE}}{b}\ C_2 + \frac{A_2}{b}$$

Considering symmetry and Equations (65) and (80),

$$\frac{1}{r}\frac{\partial V}{\partial \theta} = \frac{1}{r}\frac{\partial V}{\partial X}\frac{\partial X}{\partial \theta} = \frac{1}{r}\frac{\partial V}{\partial X}\frac{\partial X}{\partial \phi}\frac{\partial \phi}{\partial \theta} = \frac{\partial V}{\partial X}\frac{\partial X}{\partial \phi}\frac{1}{\rho}\frac{\partial \rho}{\partial r}$$

$$= \frac{\partial X}{\partial \phi}\frac{\partial V}{\partial X}\frac{1}{r - 2\varepsilon_r}\left[\frac{r}{b}\left(\frac{r^2 - b^2}{b^2}\right)^{-1/2} - \frac{2\varepsilon_r}{r - 2\varepsilon_r} + \ldots\right]$$

Relating this result to the expansion for $\frac{1}{r}\frac{\partial V}{\partial \theta}$ given in Equations (81),

$$D_1 = \frac{b}{\sqrt{2}c}\frac{\partial X}{\partial \phi}\frac{\partial V}{\partial X}$$

and

$$D_2 = -\frac{\varepsilon_r b}{2c^2}\frac{\partial X}{\partial \phi}\frac{\partial V}{\partial X} \tag{86}$$

Therefore, from Equations (83)

$$A_1 = \frac{b}{\sqrt{2}\,c}\frac{\partial X}{\partial \phi}\frac{\partial V}{\partial X}\frac{\gamma Q_{TE}}{U_{TE}^2 - \gamma Q_{TE}} \tag{87}$$

Using Equations (85), (86) and (87), the equations of motion at the trailing edge, valid for downstream differencing, are

$$\frac{\partial P}{\partial t} = \gamma F - \frac{\partial}{\partial r}\left[U_{TE}\ (P - P_{TE}) + \gamma(U - U_{TE})\right]$$

$$\frac{\partial R}{\partial t} = F - \frac{\partial}{\partial r}\left[U_{TE}\ (R - R_{TE}) + U - U_{TE}\right] \tag{88}$$

and

$$\frac{\partial U}{\partial t} = \frac{dU_\infty}{dt} - \frac{\gamma^2 b\, Q_{TE}^2}{4c^2(U_{TE}^2 - \gamma Q_{TE})^2}\left(\frac{\partial X}{\partial \phi}\frac{\partial V}{\partial X}\right)^2\left[1 + \frac{\gamma - 1}{\gamma}\frac{U_{TE}^2}{Q_{TE}}\right]$$

$$- \frac{\partial}{\partial r}\left[U_{TE}\ (U - U_{TE}) + Q_{TE}\ (P - P_{TE})\right]$$

where

$$F = \frac{\gamma b\, U_{TE}\, Q_{TE}}{4c^2 (U_{TE}^2 - \gamma Q_{TE})^2} \left(\frac{\partial X}{\partial \phi}\frac{\partial V}{\partial X}\right)^2 + \frac{r}{2c^2}\frac{\partial X}{\partial \phi}\frac{\partial V}{\partial X} - \frac{U_{TE}}{b}$$

2.3.3.2 Laminar Viscous Flow - The analysis of viscous boundary conditions is simplified somewhat by the no-slip condition. If, in addition, a constant temperature surface is assumed equal to free stream temperature, the boundary conditions to be applied to Equations (1) through (5) become

$$U = V = 0$$

$$Q = 1 = e^{P-R} \tag{89}$$

or

$$P = R$$

This last condition reduces the solid boundary analysis to that of predicting only the surface pressure which can be accomplished most accurately by constructing a characteristic equation from Equations (2), (3) and (4).

Following a procedure similar to that outlined for inviscid flow, a normal momentum equation is formed by combining Equations (2) and (3) according to the first of Equations (45). This result is then combined with Equation (4) to give the characteristic relationship

$$\frac{\partial P}{\partial T} = \frac{\partial Y}{\partial r}\left[\frac{a}{\cos\beta}\frac{\partial P}{\partial Y} - \gamma\left(\frac{\partial U}{\partial Y} - \sigma\frac{\partial V}{\partial Y}\right)\right] + F - \frac{\gamma}{a}\cos\beta\left[\frac{dU_\infty}{dT}(\cos\theta + \sigma\sin\theta)\right. \tag{90}$$

$$\left. + \frac{dV_\infty}{dT}(\sin\theta - \sigma\cos\theta) - Q\left(\frac{\partial X}{\partial r} - \frac{\sigma}{b}\frac{\partial X}{\partial \theta}\right)\frac{\partial P}{\partial X} + G - \sigma H\right]$$

where

$$F = e^{-P}\Phi + \frac{\gamma^{3/2} M_\infty}{Pr\ Re} e^{-R}\left\{\left(\frac{1}{b}\frac{\partial Y}{\partial r} + \frac{\partial^2 Y}{\partial r^2} + \frac{1}{b^2}\frac{\partial^2 Y}{\partial \theta^2}\right)\left(\frac{\partial P}{\partial Y} - \frac{\partial R}{\partial Y}\right)\right.$$

$$+ (1+\sigma^2)\left(\frac{\partial Y}{\partial r}\right)^2\left[\left(\frac{\partial P}{\partial Y} - \frac{\partial R}{\partial Y}\right)^2 + \frac{\partial^2 P}{\partial Y^2} - \frac{\partial^2 R}{\partial Y^2}\right] + 2\frac{\partial Y}{\partial r}\left(\frac{\partial X}{\partial r} - \frac{\sigma}{b}\frac{\partial X}{\partial \theta}\right)$$

$$\left.\left(\frac{\partial^2 P}{\partial X \partial Y} - \frac{\partial^2 R}{\partial X \partial Y}\right)\right\}$$

$$\Phi = (\gamma-1)\sqrt{\gamma}\ \frac{M_\infty}{Re}\left(\frac{\partial Y}{\partial r}\right)^2\left[2\left(\frac{\partial U}{\partial Y}\right)^2 + 2\sigma^2\left(\frac{\partial V}{\partial Y}\right)^2 + \left(\frac{\partial V}{\partial Y} - \sigma\frac{\partial U}{\partial Y}\right)^2\right. \tag{91}$$

$$- \frac{2}{3}\left(\frac{\partial U}{\partial Y} - \sigma \frac{\partial V}{\partial Y}\right)^2\Bigg]$$

and

$$G - \sigma H = \sqrt{\gamma}\,\frac{M_\infty}{Re}\, e^{-R}\left\{\left(\frac{4}{3}\frac{\partial^2 Y}{\partial r^2} + \frac{1}{b^2}\frac{\partial^2 Y}{\partial \theta^2} - \frac{\sigma}{3b}\frac{\partial^2 Y}{\partial r \partial \theta} + \frac{4}{3b}\frac{\partial Y}{\partial r} + \frac{7}{3}\frac{\sigma^2}{b}\frac{\partial Y}{\partial r}\right)\frac{\partial U}{\partial Y}\right.$$

$$+\left(\frac{1}{3b}\frac{\partial^2 Y}{\partial r \partial \theta} - \sigma\frac{\partial^2 Y}{\partial r^2} - \frac{4\sigma}{3b^2}\frac{\partial^2 Y}{\partial \theta^2} + \frac{4\sigma}{3b}\frac{\partial Y}{\partial \theta}\right)\frac{\partial V}{\partial Y} + \frac{4}{3}(1+\sigma^2)\left(\frac{\partial Y}{\partial r}\right)^2$$

$$\left(\frac{\partial^2 U}{\partial Y^2} - \sigma\frac{\partial^2 V}{\partial Y^2}\right) + \frac{1}{3}\frac{\partial Y}{\partial r}\left[(8+\sigma^2)\frac{\partial X}{\partial r} - \frac{7\sigma}{b}\frac{\partial X}{\partial \theta}\right]\frac{\partial^2 U}{\partial X \partial Y}$$

$$\left.+\frac{1}{3}\frac{\partial Y}{\partial r}\left[(1+8\sigma^2)\frac{1}{b}\frac{\partial X}{\partial \theta} - 7\sigma\frac{\partial X}{\partial r}\right]\frac{\partial^2 V}{\partial X \partial Y}\right\}$$

In these expressions, use has been made of Equation (44) and the additional surface conditions

$$\frac{\partial U}{\partial X} = \frac{\partial V}{\partial X} = 0$$

$$\frac{\partial^2 U}{\partial X^2} = \frac{\partial^2 V}{\partial X^2} = 0$$

$$\frac{\partial P}{\partial X} = \frac{\partial R}{\partial X}$$

and

$$\frac{\partial^2 P}{\partial X^2} = \frac{\partial^2 R}{\partial X^2}$$

obtained from Equations (89). The quantities F, G and H appearing in Equations (91) represent the viscous terms in Equations (2), (3) and (4) which have been assumed to act as forcing terms when forming the characteristic relation of Equation (90). This technique has also been used in Reference 7.

Equation (1) may be written for constant surface temperature as

$$\frac{\partial R}{\partial T} = \frac{\partial P}{\partial T} = -\frac{\partial Y}{\partial r}\left(\frac{\partial U}{\partial Y} - \sigma\frac{\partial V}{\partial Y}\right)$$

which can be incorporated into Equation (90) to eliminate the term $\frac{\partial Y}{\partial r}\left(\frac{\partial U}{\partial Y} - \sigma\frac{\partial V}{\partial Y}\right)$ giving

$$\frac{\partial P}{\partial T} = \frac{1}{1-\gamma}\left\{\frac{a}{\cos\beta}\,\frac{\partial Y}{\partial r}\,\frac{\partial P}{\partial Y} + F - \frac{\gamma}{a}\cos\beta\left[\frac{dU_\infty}{dT}(\cos\theta + \sigma\sin\theta) + \right.\right.$$

$$\left.\left.\frac{dV_\infty}{dT}(\sin\theta - \sigma\cos\theta) - Q\left(\frac{\partial X}{\partial r} - \frac{\sigma}{b}\,\frac{\partial X}{\partial\theta}\right)\frac{\partial P}{\partial X} + G - \sigma H\right]\right\} \tag{92}$$

This result may then be used to update surface pressure.

The special treatment required at points of surface discontinuity will again be illustrated for the cusped trailing edge of a non-lifting Joukowsky airfoil. For surface points near the trailing edge, Equations (1) and (4) may be combined in computational space variables as

$$\frac{\partial P}{\partial T} - \gamma\,\frac{\partial R}{\partial T} = (1-\gamma)\,\frac{\partial P}{\partial T} = F \tag{93}$$

where

$$F = e^{-P}\Phi + \frac{\gamma M_\infty^{3/2}}{Pr\ Re}\,e^{-P}\left\{\left(\frac{1}{b}\,\frac{\partial Y}{\partial r} + \frac{\partial^2 Y}{\partial r^2} + \frac{1}{b^2}\,\frac{\partial^2 Y}{\partial\theta^2}\right)\left(\frac{\partial P}{\partial Y} - \frac{\partial R}{\partial Y}\right) + \right.$$

$$(1+\sigma^2)\left(\frac{\partial Y}{\partial r}\right)^2\left[\left(\frac{\partial P}{\partial Y} - \frac{\partial R}{\partial Y}\right)^2 + \frac{\partial^2 P}{\partial Y^2} - \frac{\partial^2 R}{\partial Y^2}\right] + 2\,(1+\sigma^2)\,\frac{\partial X}{\partial\rho}\,\frac{\partial\rho}{\partial r}\,\frac{\partial Y}{\partial r} \tag{94}$$

$$\left.\left(\frac{\partial^2 P}{\partial X\partial Y} - \frac{\partial^2 R}{\partial X\partial Y}\right)\right\}$$

and

$$\Phi = (\gamma-1)\sqrt{\gamma}\,\frac{M_\infty}{Re}\left(\frac{\partial Y}{\partial r}\right)^2\left[\frac{4}{3}\left(\frac{\partial U}{\partial Y} - \sigma\,\frac{\partial V}{\partial Y}\right)^2 + \left(\frac{\partial V}{\partial Y} + \sigma\,\frac{\partial U}{\partial Y}\right)^2\right]$$

By means of Equations (65) and (66) and the fact that $\frac{\partial Y}{\partial\phi}$ and $\frac{\partial^2 Y}{\partial\phi^2}$ both vanish on the airfoil surface

$$\frac{1}{b}\,\frac{\partial Y}{\partial r} + \frac{\partial^2 Y}{\partial r^2} + \frac{1}{b^2}\,\frac{\partial^2 Y}{\partial\theta^2} = (1+\sigma^2)\left(\frac{\partial\rho}{\partial r}\right)^2\frac{\partial^2 Y}{\partial\rho^2}$$

$$+ \left(\frac{\partial^2\rho}{\partial r^2} + \frac{1}{b^2}\,\frac{\partial^2\rho}{\partial\theta^2} + \frac{1}{b}\,\frac{\partial\rho}{\partial r}\right)\frac{\partial Y}{\partial\rho}$$

Differentiation of the Cauchy-Riemann conditions gives

$$\frac{\partial^2\rho}{\partial r^2} + \frac{1}{b^2}\,\frac{\partial^2\rho}{\partial\theta^2} + \frac{1}{b}\,\frac{\partial\rho}{\partial r} = \frac{1+\sigma^2}{c}\left(\frac{\partial\rho}{\partial r}\right)^2$$

so that Equation (94) becomes

$$F = \sqrt{\gamma}\,\frac{M_\infty}{Re}\,e^{-P}\left\{(\gamma-1)\left(\frac{\partial Y}{\partial r}\right)^2\left[\frac{1}{3}\left(\frac{\partial U}{\partial Y}\right)^2 - \frac{2}{3}\,\sigma\,\frac{\partial V}{\partial Y}\,\frac{\partial U}{\partial Y} + \frac{4}{3}\left(\sigma\,\frac{\partial V}{\partial Y}\right)^2 + \left(\frac{\partial V}{\partial Y}\right)^2 + (1+\sigma^2)\left(\frac{\partial U}{\partial Y}\right)^2\right] + \frac{\gamma}{Pr}\,(1+\sigma^2)\left(\frac{\partial \rho}{\partial r}\right)^2\left[\left(\frac{\partial^2 Y}{\partial \rho^2} + \frac{1}{c}\,\frac{\partial Y}{\partial \rho}\right)\left(\frac{\partial P}{\partial Y} - \frac{\partial R}{\partial Y}\right) + \left(\frac{\partial Y}{\partial \rho}\right)^2\left\langle\left(\frac{\partial P}{\partial Y} - \frac{\partial R}{\partial Y}\right)^2 + \frac{\partial^2 P}{\partial Y^2} - \frac{\partial^2 R}{\partial Y^2}\right\rangle + 2\,\frac{\partial X}{\partial \rho}\,\frac{\partial Y}{\partial \rho}\left(\frac{\partial^2 P}{\partial X \partial Y} - \frac{\partial^2 R}{\partial X \partial Y}\right)\right]\right\}$$

In order that this term be non-singular at the trailing edge, the quantity

$$f = \left(\frac{\partial Y}{\partial \rho}\,\frac{\partial U}{\partial Y}\right)^2 + \frac{\gamma}{(\gamma-1)Pr}\left\{\left(\frac{\partial^2 Y}{\partial \rho^2} + \frac{1}{c}\,\frac{\partial Y}{\partial \rho}\right)\left(\frac{\partial P}{\partial Y} - \frac{\partial R}{\partial Y}\right) + \left(\frac{\partial Y}{\partial \rho}\right)^2\left[\left(\frac{\partial P}{\partial Y} - \frac{\partial R}{\partial Y}\right)^2 + \frac{\partial^2 P}{\partial Y^2} - \frac{\partial^2 R}{\partial Y^2}\right] + 2\,\frac{\partial X}{\partial \rho}\,\frac{\partial Y}{\partial \rho}\left(\frac{\partial^2 P}{\partial X \partial Y} - \frac{\partial^2 R}{\partial X \partial Y}\right)\right\} \tag{95}$$

must vanish. Equation (93) evaluated at the trailing edge then becomes

$$\frac{\partial P}{\partial T} = \sqrt{\gamma}\,\frac{M_\infty}{Re}\,e^{-P}\left(\frac{\partial \rho}{\partial r}\right)^2\left\{\left(\frac{\partial Y}{\partial \rho}\right)^2\left[\frac{2}{3}\,\frac{\partial U}{\partial Y}\lim_{\theta\to 0}\left(\sigma\,\frac{\partial V}{\partial Y}\right) - \frac{4}{3}\lim_{\theta\to 0}\left(\sigma\,\frac{\partial V}{\partial Y}\right)^2 - \frac{1}{3}\left(\frac{\partial U}{\partial Y}\right)^2\right] - \lim_{\theta\to 0}\left(\sigma^2 f\right)\right\}$$

From the inviscid trailing edge analysis,

$$\lim_{\theta\to 0}\left(\frac{\partial \rho}{\partial r}\right) = -\frac{3}{4}\,\frac{r}{c}$$

$$\lim_{\theta\to 0}\left(\sigma\,\frac{\partial V}{\partial Y}\right) = \alpha\,\frac{\partial^2 V}{\partial X \partial Y}$$

where

$$\alpha \equiv 3\,K_1^{\,3}\,\frac{b}{c}\,\frac{\partial X}{\partial \phi}\,\frac{\partial \rho}{\partial r}$$

Double application of L'Hospital's rule and Equation (68) gives

$$\lim_{\theta\to 0}\left(\sigma^2 f\right) = \frac{\alpha^2}{2}\,\frac{\partial^2 f}{\partial X^2}$$

Therefore, the governing equation at the trailing edge based on upstream influence is

$$\frac{\partial P}{\partial T} = \frac{3}{16}\sqrt{\gamma}\,\frac{M_\infty}{Re}\left(\frac{r}{c}\right)^2 e^{-P}\left\{\left(\frac{\partial Y}{\partial \rho}\right)^2\left[2\alpha\,\frac{\partial U}{\partial Y}\,\frac{\partial^2 V}{\partial X \partial Y} - 4\alpha^2\left(\frac{\partial^2 V}{\partial X \partial Y}\right)^2 - \left(\frac{\partial U}{\partial Y}\right)^2\right] - \frac{3}{2}\,\alpha^2\,\frac{\partial^2 f}{\partial X^2}\right\} \tag{96}$$

Along the trailing edge streamline the continuity and energy equations simplify to

$$\frac{\partial R}{\partial t} + U\,\frac{\partial R}{\partial r} + \frac{\partial U}{\partial r} + \frac{U}{r} + \frac{1}{r}\,\frac{\partial V}{\partial \theta} = 0$$

and (97)

$$\frac{\partial P}{\partial t} - \gamma\,\frac{\partial R}{\partial t} + U\left(\frac{\partial P}{\partial r} - \gamma\,\frac{\partial R}{\partial r}\right) = F$$

where

$$F = e^{-P}\,\Phi + \frac{\gamma^{3/2}\,M_\infty}{Pr\,Re}\,e^{-R}\left[\frac{1}{r}\left(\frac{\partial P}{\partial r} - \frac{\partial R}{\partial r}\right) + \left(\frac{\partial P}{\partial r} - \frac{\partial R}{\partial r}\right)^2 + \frac{\partial^2 P}{\partial r^2} - \frac{\partial^2 R}{\partial r^2} + \frac{1}{r^2}\left(\frac{\partial^2 P}{\partial \theta^2} - \frac{\partial^2 R}{\partial \theta^2}\right)\right] \tag{98}$$

and

$$\Phi = (\gamma - 1)\sqrt{\gamma}\,\frac{M_\infty}{Re}\left[2\left(\frac{\partial U}{\partial r}\right)^2 + 2\left(\frac{1}{r}\,\frac{\partial V}{\partial \theta} + \frac{U}{r}\right)^2 - \frac{2}{3}\left(\frac{\partial U}{\partial r} + \frac{U}{r} + \frac{1}{r}\,\frac{\partial V}{\partial \theta}\right)^2\right]$$

Considering the term $\frac{1}{r}\,\frac{\partial V}{\partial \theta}$ in the above equations and employing Equations (65) and the fact that the flow and coordinate geometry are symmetric

$$\frac{1}{r}\,\frac{\partial V}{\partial \theta} = \frac{1}{r}\,\frac{\partial V}{\partial X}\,\frac{\partial X}{\partial \phi}\,\frac{\partial \phi}{\partial \theta} = \frac{1}{\rho}\,\frac{\partial V}{\partial X}\,\frac{\partial X}{\partial \phi}\,\frac{\partial \rho}{\partial r}$$

From the inviscid analysis, the derivative $\frac{\partial \rho}{\partial r}$ given by Equations (80) is singular at the trailing edge. Applying L'Hospital's rule to the above expression gives the trailing edge value

$$\frac{1}{b}\,\frac{\partial V}{\partial \theta} = \frac{1}{\rho}\,\frac{\partial X}{\partial \phi}\,\lim_{r \to b}\left(\frac{\partial V}{\partial X}\,\frac{\partial \rho}{\partial r}\right) = \frac{1}{4}\,\frac{b}{c}\,\frac{\partial X}{\partial \phi}\,\frac{\partial Y}{\partial \rho}\,\frac{\partial^2 V}{\partial X \partial Y} \tag{99}$$

$$= \beta\,\frac{\partial^2 V}{\partial X \partial Y}$$

which is well-behaved and differs from the inviscid result. This implies that the derivatives $\frac{\partial U}{\partial r}$, $\frac{\partial P}{\partial r}$ and $\frac{\partial R}{\partial r}$ are also non-singular at the trailing edge. That is, near the trailing edge

$$\frac{\partial U}{\partial r} = \frac{\partial U}{\partial Y}\frac{\partial Y}{\partial \rho}\frac{\partial \rho}{\partial r} \sim O(1)$$

which indicates, according to Equations (80),

$$\frac{\partial U}{\partial Y} \sim \left(\frac{r-b}{b}\right)^{1/2}$$

This result may be used to simplify Equation (96). By similar arguments, the derivatives $\frac{\partial P}{\partial Y}$ and $\frac{\partial R}{\partial Y}$ also vanish at the trailing edge so that with reference to Equation (95)

$$\frac{\partial^2 P}{\partial Y^2} = \frac{\partial^2 R}{\partial Y^2} \tag{100}$$

Considering the remaining terms in Equations (98) and using

$$\frac{\partial^2 \rho}{\partial r^2} + \frac{1}{r^2}\frac{\partial^2 \rho}{\partial \theta^2} + \frac{1}{r}\frac{\partial \rho}{\partial r} = \frac{1}{\rho}\left(\frac{\partial \rho}{\partial r}\right)^2$$

obtained by differentiating the Cauchy-Riemann conditions, then

$$\frac{1}{r}\frac{\partial P}{\partial r} + \frac{\partial^2 P}{\partial r^2} + \frac{1}{r^2}\frac{\partial^2 P}{\partial \theta^2} = \left(\frac{\partial \rho}{\partial r}\right)^2\left[\frac{\partial P}{\partial Y}\left(\frac{\partial^2 Y}{\partial \rho^2} + \frac{1}{\rho}\frac{\partial Y}{\partial \rho} + \frac{1}{\rho^2}\frac{\partial^2 Y}{\partial \phi^2}\right)\right.$$

$$\left. + \frac{\partial^2 P}{\partial Y^2}\left(\frac{\partial Y}{\partial \rho}\right)^2 + \frac{1}{\rho^2}\frac{\partial^2 P}{\partial X^2}\left(\frac{\partial X}{\partial \phi}\right)^2\right]$$

Therefore, Equations (98) become

$$F = e^{-P}\Phi + \frac{\gamma^{3/2}M_\infty}{Pr\,Re}e^{-R}\left\{\left(\frac{\partial P}{\partial r} - \frac{\partial R}{\partial r}\right)^2 + \left(\frac{\partial \rho}{\partial r}\right)^2\left[\left(\frac{\partial P}{\partial Y} - \frac{\partial R}{\partial Y}\right)\left(\frac{\partial^2 Y}{\partial \rho^2} + \right.\right.\right.$$

$$\left.\left.\left.\frac{1}{\rho}\frac{\partial Y}{\partial \rho} + \frac{1}{\rho^2}\frac{\partial^2 Y}{\partial \phi^2}\right) + \left(\frac{\partial Y}{\partial \rho}\right)^2\left(\frac{\partial^2 P}{\partial Y^2} - \frac{\partial^2 R}{\partial Y^2}\right) + \frac{1}{\rho^2}\left(\frac{\partial X}{\partial \phi}\right)^2\left(\frac{\partial^2 P}{\partial X^2} - \frac{\partial^2 R}{\partial X^2}\right)\right]\right\} \tag{101}$$

which implies that the quantity

$$g = \left(\frac{\partial P}{\partial Y} - \frac{\partial R}{\partial Y}\right)\left(\frac{\partial^2 Y}{\partial \rho^2} + \frac{1}{\rho}\frac{\partial Y}{\partial \rho} + \frac{1}{\rho^2}\frac{\partial^2 Y}{\partial \phi^2}\right) + \left(\frac{\partial Y}{\partial \rho}\right)^2\left(\frac{\partial^2 P}{\partial Y^2} - \frac{\partial^2 R}{\partial Y^2}\right)$$

$$+ \frac{1}{\rho^2}\left(\frac{\partial X}{\partial \phi}\right)^2\left(\frac{\partial^2 P}{\partial X^2} - \frac{\partial^2 R}{\partial X^2}\right)$$

must vanish at the trailing edge. This requirement is ensured by Equation (100) and its preceding arguments.

Using Equation (99), Equation (101) evaluated at the trailing edge then becomes

$$F = \sqrt{\gamma}\,\frac{M_\infty}{Re}\,e^{-P}\left\{(1-\gamma)\left[\frac{2}{3}\left(\frac{\partial U}{\partial r} + \beta\,\frac{\partial^2 V}{\partial X \partial Y}\right)^2 - 2\left(\frac{\partial U}{\partial r}\right)^2 - 2\beta^2\left(\frac{\partial^2 V}{\partial X \partial Y}\right)^2\right]\right.$$

$$\left. + \frac{\gamma}{Pr}\lim_{r \to b}\left[\left(\frac{\partial \rho}{\partial r}\right)^2 g\right]\right\}$$

Application of L'Hospital's rule gives

$$\lim_{r \to b}\left[\left(\frac{\partial \rho}{\partial r}\right)^2 g\right] = \frac{b}{8}\frac{\partial g}{\partial r}$$

Therefore, from Equations (97) the governing equation at the trailing edge based on downstream influence is

$$\frac{\partial P}{\partial t} = \sqrt{\gamma}\,\frac{M_\infty}{Re}\,e^{-P}\left[\frac{2}{3}\left(\frac{\partial U}{\partial r} + \beta\,\frac{\partial^2 V}{\partial X \partial Y}\right)^2 - 2\left(\frac{\partial U}{\partial r}\right)^2 - 2\beta^2\left(\frac{\partial^2 V}{\partial X \partial Y}\right)^2\right.$$

$$\left. - \frac{\gamma b}{8(\gamma-1)\,Pr}\,\frac{\partial g}{\partial r}\right] \qquad (102)$$

2.3.4 Symmetry or Identity Conditions - Boundary conditions at X = 0 and X = 1 are much simpler to determine. If the body and flow field are symmetrical, an extra row of nodal points is added below the symmetry boundary both fore and aft. Symmetry or anti-symmetry conditions on the flow variables are then imposed along both of these extra rows of points. If the flow field is not symmetric, the X = 0 and X = 1 rows of nodal points are made to overlap by one grid interval at some point in the field (see Figure 2). Identity conditions are then imposed on the two overlapping rows of points.

2.4 TDC Computer Program Organization

A flow chart of the TDC program is presented in Figure 7. Subroutine INITAL handles the input and storage of the body geometry and its surface derivatives and sets the initial values (normally zero) of the dependent variables P, R, U and V. For some small time t_o, the outer wave location is computed (see Section 2.3.1) by assuming a propagation velocity equal to free stream sonic velocity. This wave location initially serves as the outer boundary of the physical plane and moves with the body for $0 < t \leq t_o$. For $t > t_o$, the physical plane is allowed to expand in a normal fashion with the outer wave location and properties determined by subroutine OUTERW as explained earlier (see Section 2.3.2.).

Subroutine DIFFER contains the finite difference equivalent of Equations 1 through 5 and updates the dependent variables, P, R, U and V at each interior point of the computational space. The allowable time step-size is computed in this subroutine by means of the Courant-Friederichs-Lewy (CFL) rule as modified for viscous flow by Moretti (Reference 4). That is,

$$\Delta T = \frac{kd_{min}}{\left| \sqrt{U^2 + V^2} + a + \frac{2\sqrt{\gamma}M_\infty}{\rho Re\, d_{min}} \right|_{max}} \tag{103}$$

where d_{min} is the minimum spatial increment in the flow field, a is the local speed of sound, and k is a safety factor less than unity.

Subroutine TRANSF, called by DIFFER, analytically computes the derivatives of the transformation functions X and Y employed in mapping the physical space onto the computational space. The choice of these transformation functions is entirely arbitrary, being constructed to suit the point distribution requirements of each given type of problem. Subroutine BNDARY computes conditions at the boundaries of the computational space shown in Figure 1. The nature of these boundary conditions will vary somewhat with each given class of problems and the assumptions concerning the type of flow, such as inviscid flow, isothermal or adiabatic wall, etc.

Subroutine OUTPUT writes out the dependent variables, outer wave geometrical characteristics, and other parameters of interest after each chosen increment in time steps. All of the information in machine storage may also be stored on tape after an arbitrary number of time steps so that the computations may be resumed at a later date.

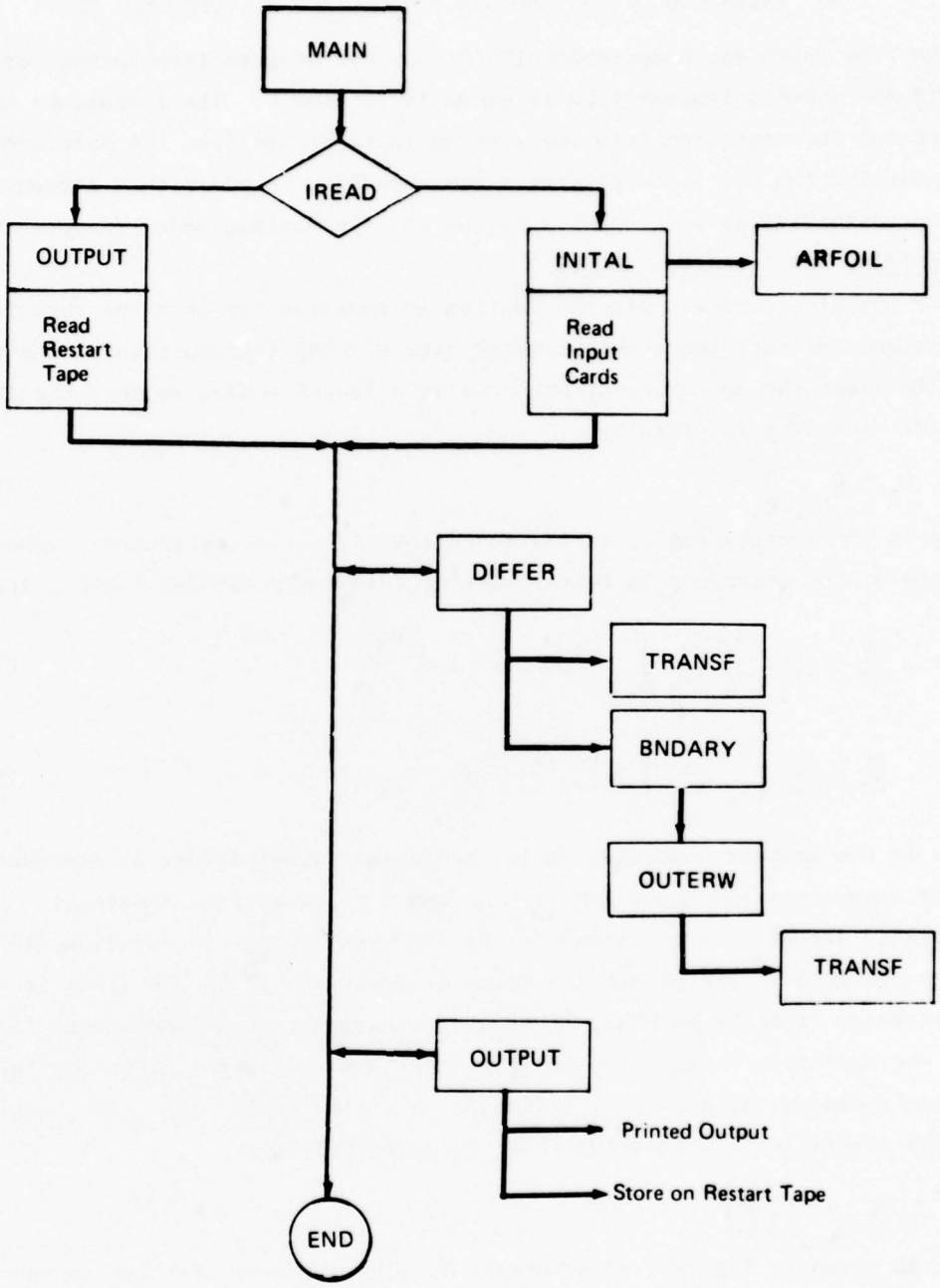


FIGURE 7. ORGANIZATION OF TIME DEPENDENT COMPUTATION (TDC) COMPUTER PROGRAM

3. EXTENSION OF TDC PROGRAM FORMULATION TO TURBULENT FLOW

The Time Dependent Computation (TDC) computer program formulation for inviscid and viscous laminar flow is given in Section 2. The turbulence model selected for incorporation into the program is fashioned from the Extended Energy-Dissipation model of Spalding (Reference 8) with additional corrections for compressibility as developed by Wilcox for the Saffman model (Reference 9).

3.1 Spalding k-ε Turbulence Model

The turbulence model selected employs an equation for both the turbulence energy k and the turbulence energy decay rate ε. The introduction of the decay rate eliminates the necessity of prescribing a length scale, so that the turbulent eddy viscosity is given by

$$\mu_t = C_\mu \rho \frac{k^2}{\varepsilon} \tag{104}$$

where ρ is the density and C_μ is the turbulent viscosity coefficient. From Reference 9, the equations in rectangular coordinates governing k and ε are

$$\rho \frac{Dk}{Dt} = \frac{\partial}{\partial x_j}\left(\frac{\mu_t}{\sigma_k}\frac{\partial k}{\partial x_j}\right) + \frac{\mu_t}{\mu}\Phi - \rho\varepsilon - \xi\rho k \frac{\partial u_j}{\partial x_j} \tag{105}$$

$$\rho \frac{D\varepsilon}{Dt} = \frac{\partial}{\partial x_j}\left(\frac{\mu_t}{\sigma_\varepsilon}\frac{\partial \varepsilon}{\partial x_j}\right) + C_{\varepsilon 1}\frac{\varepsilon}{k}\frac{\mu_t}{\mu}\Phi - C_{\varepsilon 2}\rho\frac{\varepsilon^2}{k} \tag{106}$$

where μ is the laminar viscosity, Φ is the laminar dissipation, u_i represents velocity components and σ_k, σ_ε, $C_{\varepsilon 1}$, $C_{\varepsilon 2}$ and ξ are empirical constants. Compressibility effects are accounted for by the term $\xi\rho k \frac{\partial u_j}{\partial x_j}$ in Equation (105).

The use of Φ in the production terms of Equations (105) and (106) is a generalization from the boundary layer approximation to two-dimensional flow of the corresponding terms in Spalding's model and are identical to the terms in Wilcox's compressible form of Saffman's model (Reference 10). The turbulent viscosity coefficient in Equation (104) is evaluated from

$$C_\mu = .09\ f\left(\frac{\bar{P}}{\varepsilon}\right)$$

where f is given in Figure 1 of Reference 8. The argument of this function is

$$\frac{\bar{P}}{\varepsilon} = \int \tau_t \frac{\mu_t}{\mu}\Phi\, dy \left[\int \tau_t\, dy\right]^{-1}$$

where τ_t is the turbulent shear stress and the integrations are carried out across the viscous region.

The values of the empirical constants appearing in Equations (105) and (106) are given in Reference 8 as

$$\sigma_k = 1.0 \qquad C_{\varepsilon 1} = 1.40$$

$$\sigma_\varepsilon = 1.3 \qquad C_{\varepsilon 2} = 1.94$$

The value of ξ was determined in Reference 10 as

$$\xi = 2.5$$

Hoffman (Reference 11) has examined the behavior of the Spalding k-ε turbulence model for consistency at a turbulent/non-turbulent interface and recommends the somewhat different set of constants

$$\sigma_k = 2.0 \qquad C_{\varepsilon 1} = 1.81$$

$$\sigma_\varepsilon = 3.0 \qquad C_{\varepsilon 2} = 2.00$$

Improved agreement with experimental results for fully developed channel flow was obtained with these values.

3.2 Equations of Motion

The turbulence model described above introduces additional terms and modifications into the Navier-Stokes equations as presented in Section 2 to make them valid for turbulent flow. The dependent variables P, R, U and V now denote mean instead of instantaneous values of pressure, density and velocity. Under the assumptions of a perfect gas with constant laminar viscosity and thermal conductivity, the equations of motion in polar coordinates are

$$\frac{\partial R}{\partial t} + U\frac{\partial R}{\partial r} + \frac{V}{r}\frac{\partial R}{\partial \theta} + Z_1 = 0 \tag{107}$$

$$\frac{\partial U}{\partial t} + U\frac{\partial U}{\partial r} + \frac{V}{r}\frac{\partial U}{\partial \theta} - \frac{V^2}{r} = \frac{dU_\infty}{dt}\cos\theta + \frac{dV_\infty}{dt}\sin\theta - Q\frac{\partial P}{\partial r} \tag{108}$$

$$+ \left(1 + \frac{\mu_t Re}{\sqrt{\gamma}\, M_\infty}\right)e^{-R} Z_r - \frac{2}{3}\left(\frac{\partial K}{\partial r} + K\frac{\partial R}{\partial r}\right) + \left(2\frac{\partial U}{\partial r}\frac{\partial \mu_t}{\partial r}\right.$$

$$\left. + \frac{Z_2}{r}\frac{\partial \mu_t}{\partial \theta} - \frac{2}{3}Z_1\frac{\partial \mu_t}{\partial r}\right)e^{-R}$$

$$\frac{\partial V}{\partial t} + U\frac{\partial V}{\partial r} + \frac{V}{r}\frac{\partial V}{\partial \theta} + \frac{UV}{r} = \frac{dV_\infty}{dt}\cos\theta - \frac{dU_\infty}{dt}\sin\theta - \frac{Q}{r}\frac{\partial P}{\partial \theta}$$

$$+ \left(1 + \frac{\mu_t Re}{\sqrt{\gamma}\, M_\infty}\right) e^{-R} Z_\theta - \frac{2}{3}\frac{1}{r}\left(\frac{\partial K}{\partial \theta} + K\frac{\partial R}{\partial \theta}\right) + \left(2\frac{Z_3}{r}\frac{\partial \mu_t}{\partial \theta}\right. \tag{109}$$

$$\left. + Z_2\frac{\partial \mu_t}{\partial r} - \frac{2}{3}\frac{Z_1}{r}\frac{\partial \mu_t}{\partial \theta}\right) e^{-R}$$

$$\frac{\partial P}{\partial t} + U\frac{\partial P}{\partial r} + \frac{V}{r}\frac{\partial P}{\partial \theta} = \left(1 + \frac{\mu_t Re}{\sqrt{\gamma} M_\infty}\right) e^{-P}\Phi + \gamma e^{-R}\left(1 + \frac{\mu_t Re}{\sqrt{\gamma} M_\infty}\frac{Pr_L}{Pr_T}\right) Z_e$$

$$+ \gamma\frac{e^{-R}}{Pr_T}\psi_T - \left[\gamma + \frac{2}{3}(\gamma - 1)\frac{K}{Q}\right] Z_1 \tag{110}$$

$$\frac{\partial K}{\partial t} + U\frac{\partial K}{\partial r} + \frac{V}{r}\frac{\partial K}{\partial \theta} = \left[\frac{\psi_K}{\sigma_k} + \left(\frac{\mu_t Re}{\sqrt{\gamma} M_\infty}\right)\frac{\Phi}{\gamma - 1}\right] e^{-R} - E - \xi K Z_1 \tag{111}$$

and

$$\frac{\partial E}{\partial t} + U\frac{\partial E}{\partial r} + \frac{V}{r}\frac{\partial E}{\partial \theta} = \left[\frac{\psi_E}{\sigma_\varepsilon} + C_{\varepsilon 1}\frac{\mu_t Re}{\sqrt{\gamma} M_\infty}\frac{E}{K}\frac{\Phi}{\gamma - 1}\right] e^{-R} - C_{\varepsilon 2}\frac{E^2}{K} \tag{112}$$

where

$$Z_1 = \frac{\partial U}{\partial r} + \frac{U}{r} + \frac{1}{r}\frac{\partial V}{\partial \theta}$$

$$Z_2 = \frac{1}{r}\frac{\partial U}{\partial \theta} - \frac{V}{r} + \frac{\partial V}{\partial r}$$

$$Z_3 = \frac{1}{r}\frac{\partial V}{\partial \theta} + \frac{U}{r}$$

$$Z_r = \sqrt{\gamma}\,\frac{M_\infty}{Re}\left[\frac{4}{3}\left(\frac{\partial^2 U}{\partial r^2} + \frac{1}{r}\frac{\partial U}{\partial r} - \frac{U}{r^2}\right) + \frac{1}{r^2}\frac{\partial^2 U}{\partial \theta^2} - \frac{7}{3}\frac{1}{r^2}\frac{\partial V}{\partial \theta} + \frac{1}{3}\frac{1}{r}\frac{\partial^2 V}{\partial r \partial \theta}\right]$$

$$Z_\theta = \sqrt{\gamma}\,\frac{M_\infty}{Re}\left[\frac{\partial^2 V}{\partial r^2} + \frac{1}{r}\frac{\partial V}{\partial r} - \frac{V}{r^2} + \frac{4}{3}\frac{1}{r^2}\frac{\partial^2 V}{\partial \theta^2} + \frac{7}{3}\frac{1}{r^2}\frac{\partial U}{\partial \theta} + \frac{1}{3}\frac{1}{r}\frac{\partial^2 U}{\partial r \partial \theta}\right]$$

$$Z_e = \frac{\sqrt{\gamma}\, M_\infty}{Pr_L Re} \left\{ \frac{1}{r}\left(\frac{\partial P}{\partial r} - \frac{\partial R}{\partial r}\right) + \left(\frac{\partial P}{\partial r} - \frac{\partial R}{\partial r}\right)^2 + \frac{\partial^2 P}{\partial r^2} - \frac{\partial^2 R}{\partial r^2} + \frac{1}{r^2}\left[\left(\frac{\partial P}{\partial \theta} - \frac{\partial R}{\partial \theta}\right)^2 + \frac{\partial^2 P}{\partial \theta^2} - \frac{\partial^2 R}{\partial \theta^2}\right]\right\}$$

$$\Phi = (\gamma-1)\sqrt{\gamma}\,\frac{M_\infty}{Re}\left[2\left(\frac{\partial U}{\partial r}\right)^2 + Z_2^2 + 2Z_3^2 - \frac{2}{3}Z_1^2\right]$$

$$\mu_t = C_\mu e^R \frac{K^2}{E}$$

$$\psi_K = \mu_t\left(\frac{\partial^2 K}{\partial r^2} + \frac{1}{r}\frac{\partial K}{\partial r} + \frac{1}{r^2}\frac{\partial^2 K}{\partial \theta^2}\right) + \frac{\partial K}{\partial r}\frac{\partial \mu_t}{\partial r} + \frac{1}{r^2}\frac{\partial K}{\partial \theta}\frac{\partial \mu_t}{\partial \theta}$$

$$\psi_E = \mu_t\left(\frac{\partial^2 E}{\partial r^2} + \frac{1}{r}\frac{\partial E}{\partial r} + \frac{1}{r^2}\frac{\partial^2 E}{\partial \theta^2}\right) + \frac{\partial E}{\partial r}\frac{\partial \mu_t}{\partial r} + \frac{1}{r^2}\frac{\partial E}{\partial \theta}\frac{\partial \mu_t}{\partial \theta}$$

and

$$\psi_T = \left(\frac{\partial P}{\partial r} - \frac{\partial R}{\partial r}\right)\frac{\partial \mu_t}{\partial r} - \frac{1}{r^2}\left(\frac{\partial P}{\partial \theta} - \frac{\partial R}{\partial \theta}\right)\frac{\partial \mu_t}{\partial \theta}$$

The symbols used in these equations are defined as follows:

E - Turbulence energy decay rate non-dimensionalized by $\frac{1}{L}\left(\frac{p_\infty}{\rho_\infty}\right)^{3/2}$

K - Turbulence energy non-dimensionalized by p_∞/ρ_∞

L - Reference length

P - Log (p/p_∞)

Q - Non-dimensional temperature, e^{P-R}

R - Log (ρ/ρ_∞)

U - Radial velocity non-dimensionalized by $\sqrt{p_\infty/\rho_\infty}$ (mean)

V - Angular velocity non-dimensionalized by $\sqrt{p_\infty/\rho_\infty}$ (mean)

p - Static pressure (mean)

r - Radial coordinate non-dimensionalized by L

t - Time non-dimensionalized by $L\sqrt{\rho_\infty/p_\infty}$

Φ - Laminar dissipation function

ρ - Mass density (mean)

θ - Polar angle

γ - Ratio of specific heats

ξ - Turbulence model constant

M_∞ - Free stream Mach number

Re - Free stream Reynolds number

Pr_L - Laminar Prandtl number

Pr_T - Turbulent Prandtl number

U_∞ - Longitudinal free stream velocity component

V_∞ - Vertical free stream velocity component

P_∞ - Free stream static pressure

ρ_∞ - Free stream mass density

μ_t - Turbulent eddy viscosity non-dimensionalized by $L\sqrt{P_\infty \rho_\infty}$

C_μ - Turbulent viscosity coefficient

σ_k - Turbulence model constant

σ_ε - Turbulence model constant

$C_{\varepsilon 1}$ - Turbulence model constant

$C_{\varepsilon 2}$ - Turbulence model constant

The finite difference equivalent of the above equations of motion are contained in subroutine DIFFER (see Section 2.4) where the dependent variables are updated at interior points of the computational space. If conditions are such that at some point in the flow field transition to turbulent flow occurs, the above equations are employed to determine flow properties at all downstream and all transverse locations likely to be affected.

3.3 Boundary Conditions

Turbulent flow boundary point calculations, to a certain extent, are the same as for laminar flow provided the turbulent flow is confined to the body boundary layer and wake region. Initially, the dependent variables P, R, U, V, E and K are each zero with the outer wave front boundary location determined as described in Section 2.3.1. Properties immediately behind the moving outer perturbation wave can again be determined by assuming inviscid conditions as in Section 2.3.2.

It is advantageous to avoid calculating turbulence properties directly very near a solid boundary using Equations (111) and (112) because of the extremely small grid spacings required to obtain adequate resolution of the rapid variation of k and ε across the laminar sublayer. This difficulty can be avoided by imposing fictitious values of k, ε and slip velocity at the surface such that reasonably accurate spatial derivatives normal to the surface can still be

obtained by conventional finite differencing with not too fine a mesh. The necessary approximations to the turbulent flow properties near the surface can be obtained using "law-of-the-wall" relationships. These relations are

$$u^+ = \frac{1}{A} \log (By^+) \tag{113}$$

$$k^+ = C_\mu^{-1/2} \tag{114}$$

and

$$\varepsilon^+ = \frac{1}{Ay^+} \tag{115}$$

where by definition

$$u^+ \equiv \frac{u}{u_\tau} \tag{116}$$

$$k^+ \equiv \sqrt{\frac{\rho_w}{\rho}} \frac{k}{u_\tau^2} \tag{117}$$

$$\varepsilon^+ \equiv \frac{\rho_w \mu_w}{\tau_w^2} \varepsilon \tag{118}$$

$$y^+ \equiv \frac{u_\tau \rho_w}{\mu_w} y \tag{119}$$

$$u_\tau \equiv \sqrt{\frac{\tau_w}{\rho_w}} \tag{120}$$

$A = .4187$

$B = 9.793$

and y is the distance normal to the surface, u is velocity parallel to the surface and ρ_w, μ_w and τ_w denote surface values of density, laminar viscosity and shear stress.

Because of the logarithmic variation of u and the inverse power variation of ε, the above equations are not valid at the surface. However, several simplifying assumptions can be made to achieve the desired approximate result. First, the shear stress τ is assumed to be constant near the surface. Next, values of u^+, k^+ and ε^+ are determined at a point p (see Figure 8) near the

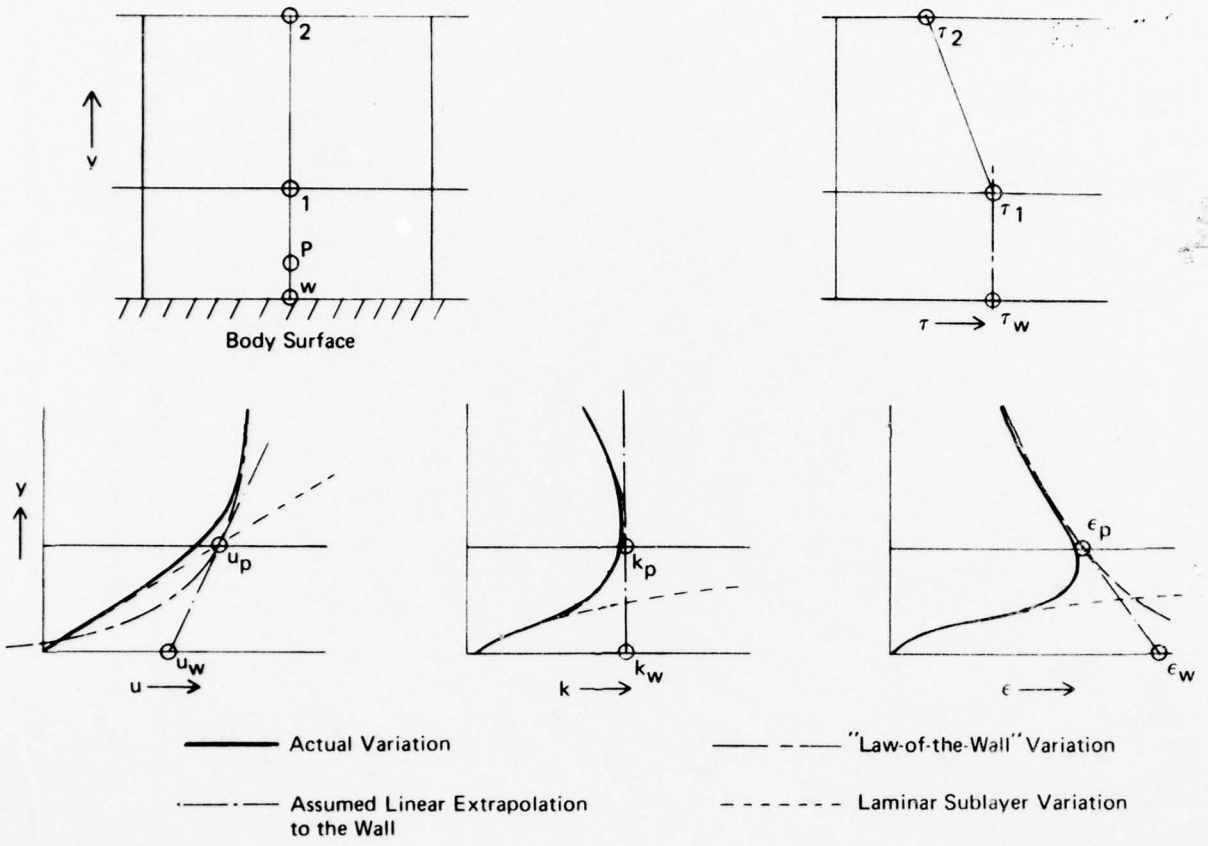


FIGURE 8. "LAW-OF-THE-WALL" BOUNDARY CONDITIONS

inner edge of the "law-of-the-wall" region and surface values are extrapolated linearly from this point. The point p is chosen to coincide with the location at which the velocity variation of Equation (113) matches the laminar sublayer law $u^+ \sim y^+$, namely $y_p^+ = 11.63$. The first grid point outward from the surface should lie near the outer limit of the "law-of-the-wall" region where y^+ is approximately 100 to 200 and the wall shear stress will be assumed to be the same as at this point.

The necessary slopes for extrapolating to the fictitious surface values can be obtained by differentiating Equations (113) through (115). The surface values of u^+, k^+ and ε^+ are then given by

$$u_w^+ = \frac{1}{A}\left[\log\left(By_p^+\right) - 1\right] = 8.921$$

$$k_w^+ = C_\mu^{-1/2} = 3.333\, f^{-1/2} \tag{121}$$

and

$$\varepsilon_w^+ = \frac{2}{Ay_p^+} = .4107$$

From Equations (116) through (120), the surface values of k, ε and velocity in non-dimensional form are

$$K_w = 3.333\, f^{-1/2}\, \tau_w\, e^{-R_w}$$

$$E_w = .4107\, e^{-R_w}\, \frac{Re}{\sqrt{\gamma} M_\infty}\, \tau_w^2$$

$$V_w = -8.921\,(1 + \sigma^2)^{-1/2}\, e^{-\frac{1}{2}R_w}\, \tau_w^{1/2} \tag{122}$$

$$U_w = \sigma V_w$$

and

$$\sigma = \frac{1}{b}\frac{db}{d\theta}$$

where R_w denotes the surface value of R and b is the radial coordinate describing the body surface. Note that the slip velocity is non-zero for the turbulent boundary layer only.

Surface values of pressure for turbulent flow can be approximated using the characteristics relationship developed in Section 2.3.3.2. The assumption underlying such a prediction is that the turbulence quantities in Equations (108), (109) and (110) are negligible at the surface. The analysis of Section 2.3.3.2 assumes a constant wall temperature equal to free stream temperature which implies equality of P and R along the surface. At a sharp trailing edge, the above approximation using the "law-of-the-wall" relations will not be valid. However, values of E_w, K_w, U_w and V_w can be approximated by simple extrapolation.

4. INVISCID SAMPLE CASES

Several exact inviscid two-dimensional flow field methods are available for the purpose of validating the results of the TDC Program:

- Douglas Neuman Program (Reference 12) for incompressible potential flow
- Garabedian-Korn Analysis Program (Reference 13) for subcritical or supercritical airfoil flow
- Catherall-Sells Program (Reference 14) for subcritical flow.

In this section, calculations by the Catherall-Sells Program are used as the basis for comparison. This method uses a relaxation technique to solve the subsonic, inviscid flow equations in a computational space consisting of a polar grid inside a circle. Comparisons of TDC Program calculations with the steady-state calculations obtained from the Catherall-Sells Program were used to determine the number of grid points needed for accurate results, the time of convergence to steady state values at the body surface, and the rate of growth of the steady state region around the body.

4.1 Non-Lifting Flow Past a Circular Cylinder

Sample results for inviscid flow past a circular cylinder of unit radius are presented in Figures 10 and 15 for several subcritical free stream Mach numbers. The grid system for these cases consisted of rays of points from the center of the cylinder equally spaced over the upper surface in the angular direction as shown in Figure 9. The radial distribution of points along each ray is such that points are concentrated near the body and near the outer perturbation wave where gradients tend to be largest. The polar angle θ is measured from the downstream axis while r is measured outward from the center of the cylinder. The pressure coefficient is defined as

$$C_p = \frac{\log P - 1}{1/2\ \gamma\ M_\infty^2}$$

The transformation functions X and Y for this case were chosen similar to those of Reference 1, namely

$$X = \frac{\theta}{\pi}$$

$$Y = \frac{1}{2} + \frac{1}{2\alpha} \log \left[\frac{1 + (2Z - 1) \tanh(\alpha/2)}{1 - (2Z - 1) \tanh(\alpha/2)} \right]$$

where $\alpha = \alpha(t)$ and

$$Z = \frac{r - 1}{s - 1}$$

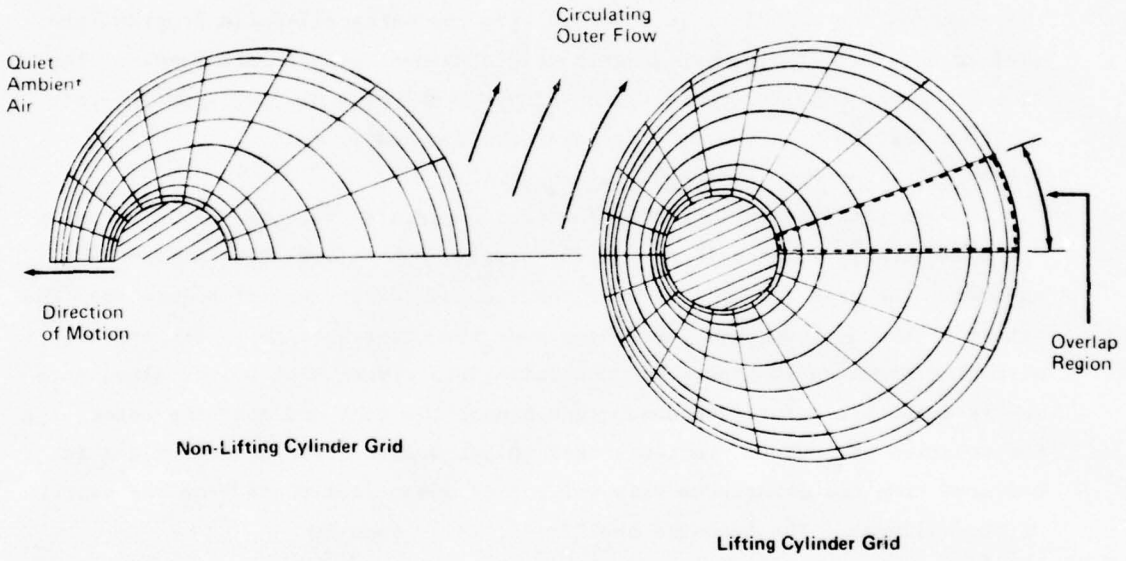


FIGURE 9. GRID GEOMETRY FOR CYLINDER FLOW

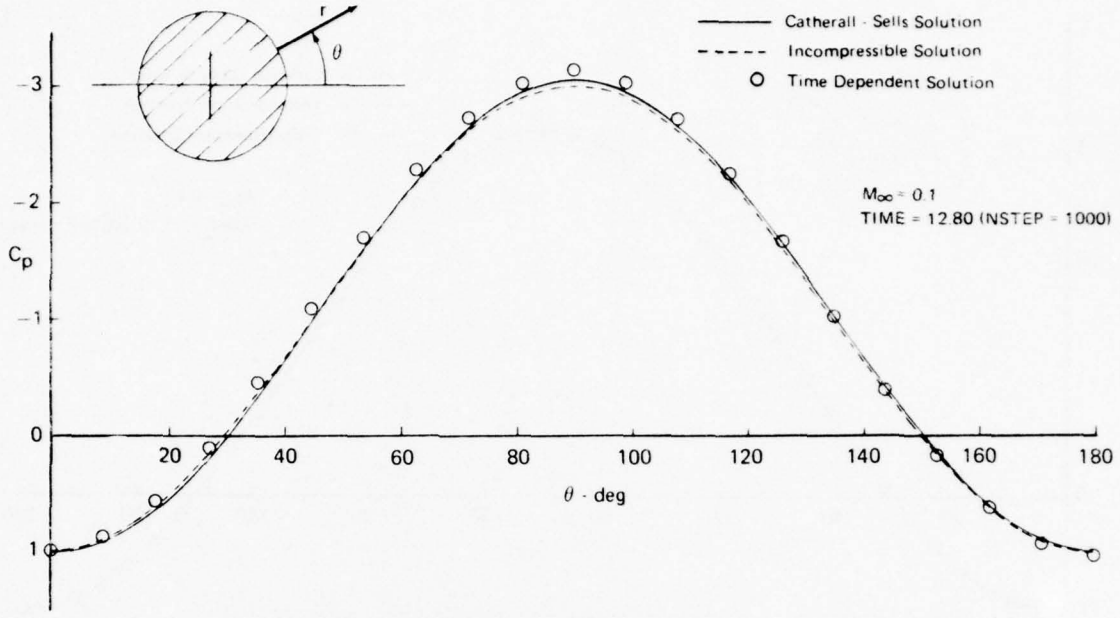


FIGURE 10. CYLINDER: SURFACE PRESSURE DISTRIBUTION

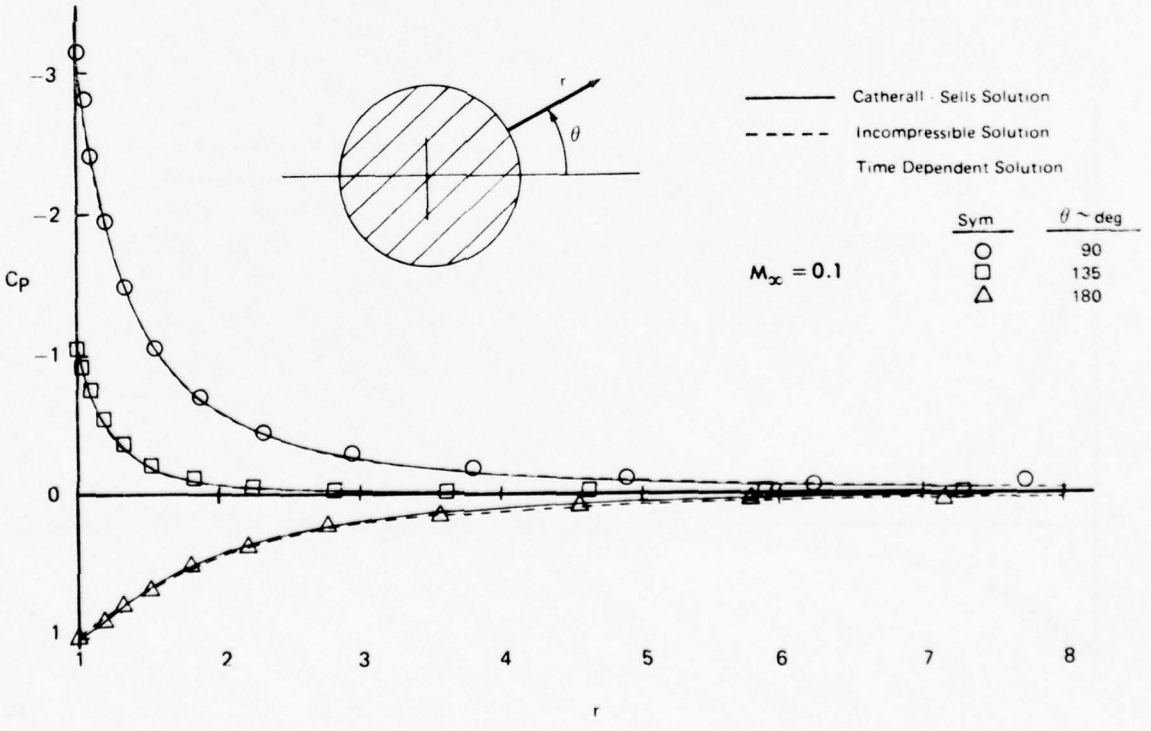


FIGURE 11. CYLINDER: NEAR-FIELD PRESSURE DISTRIBUTION

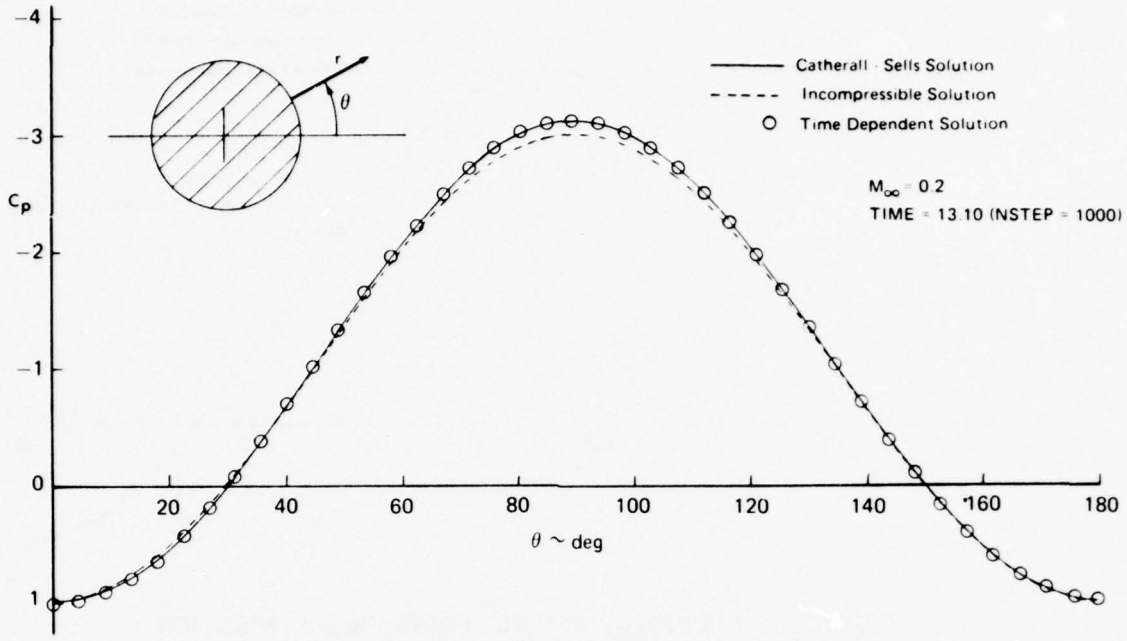


FIGURE 12. CYLINDER: SURFACE PRESSURE DISTRIBUTION

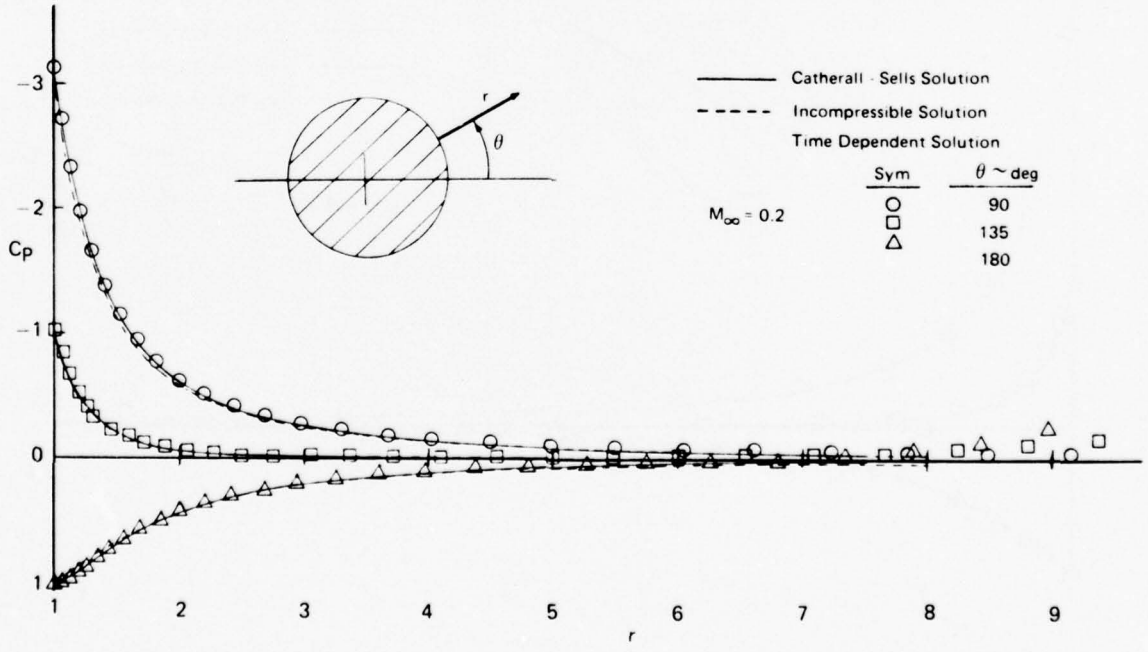


FIGURE 13. CYLINDER: NEAR-FIELD PRESSURE DISTRIBUTION

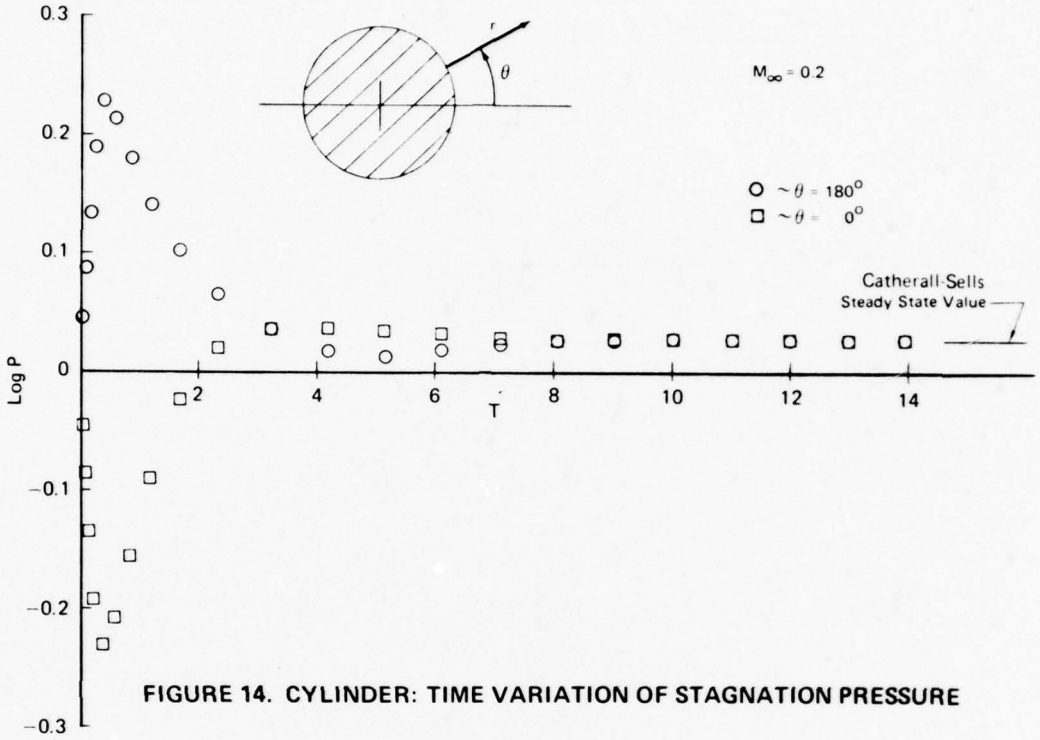


FIGURE 14. CYLINDER: TIME VARIATION OF STAGNATION PRESSURE

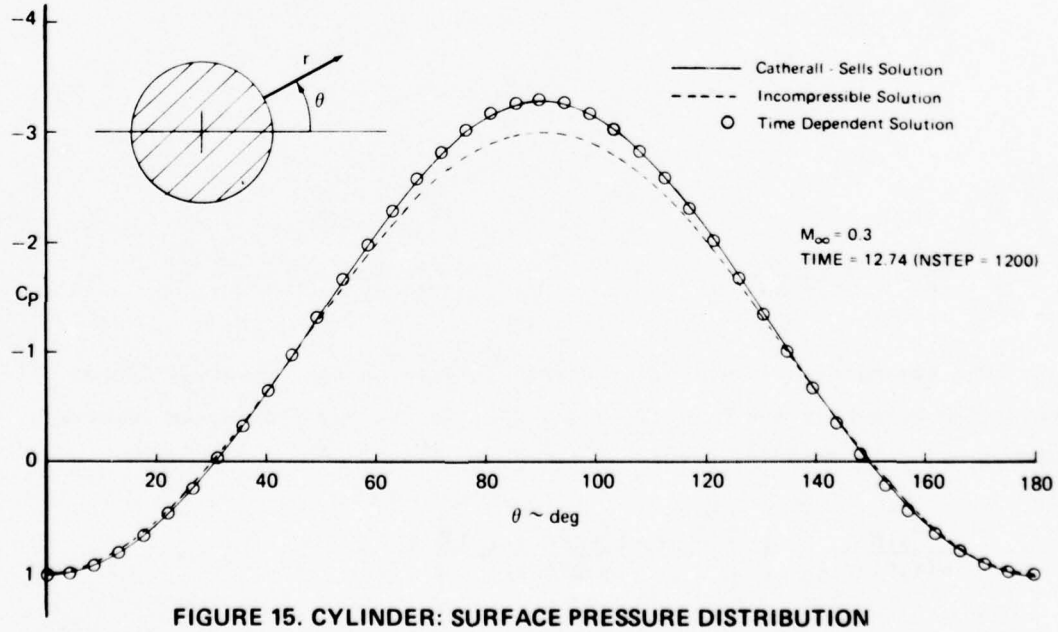


FIGURE 15. CYLINDER: SURFACE PRESSURE DISTRIBUTION

The derivatives of these functions required in the course of the numerical computation are

$$\frac{\partial X}{\partial t} = \frac{\partial X}{\partial r} = 0$$

$$\frac{\partial X}{\partial \theta} = \frac{1}{\pi}$$

$$\frac{\partial^2 X}{\partial t^2} = \frac{\partial^2 X}{\partial t \partial r} = \frac{\partial^2 X}{\partial t \partial \theta} = \frac{\partial^2 X}{\partial r^2} = \frac{\partial^2 X}{\partial r \partial \theta} = \frac{\partial^2 X}{\partial \theta^2} = 0$$

$$\frac{\partial Y}{\partial t} = \frac{\partial Y}{\partial Z}\frac{\partial Z}{\partial t} + \frac{\partial Y}{\partial \alpha}\frac{d\alpha}{dt}$$

$$\frac{\partial Y}{\partial r} = \frac{\partial Y}{\partial Z}\frac{\partial Z}{\partial r}$$

and

$$\frac{\partial Y}{\partial \theta} = \frac{\partial Y}{\partial Z}\frac{\partial Z}{\partial \theta}$$

where

$$\frac{\partial Y}{\partial Z} = \frac{2}{\alpha}\tanh(\alpha/2)\left[1 - (2Z - 1)^2 \tanh^2(\alpha/2)\right]^{-1}$$

$$\frac{\partial Z}{\partial r} = \frac{1}{s - 1}$$

$$\frac{\partial Z}{\partial t} = -Z\frac{\partial Z}{\partial r}\frac{\partial s}{\partial t}$$

and

$$\frac{\partial Z}{\partial \theta} = -Z\frac{\partial Z}{\partial r}\frac{\partial s}{\partial \theta}$$

The parameter α is initially chosen to give an approximately linear variation between r and Y (e.g., $\alpha = 1.0$). As the physical space expands with time, α is adjusted according to

$$\frac{d_{min}}{s(\pi,t) - 1} = \frac{1}{2}\left\{1 + \frac{\tanh\left[\alpha(\Delta Y - 1/2)\right]}{\tanh(\alpha/2)}\right\}$$

to maintain a constant spacing d_{min} between the first interior point and the body along the forward stagnation streamline. The time derivative of α required in the above expressions is obtained from this equation as

$$\frac{d\alpha}{dt} = -2\frac{d_{min}\tanh(\alpha/2)}{\left[s(\pi,t)-1\right]^2}\frac{\partial s}{\partial t}(\pi,t)\left\{(\Delta Y-\frac{1}{2})\operatorname{sech}^2\left[\alpha(\Delta Y-1/2)\right]\right.$$

$$\left.-\frac{\tanh\left[\alpha(\Delta Y-1/2)\right]}{\sinh\alpha}\right\}^{-1}$$

Figure 10 compares the calculated surface pressure distribution for free stream Mach number of 0.1 with the exact incompressible solution and the Catherall-Sells solution. Reasonable accuracy is obtained with only 21 upper surface points and 31 points in the radial direction. The non-dimensional time $T = 12.8$ corresponds to 1000 time steps. Figure 11 shows the calculated pressure distribution near the cylinder compared with the Catherall-Sells solution and indicates a steady flow region extending outward approximately seven radii. The effect of the coordinate stretching function Y is clearly evident in that the point spacing near the body where gradients are large is much smaller than farther out in the flow field.

Figure 12 compares the calculated surface pressure distribution for free stream Mach number of 0.2 with the Catherall-Sells solution. The incompressible solution is also shown for reference. Excellent agreement (less than 0.5% error)is achieved in this case with 41 points in the angular direction and 51 points in the radial direction. Figure 13 shows the near-field pressure distribution compared with the Catherall-Sells solution and indicates a steady flow region extending outward approximately eight radii. Figure 14 presents a time history of the upstream and downstream stagnation pressures and indicates at which time steady conditions first begin to appear near the body. Figure 15 compares the calculated surface pressure distribution for free stream Mach number of 0.3 with the Catherall-Sells solution, again with good agreement. Critical free stream Mach number for a circular cylinder is approximately 0.4.

4.2 Lifting Flow Past a Circular Cylinder

Sample results for inviscid flow past a circular cylinder with arbitrary circulation are presented in Figures 16 through 21 for subcritical free stream Mach numbers of 0.1 and 0.2. The grid arrangement and transformation functions X and Y were similar to those for the above non-lifting case except for extending around the lower half of the cylinder also, as shown in Figure 9.

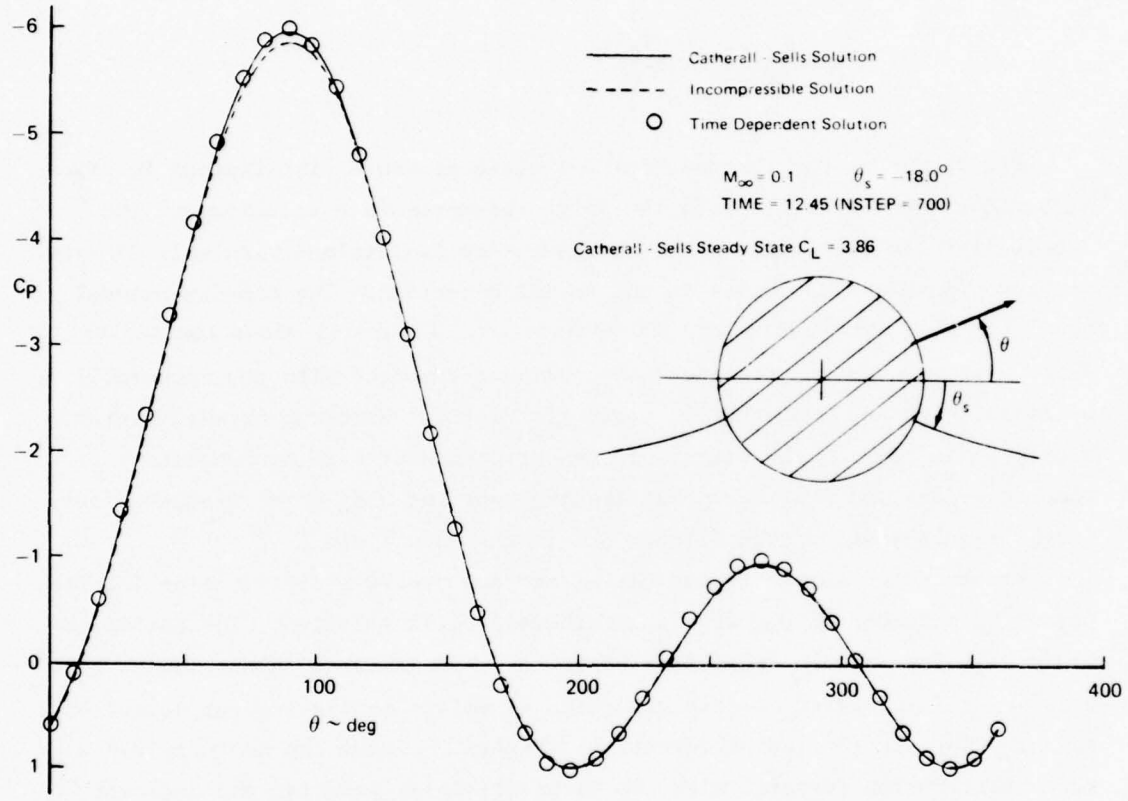


FIGURE 16. CIRCULAR CYLINDER WITH CIRCULATION (INVISCID) SURFACE PRESSURE DISTRIBUTION

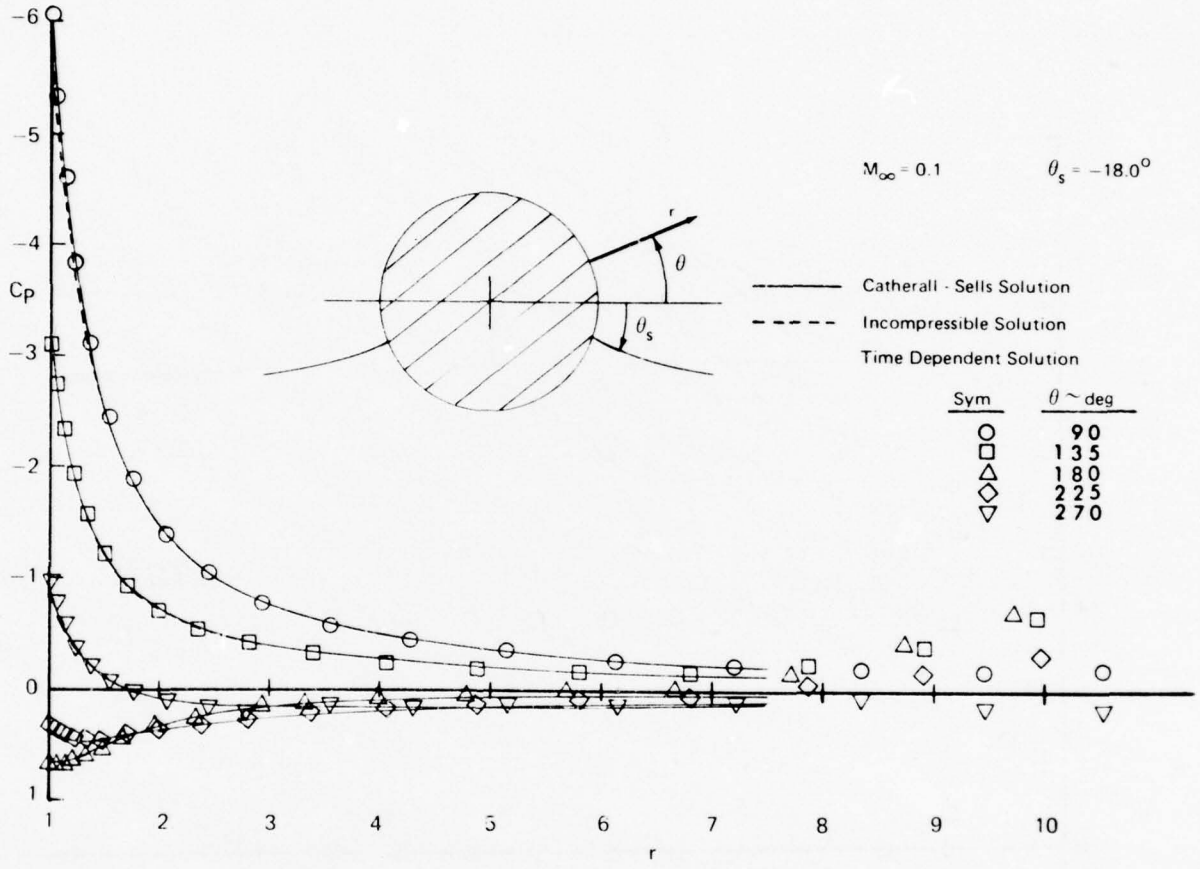


FIGURE 17. CIRCULAR CYLINDER WITH CIRCULATION (INVISCID) NEAR-FIELD PRESSURE DISTRIBUTION

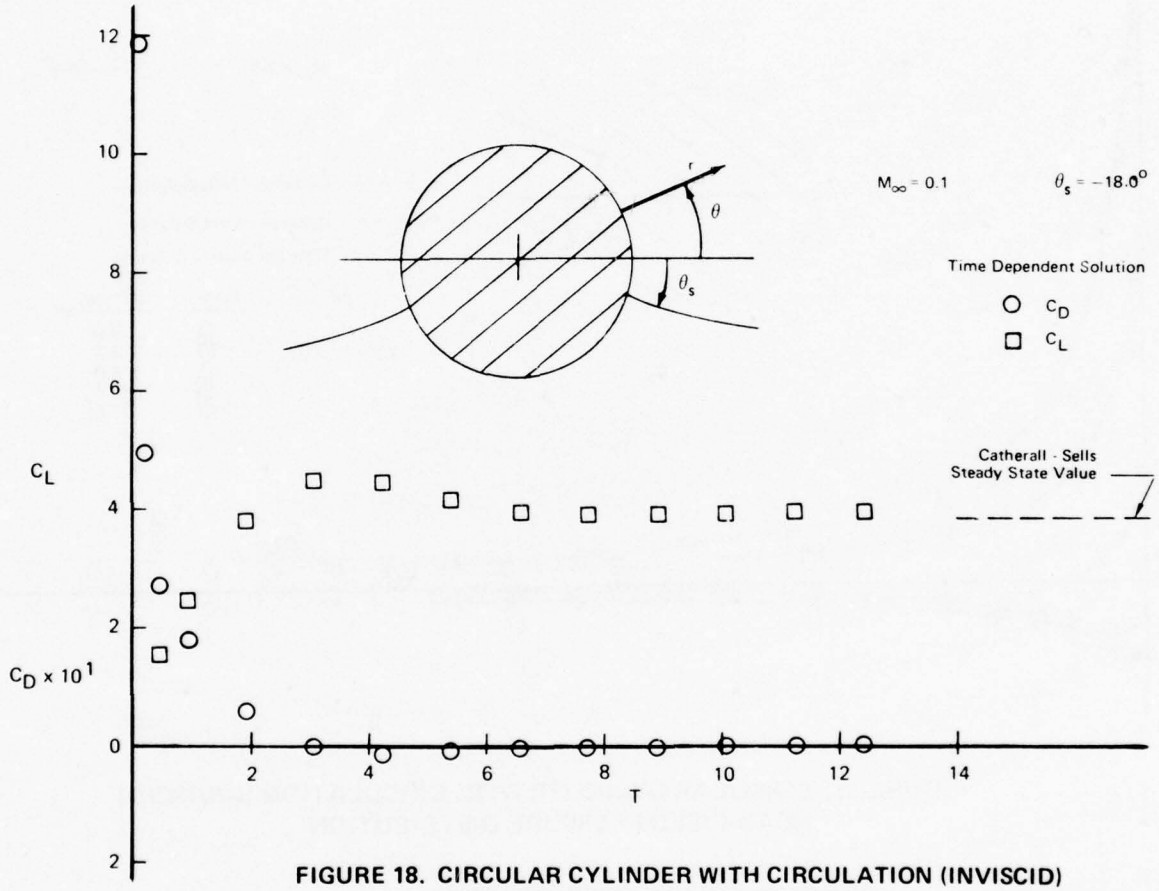


FIGURE 18. CIRCULAR CYLINDER WITH CIRCULATION (INVISCID) TIME VARIATION OF LIFT AND DRAG

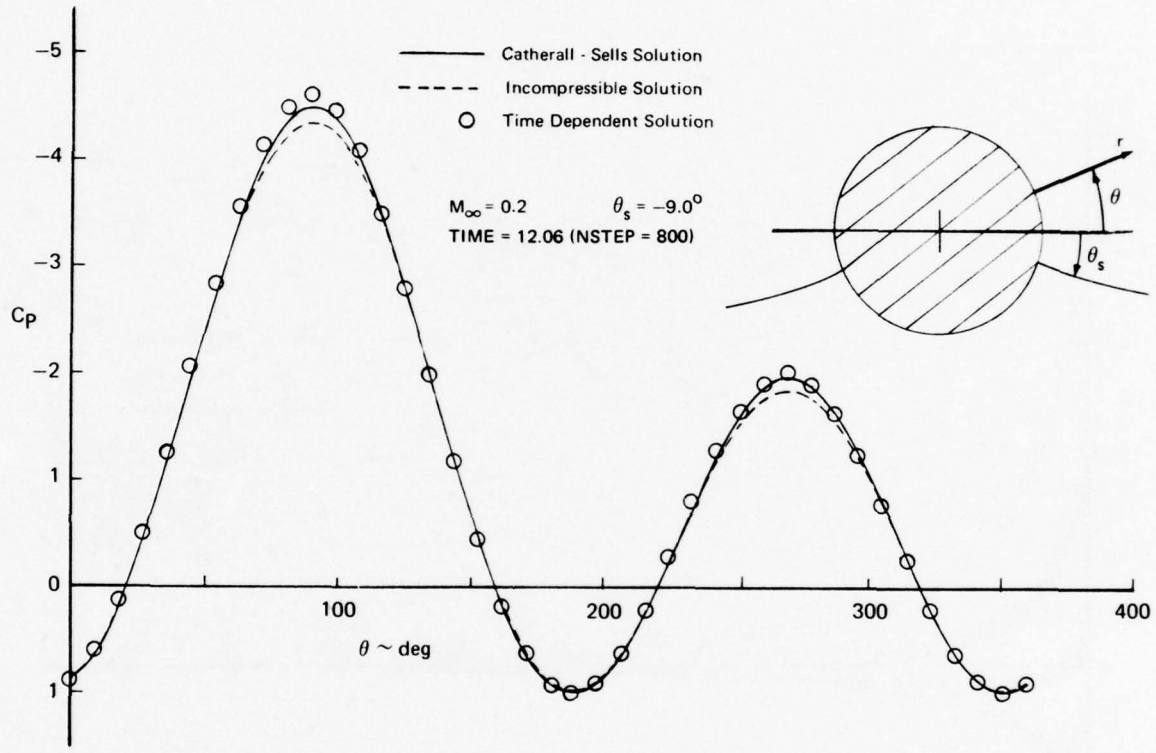


FIGURE 19. CIRCULAR CYLINDER WITH CIRCULATION (INVISCID) SURFACE PRESSURE DISTRIBUTION

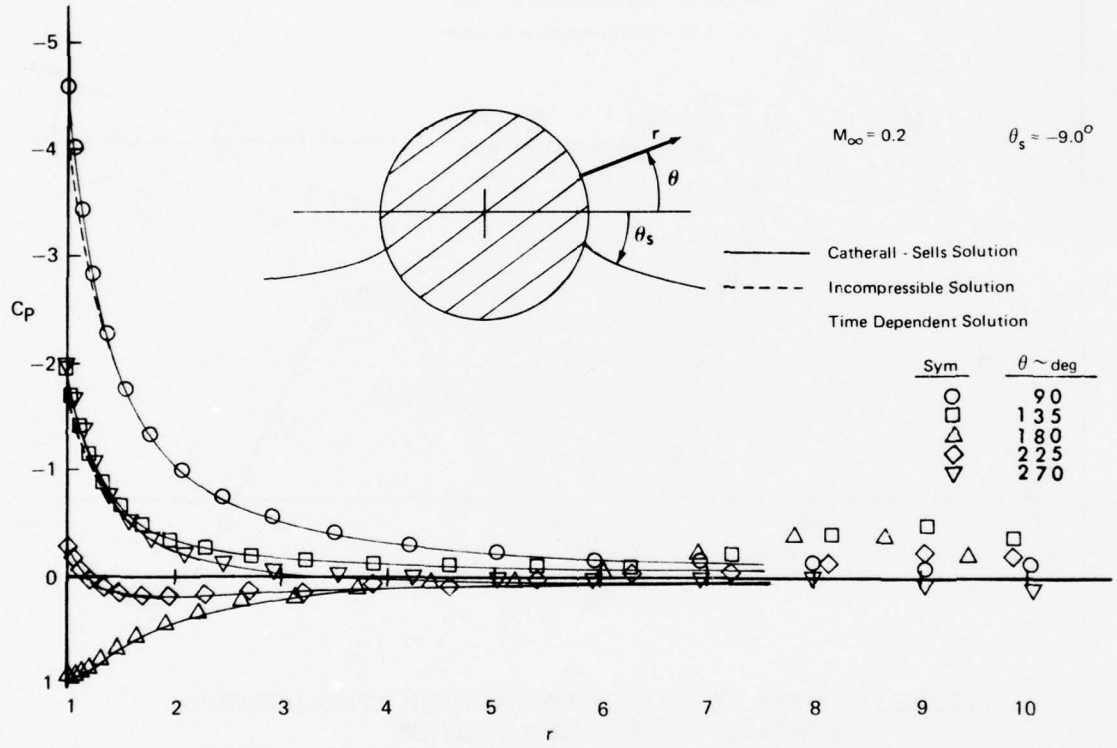


FIGURE 20. CIRCULAR CYLINDER WITH CIRCULATION (INVISCID) NEAR-FIELD PRESSURE DISTRIBUTION

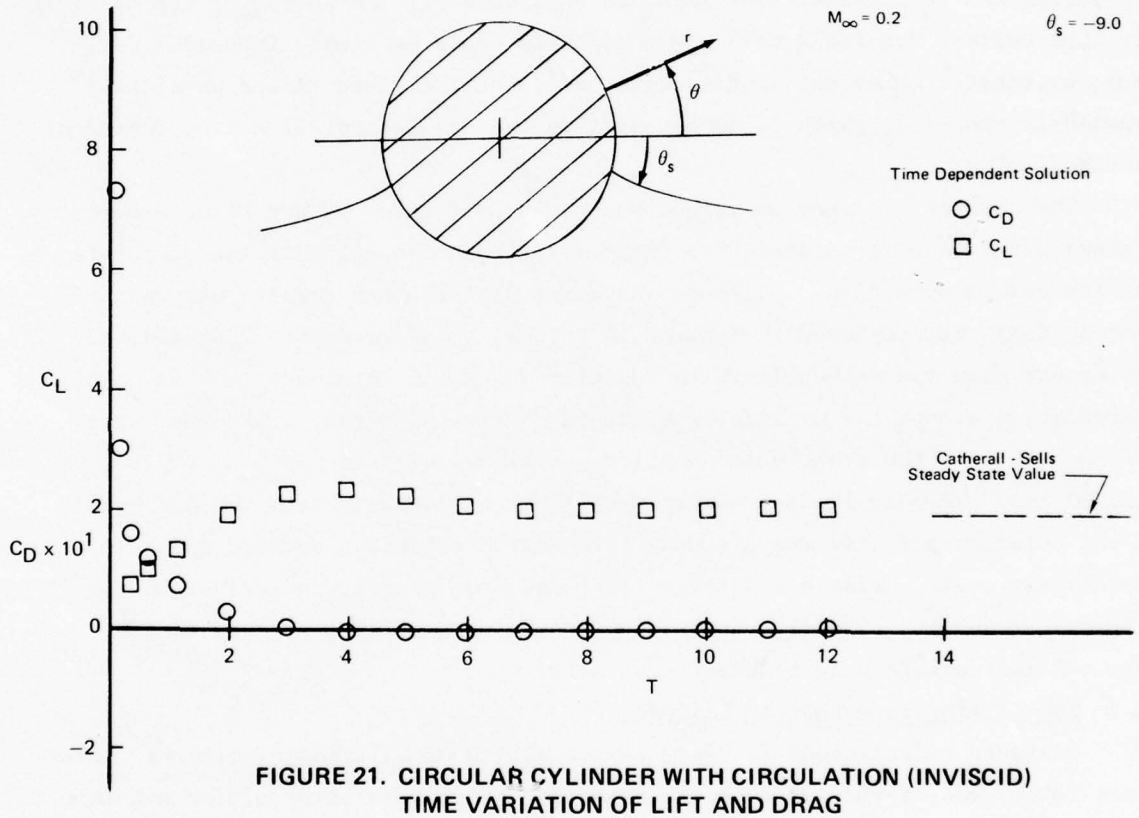


FIGURE 21. CIRCULAR CYLINDER WITH CIRCULATION (INVISCID) TIME VARIATION OF LIFT AND DRAG

Due to the absence of any flow symmetry, the grid system has an overlap region near $\theta = 0$ for simple specification of boundary conditions at $X = 0$ and $X = 1$ of the computational space.

The TDC solutions were obtained by assuming that initially the cylinder was surrounded by a compressible vortex flow of arbitrary circulation concentric with the cylinder. The cylinder was subsequently accelerated smoothly from rest to free stream velocity with the vortex center coincident with the center of the cylinder. Outside of the initial perturbation wave, the combination of vortex and rectilinear flow remained unaffected by the motion of the cylinder so that correct far-field boundary conditions could be simply imposed. Careful, systematic numerical studies have indicated that this is the physically realistic manner in which to impose lift in the development of a time dependent inviscid flow.

The surface pressure distributions shown in Figures 16 and 19 were obtained with 40 points distributed uniformly around the cylinder and 31 points in the radial direction. Although the point distribution density was approximately half that employed in Figures 12 and 13, good agreement (approximately 1% error) with the Catherall-Sells solution was still obtained. The value of circulation around the cylinder was chosen to fix the steady state rear stagnation point at the preselected angular position designated by θ_s. Figures 17 and 20 show the near-field pressure distributions compared with the Catherall-Sells solution and indicate a steady flow region extending outward approximately six radii. Time histories of lift and drag coefficient are shown in Figures 18 and 21. The drag coefficient behavior clearly demonstrates the virtual mass effect before decaying to zero.

4.3 Non-Lifting Flow Past an Ellipse

Inviscid calculations for flow past a series of ellipses of various thickness ratios and at various free stream Mach numbers have been carried out in a manner similar to that for the cylinder cases described above. Sample results are presented in Figures 22 and 23.

The family of ellipses was defined by

$$b = \left[1 + \varepsilon \sin^2\theta\right]^{-1/2}$$

where the parameter ε is related to the body thickness ratio h by

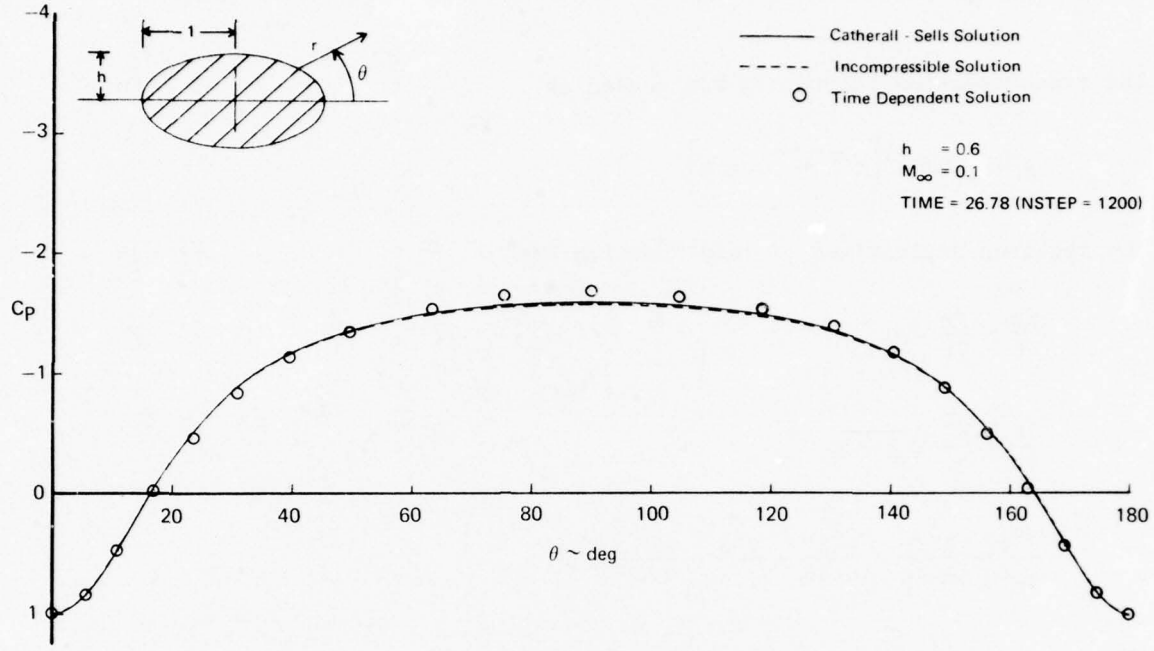


FIGURE 22. ELLIPSE: SURFACE PRESSURE DISTRIBUTION

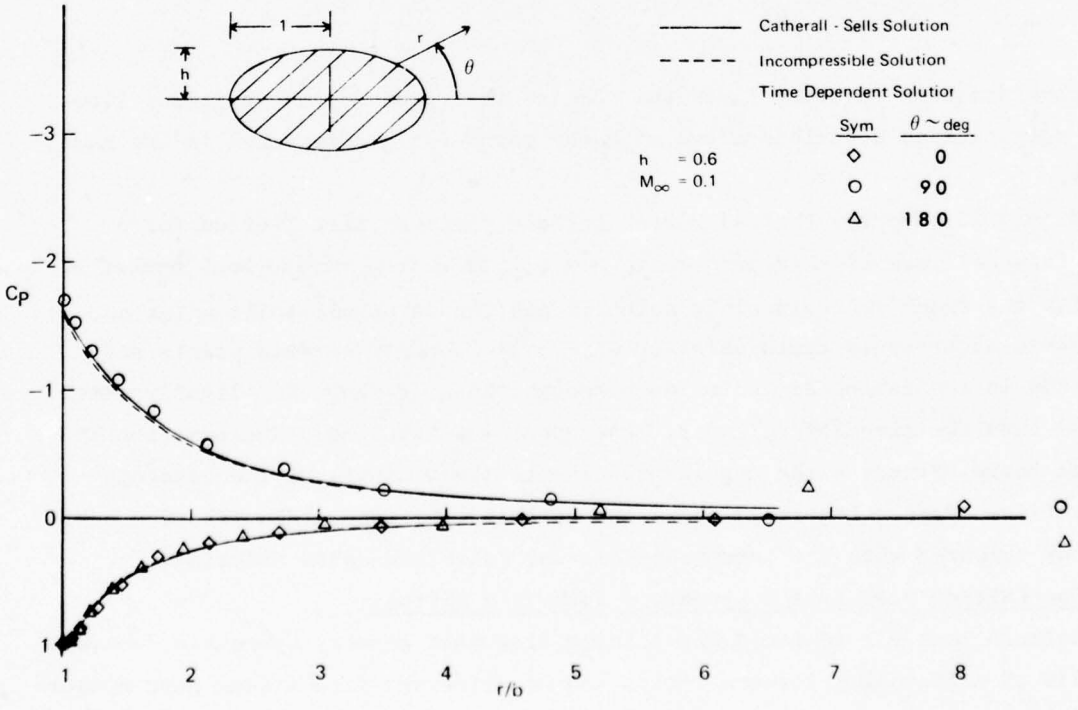


FIGURE 23. ELLIPSE: NEAR-FIELD PRESSURE DISTRIBUTION

$$\varepsilon = \frac{1}{h^2} - 1$$

The transformation function X was chosen as

$$X = \frac{1}{\pi} \tan^{-1}\left[\sqrt{1 + \varepsilon}\ \tan\theta\right]$$

The required derivatives of this function are

$$\frac{\partial X}{\partial t} = \frac{\partial X}{\partial r} = 0$$

$$\frac{\partial X}{\partial \theta} = \frac{b^2}{\pi} \sqrt{1 + \varepsilon}$$

$$\frac{\partial^2 X}{\partial t^2} = \frac{\partial^2 X}{\partial t \partial r} = \frac{\partial^2 X}{\partial t \partial \theta} = \frac{\partial^2 X}{\partial r^2} = \frac{\partial^2 X}{\partial r \partial \theta} = 0$$

and

$$\frac{\partial^2 X}{\partial \theta^2} = \frac{2b}{\pi} \sqrt{1 + \varepsilon}\ \ \frac{db}{d\theta}$$

The transformation function Y was the same as that used for the cylinder flow field computations described above with the parameter α determined in the same manner.

Figure 22 compares the calculated surface pressure distribution for a non-lifting ellipse of thickness ratio h = 0.6 at a free stream Mach number of 0.1 with the exact incompressible solution and the Catherall-Sells solution. Reasonable accuracy is again obtained with only 21 upper surface points and 30 points in the radial direction even though the body shape is slightly more complex than the circular cylinder. The angular stretching transformation X defined above decreases the angular spacing in the vicinity of the leading and trailing edges. Figure 23 shows the calculated pressure distribution near the body compared with the incompressible and Catherall-Sells solutions.

4.4 Non-Lifting Flow Past a Symmetric Joukowsky Airfoil

Calculations for inviscid non-lifting flow past several symmetric Joukowsky airfoils of different thickness ratios and at different free stream Mach numbers have been carried out. Sample results are presented in Figures 24 through 32.

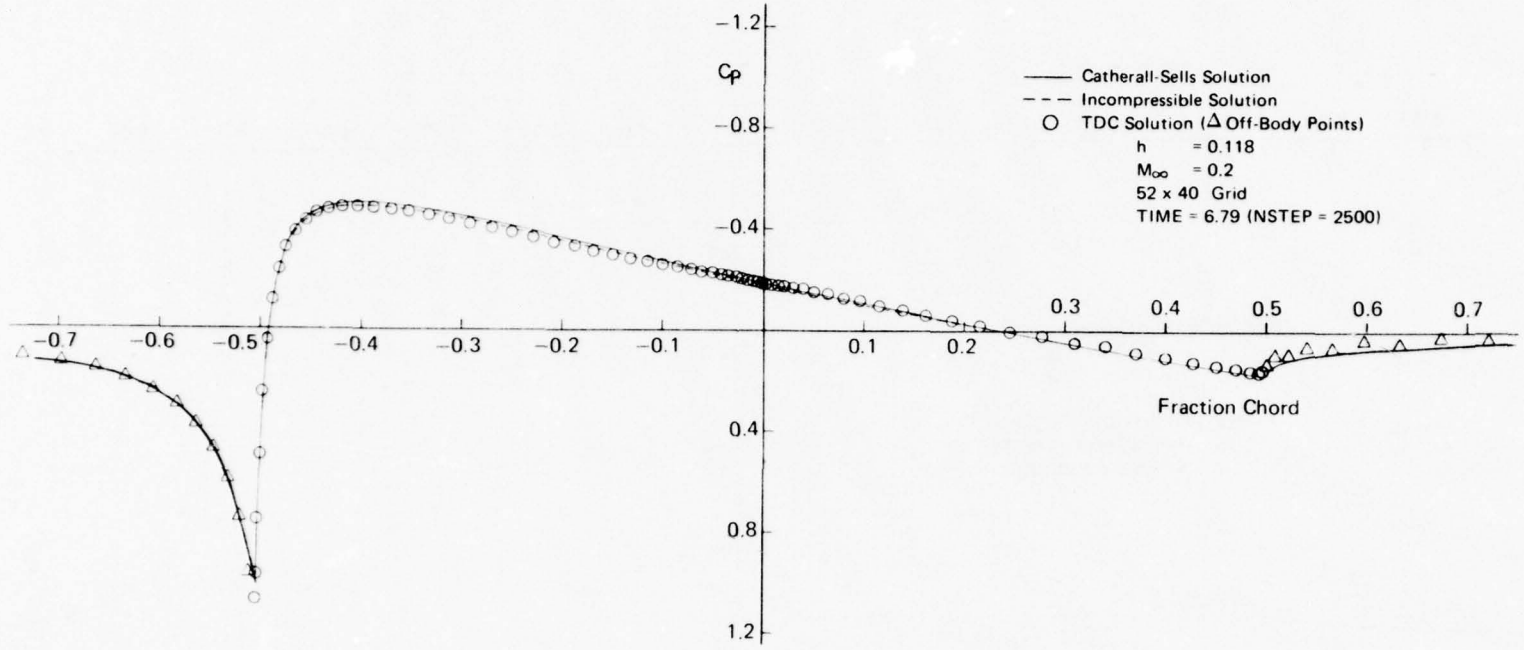


FIGURE 24. JOUKOWSKY AIRFOIL: SURFACE PRESSURE DISTRIBUTION (INVISCID)

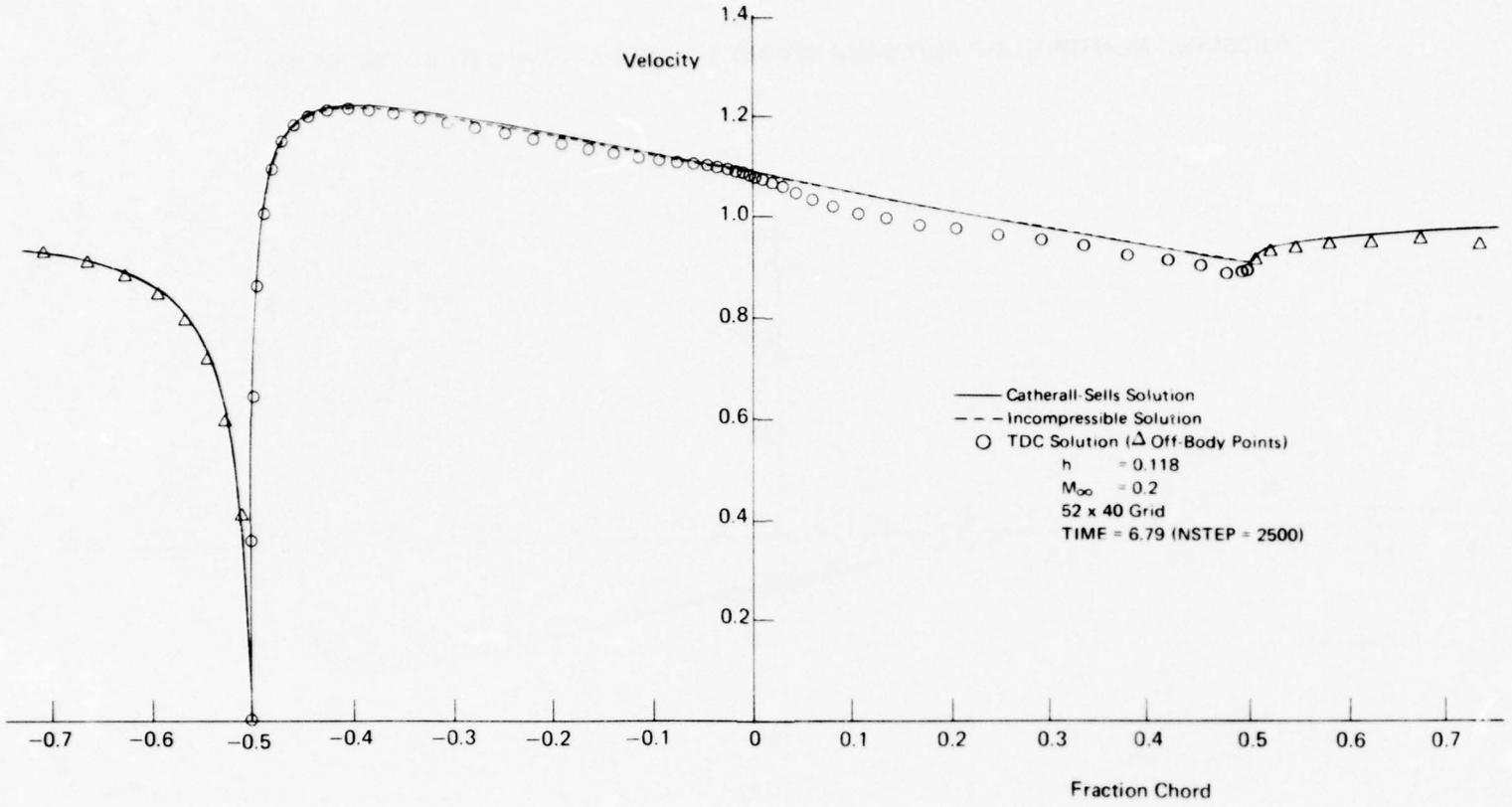


FIGURE 25. JOUKOWSKY AIRFOIL: SURFACE VELOCITY DISTRIBUTION (INVISCID)

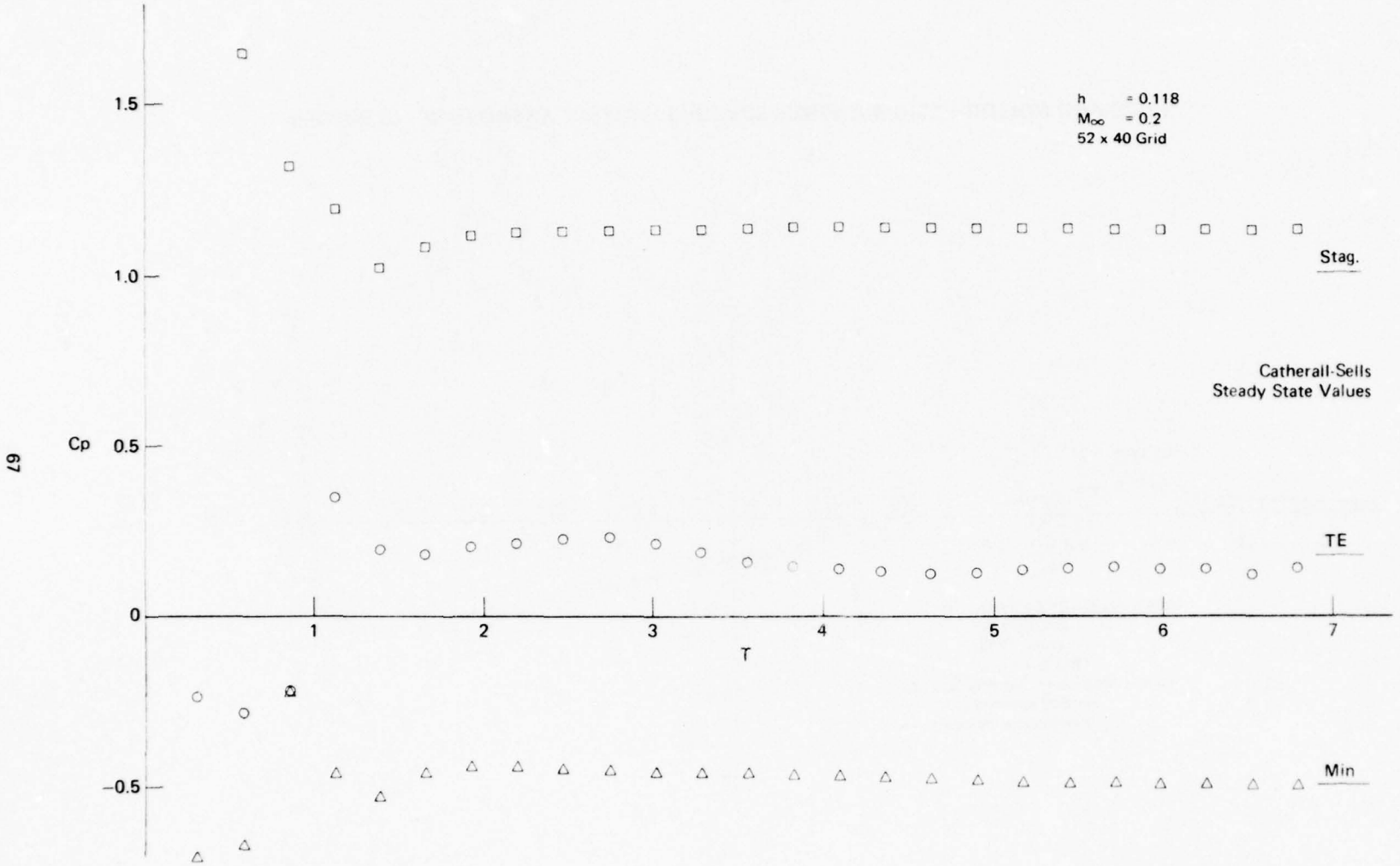


FIGURE 26. JOUKOWSKY AIRFOIL: TIME VARIATION OF STAGNATION, MINIMUM AND TRAILING EDGE PRESSURES (INVISCID)

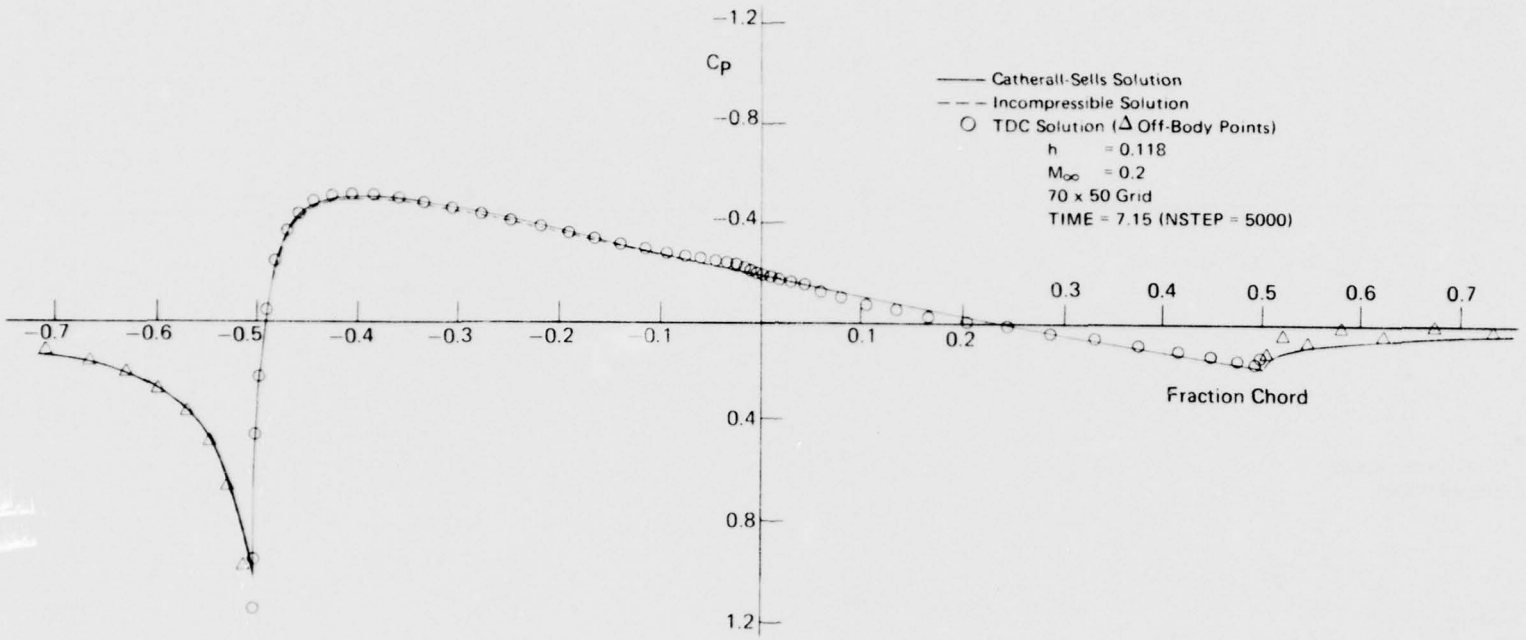


FIGURE 27. JOUKOWSKY AIRFOIL: SURFACE PRESSURE DISTRIBUTION (INVISCID)

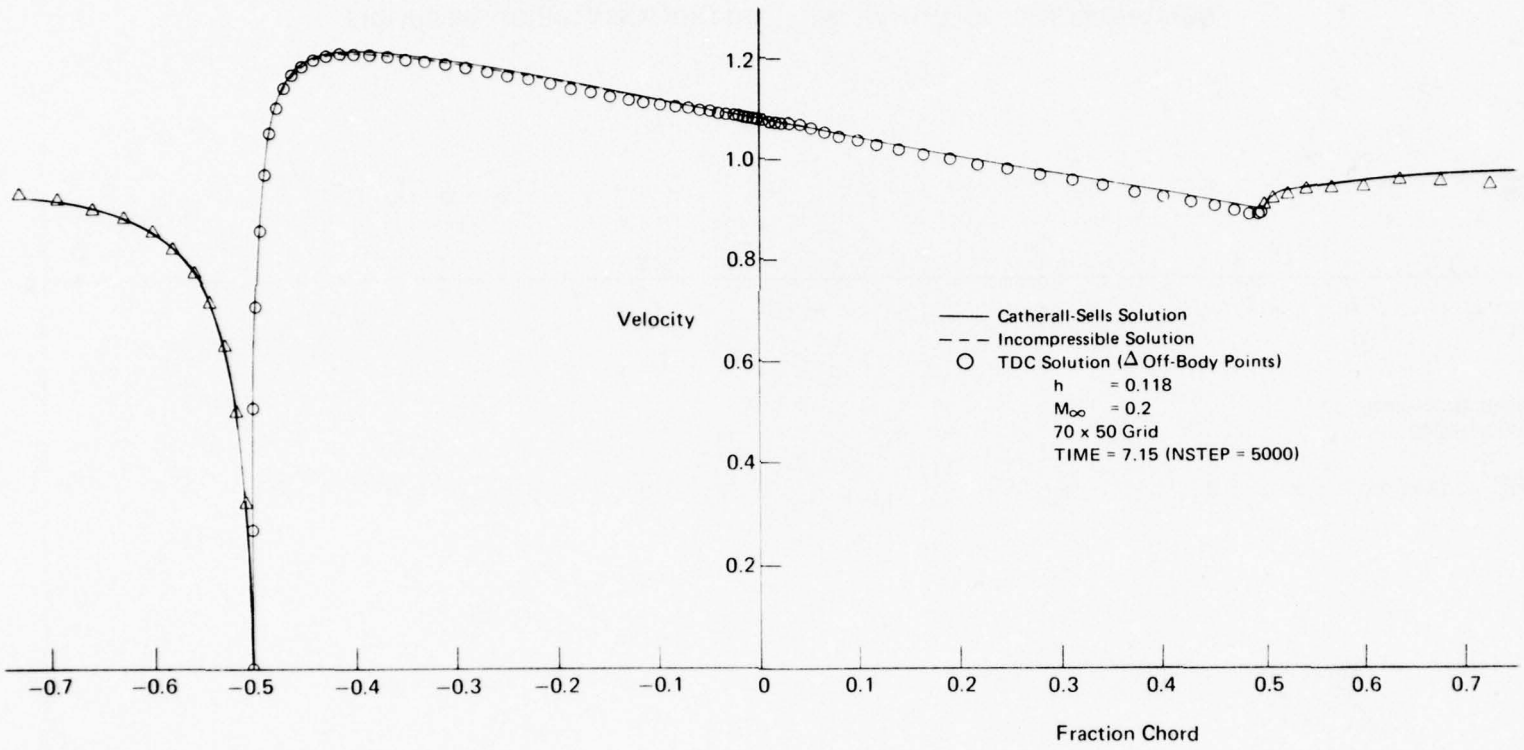


FIGURE 28. JOUKOWSKY AIRFOIL: SURFACE VELOCITY DISTRIBUTION (INVISCID)

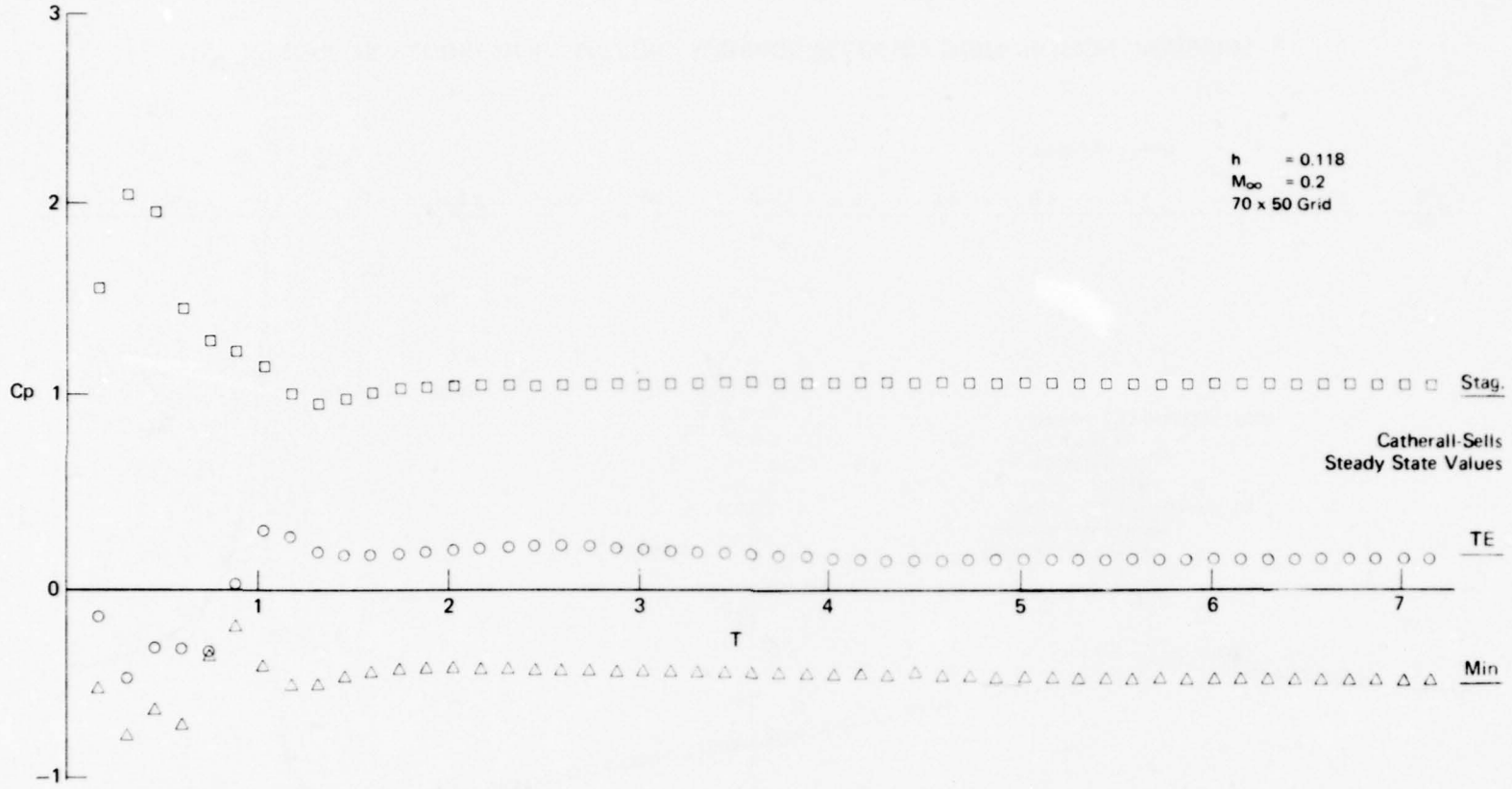


FIGURE 29. JOUKOWSKY AIRFOIL: TIME VARIATION OF STAGNATION, MINIMUM AND TRAILING EDGE PRESSURES (INVISCID)

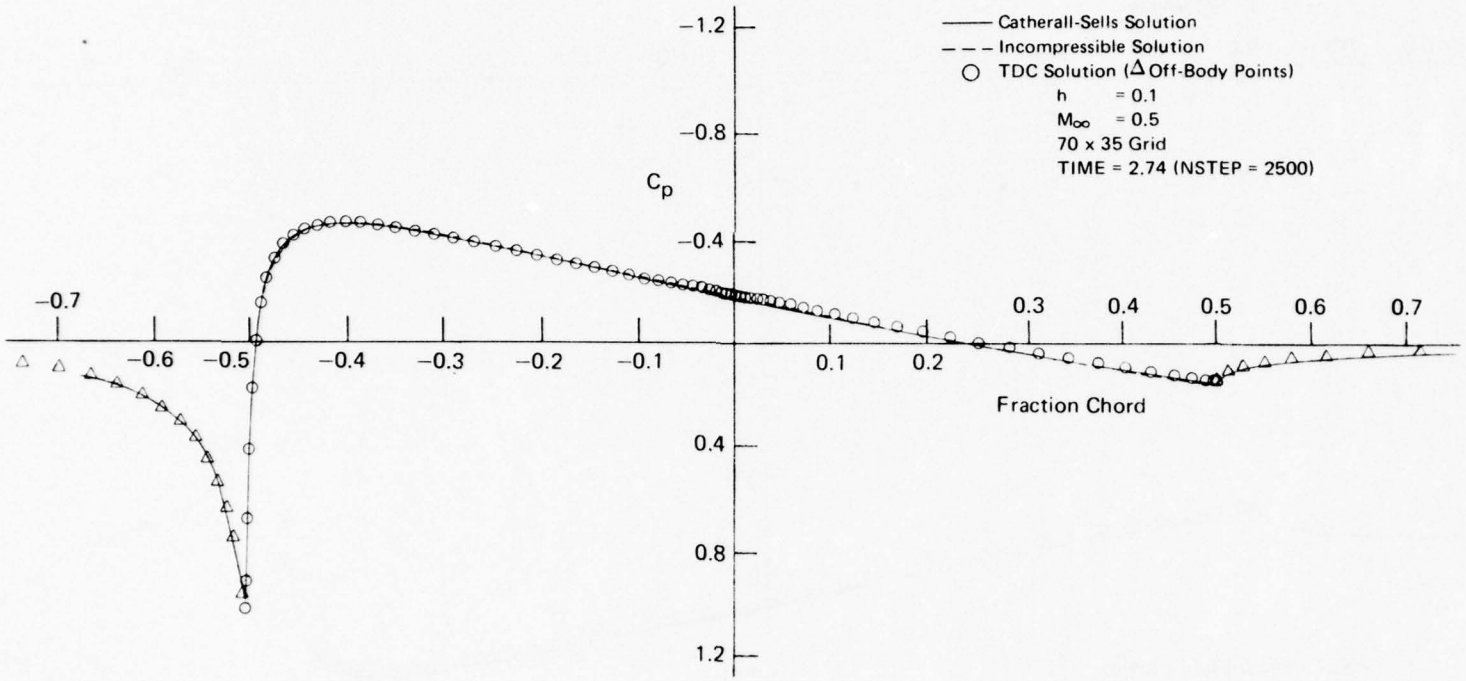


FIGURE 30. JOUKOWSKY AIRFOIL: SURFACE PRESSURE DISTRIBUTION (INVISCID)

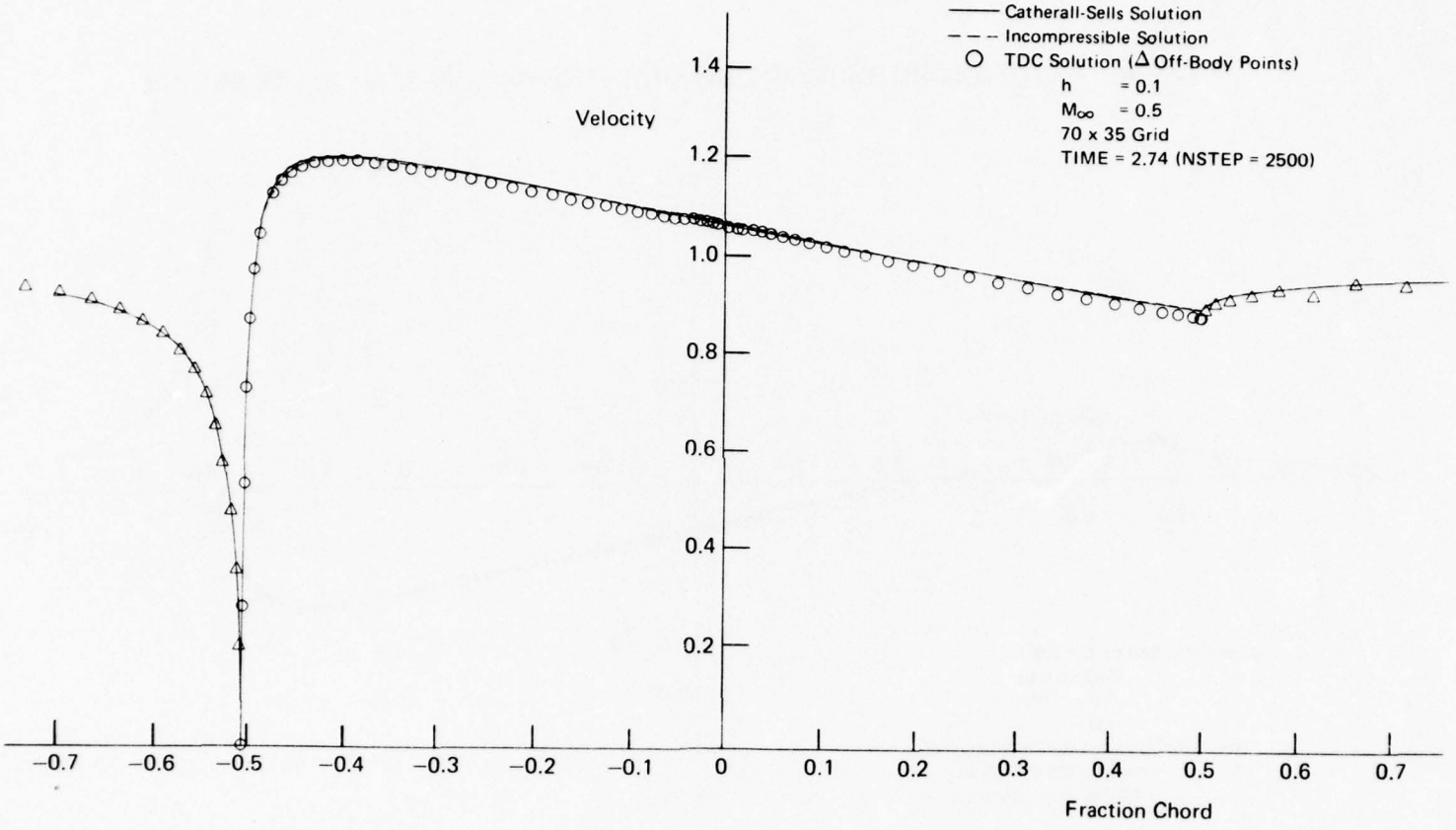


FIGURE 31. JOUKOWSKY AIRFOIL: SURFACE VELOCITY DISTRIBUTION (INVISCID)

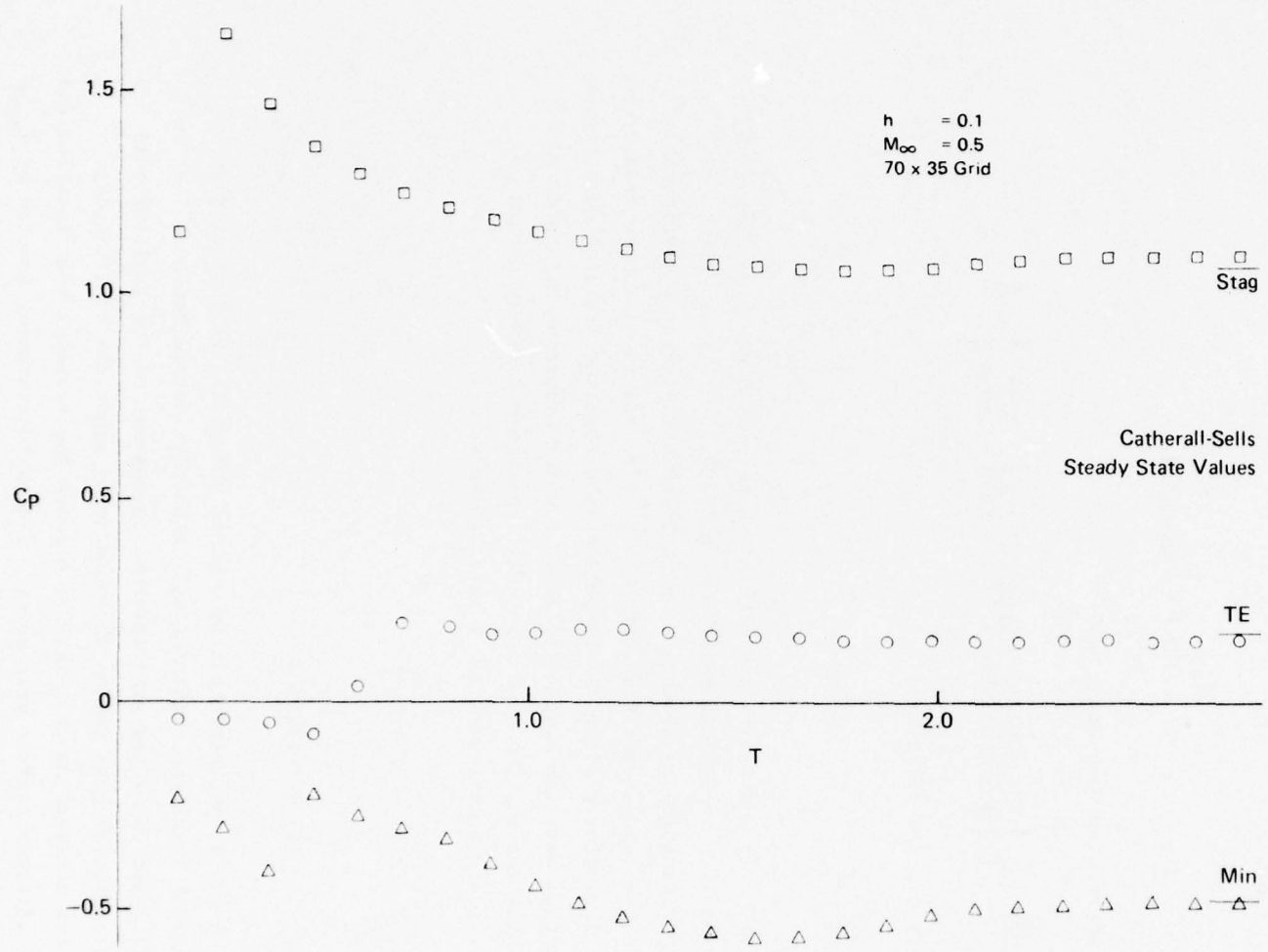


FIGURE 32. JOUKOWSKY AIRFOIL: TIME VARIATION OF STAGNATION, MINIMUM AND TRAILING EDGE PRESSURES (INVISCID)

The transformation functions X and Y chosen for this family of body shapes are defined by

$$\frac{\phi}{\pi} = 1 - X - \tau \sin(\pi X)\cos(\pi X)\left[1 - \cos(\pi X)\right]$$

where τ is an arbitrary constant and

$$Y = \frac{1}{2\alpha} \log \left\{ \frac{1 + Z\left[\tanh(\alpha + \beta) - \tanh\beta\right] + \tanh\beta}{1 - Z\left[\tanh(\alpha + \beta) - \tanh\beta\right] - \tanh\beta} \right\} - \frac{\beta}{\alpha}$$

where $\alpha = \alpha(\phi,t)$, $\beta = \beta(\phi,t)$ and

$$Z = \frac{\rho - c}{S - c}$$

The quantities ρ, ϕ and $S(\phi,t)$ are related to the Joukowsky transformation referred to earlier in Equations (7) through (10).

The transformation parameter τ, an input quantity, exerts considerable influence on the angular distribution of body grid points as can be seen from Figure 33. Its primary effect is to pull points from the trailing edge region and cluster them near the surface inflection point occurring at approximately mid-chord while leaving the nose point distribution relatively unchanged.

The arbitrary functions α and β were chosen as

$$\alpha(\phi,t) = \zeta(t) + \psi(t)\sin^2\phi$$

and

$$\beta(\phi,t) = \xi(t) + \delta(t)\sin^2\phi$$

where ζ, ψ, ξ and δ are determined to control the radial grid spacing at several critical locations. Initially, ζ and ξ are determined such that in the physical space the first grid interval downstream of the trailing edge and the last interval just inside the outer wave along the trailing edge streamline are the same as the distance between the trailing edge location and the nearest adjacent surface grid point. This grid distance, denoted by d_{min}, is typically the smallest in the flow field and is used in the CFL rule (Equation (103)) to determine the allowable time step ΔT. Equal upstream and downstream spacing at the trailing edge is advantageous when implementing the trailing edge

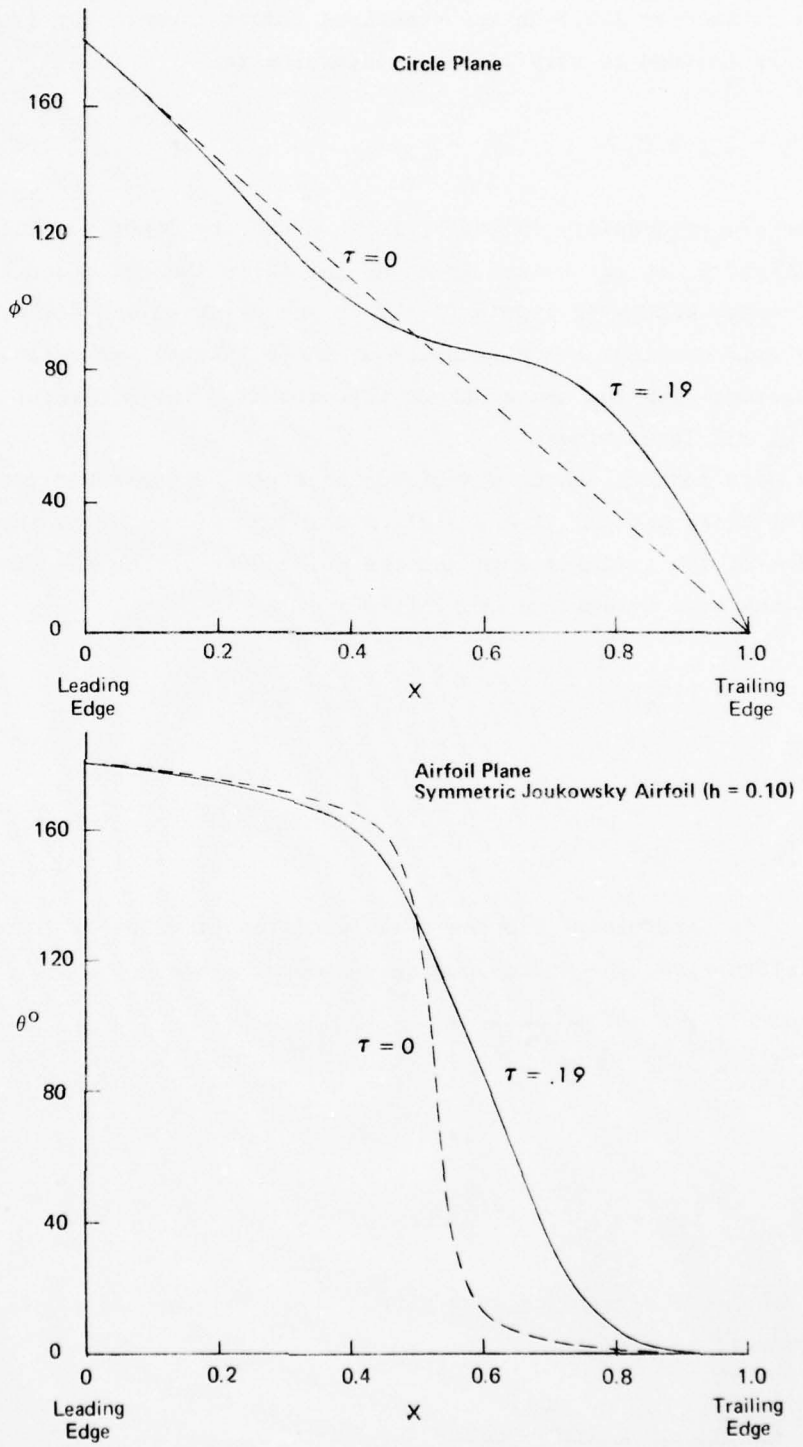


FIGURE 33. EFFECT OF TRANSFORMATION PARAMETER τ ON ANGULAR DISTRIBUTION OF BODY GRID POINTS

analysis of Section 2.3.3 in the numerical computations. For later times, ζ and ξ are assumed to vary linearly according to

$$\zeta = S_\zeta \xi + C_\zeta$$

where the proportionality factor S_ζ is an arbitrary input quantity (e.g., $S_\zeta = -0.2$) and C_ζ is determined from the initial values of ζ and ξ. When the physical space begins to expand ($t > t_o$), the upstream and downstream trailing edge grid spacings are maintained at their initial values and this condition, together with the above linear relationship, is sufficient to determine ζ and ξ at all later times.

The grid control scheme described above may be expressed mathematically in the following manner. The radial coordinates of the point immediately downstream of the trailing edge and the point just inside the outer wave on the trailing edge streamline are initially

$$r_2 = b + d_{min}$$

and

$$r_n = s(0,t_o) - d_{min}$$

where d_{min} is determined from the transformation function X. From the Joukowsky transformation, the corresponding values of ρ are

$$\rho_2 = \frac{1}{2}\left[r_2 + \sqrt{r_2^2 - b^2} \right] - \varepsilon_r$$

and

$$\rho_n = \frac{1}{2}\left[r_n + \sqrt{r_n^2 - b^2} \right] - \varepsilon_r$$

where b denotes the trailing edge coordinate. The initial values of ζ and ξ are determined to satisfy

$$\frac{\rho_2 - c}{s(0,t_o) - c} = \frac{\tanh(\zeta\Delta Y + \xi) - \tanh\xi}{\tanh(\zeta + \xi) - \tanh\xi}$$

and

$$\frac{\rho_n - c}{S(0,t_o) - c} = \frac{\tanh(\zeta + \xi - \zeta\Delta Y) - \tanh\xi}{\tanh(\zeta + \xi) - \tanh\xi}$$

After the physical space begins to expand, ρ_2 is held constant and ζ and ξ are determined to satisfy

$$\rho_2 = c + \left[S(0,t) - c\right] \frac{\tanh(\zeta\Delta Y + \xi) - \tanh\xi}{\tanh(\zeta + \xi) - \tanh\xi}$$

and

$$\zeta = S_\zeta \xi + C_\zeta$$

The time derivatives of ζ and ξ are obtained from these relations as

$$\frac{d\xi}{dt} = \frac{\partial S}{\partial t}(0,t) \frac{\tanh(\zeta\Delta Y + \xi) - \tanh\xi}{S(0,t) - c} \left\{ \operatorname{sech}^2\xi - \operatorname{sech}^2(\zeta\Delta Y + \xi)(S_\zeta \Delta Y + 1) + \left[\operatorname{sech}^2(\zeta + \xi)(S_\zeta + 1) - \operatorname{sech}^2\xi\right] \frac{\rho_2 - c}{S(0,t) - c} \right\}^{-1}$$

and

$$\frac{d\zeta}{dt} = S_\zeta \frac{d\xi}{dt}$$

Similar conditions are imposed along the constant X coordinate line originating from the first surface grid point upstream of the body surface inflection point where σ defined in Equations (43) vanishes. That is, at time zero the outward spacing at the body surface and at the outer wave along this grid line are set equal to d_{min} to determine initial values of ψ and δ. A linear relationship of the form

$$\psi = S_\psi \delta + C_\psi$$

is assumed, where S_ψ is an input variable (e.g., $S_\psi = -.5$) and C_ψ is determined from the initial values of ψ and δ. After the physical space begins to expand, the outward spacing near the inflection point is kept equal to d_{min} so that ψ and δ can be determined at all later times.

The derivatives of the transformation functions X and Y are given by

$$\frac{\partial X}{\partial t} = \frac{\partial^2 X}{\partial t^2} = \frac{\partial^2 X}{\partial t \partial r} = \frac{\partial^2 X}{\partial t \partial \theta} = 0$$

$$\frac{\partial X}{\partial r} = \frac{\partial X}{\partial \phi} \frac{\partial \phi}{\partial r}$$

$$\frac{\partial X}{\partial \theta} = \frac{\partial X}{\partial \phi} \frac{\partial \phi}{\partial \theta}$$

$$\frac{\partial^2 X}{\partial r^2} = \frac{\partial^2 X}{\partial \phi^2} \left(\frac{\partial \phi}{\partial r}\right)^2 + \frac{\partial X}{\partial \phi} \frac{\partial^2 \phi}{\partial r^2}$$

$$\frac{\partial^2 X}{\partial \theta^2} = \frac{\partial^2 X}{\partial \phi^2} \left(\frac{\partial \phi}{\partial \theta}\right)^2 + \frac{\partial X}{\partial \phi} \frac{\partial^2 \phi}{\partial \theta^2}$$

$$\frac{\partial^2 X}{\partial r \partial \theta} = \frac{\partial^2 X}{\partial \phi^2} \frac{\partial \phi}{\partial r} \frac{\partial \phi}{\partial \theta} + \frac{\partial X}{\partial \phi} \frac{\partial^2 \phi}{\partial r \partial \theta}$$

$$\frac{\partial Y}{\partial t} = \frac{\partial Y}{\partial \alpha} \frac{\partial \alpha}{\partial t} + \frac{\partial Y}{\partial \beta} \frac{\partial \beta}{\partial t} + \frac{\partial Y}{\partial Z} \frac{\partial Z}{\partial t}$$

$$\frac{\partial Y}{\partial r} = \left(\frac{\partial Y}{\partial \alpha} \frac{\partial \alpha}{\partial \phi} + \frac{\partial Y}{\partial \beta} \frac{\partial \beta}{\partial \phi}\right) \frac{\partial \phi}{\partial r} + \frac{\partial Y}{\partial Z} \frac{\partial Z}{\partial r}$$

and

$$\frac{\partial Y}{\partial \theta} = \left(\frac{\partial Y}{\partial \alpha} \frac{\partial \alpha}{\partial \phi} + \frac{\partial Y}{\partial \beta} \frac{\partial \beta}{\partial \phi}\right) \frac{\partial \phi}{\partial \theta} + \frac{\partial Y}{\partial Z} \frac{\partial Z}{\partial \theta}$$

where

$$\frac{\partial X}{\partial \phi} = -\frac{1}{\pi}\left[1 - \pi\tau\left[1 - 2\cos(\pi X) - 2\cos^2(\pi X) + 3\cos^3(\pi X)\right]\right]^{-1}$$

$$\frac{\partial^2 X}{\partial \phi^2} = \pi^3 \tau \left(\frac{\partial X}{\partial \phi}\right)^3 \sin(\pi X)\left[9\cos^2(\pi X) - 4\cos(\pi X) - 2\right]$$

$$\frac{\partial Y}{\partial \alpha} = \frac{Z \operatorname{sech}^2(\alpha + \beta)}{\alpha \operatorname{sech}^2(\alpha Y + \beta)} - \frac{Y}{\alpha}$$

$$\frac{\partial Y}{\partial \beta} = \frac{Z \operatorname{sech}^2(\alpha + \beta) + (1 - Z)\operatorname{sech}^2\beta}{\alpha \operatorname{sech}^2(\alpha Y + \beta)} - \frac{1}{\alpha}$$

$$\frac{\partial Y}{\partial Z} = \frac{\tanh(\alpha + \beta) - \tanh\beta}{\alpha \operatorname{sech}^2(\alpha Y + \beta)}$$

$$\frac{\partial \alpha}{\partial \phi} = 2\ \psi \sin\phi \cos\phi$$

$$\frac{\partial \alpha}{\partial t} = \frac{d\zeta}{dt} + \sin^2\phi \frac{d\psi}{dt}$$

$$\frac{\partial \beta}{\partial \phi} = 2\ \delta \sin\phi \cos\phi$$

$$\frac{\partial \beta}{\partial t} = \frac{d\zeta}{dt} + \sin^2\phi \frac{d\delta}{dt}$$

$$\frac{\partial Z}{\partial r} = \frac{1}{S - c}\left(\frac{\partial \rho}{\partial r} - Z \frac{\partial \phi}{\partial r} \frac{\partial S}{\partial \phi}\right)$$

$$\frac{\partial Z}{\partial \theta} = \frac{1}{S - c}\left(\frac{\partial \rho}{\partial \theta} - Z \frac{\partial \phi}{\partial \theta} \frac{\partial S}{\partial \phi}\right)$$

and

$$\frac{\partial Z}{\partial t} = \frac{-Z}{S - c} \frac{\partial S}{\partial t}$$

The derivatives of ρ and ϕ are obtained from the Joukowsky transformation as

$$\frac{\partial \rho}{\partial r} = \frac{1}{2} \frac{r\ A\ D}{A^2 + B^2}$$

$$\frac{\partial \rho}{\partial \theta} = \frac{r\ B}{A} \frac{\partial \rho}{\partial r}$$

$$\frac{\partial \phi}{\partial r} = -\frac{1}{\rho r}\frac{\partial \rho}{\partial \theta}$$

and

$$\frac{\partial \phi}{\partial \theta} = \frac{r}{\rho}\frac{\partial \rho}{\partial r}$$

Cauchy-Riemann Conditions

where

$$A = \left(D + a^2 - \frac{r^2}{2}\right)(\rho + \varepsilon_r \cos\phi) - 2a^2\rho \sin^2\phi$$

$$B = \left(D + a^2 - \frac{r^2}{2}\right)\varepsilon_r \sin\phi + 2a^2\rho \sin\phi \cos\phi$$

and

$$D = \rho^2 + 2\varepsilon_r \rho \cos\phi + \varepsilon_r^2$$

Straightforward differentiation of the above expressions yields the derivatives

$$\frac{\partial^2 \phi}{\partial r^2}, \frac{\partial^2 \phi}{\partial \theta^2} \text{ and } \frac{\partial^2 \phi}{\partial r \partial \theta}.$$

Figures 24 and 25 compare the calculated surface pressure and velocity distributions for an airfoil thickness ratio h = 0.118 at a free stream Mach number of 0.2 with the incompressible solution and the Catherall-Sells solution. Some off-body points along the upstream and downstream symmetry streamlines are also shown to indicate the extent of the steady flow region about the airfoil. Good agreement for this complex shape is obtained with 51 surface points and 40 points in the radial direction. The accuracy of the singular trailing edge analysis of Section 2.3.3.1 is also seen to be quite good. The effectiveness of the angular transformation function X can be seen from the decreased grid spacing in the neighborhood of the surface inflection point. The time variation of stagnation, minimum and trailing edge pressures is shown in Figure 26 and indicates when steady state conditions around the body are first approached. The reason for this particular choice of thickness ratio is the existence of experimental data (Reference 15), including boundary layer measurements, with which the viscous TDC calculations may be compared.

Figures 27, 28 and 29 show comparisons for the same flow conditions and a much larger number of grid points (i.e., 70 surface points and 50 radial points). Increased accuracy is obtained especially in the trailing edge region and the surface velocity prediction. Figures 30, 31 and 32 present comparisons for an airfoil thickness ratio h = 0.10 and a free stream Mach number of 0.5. These predictions were made with 70 surface points and 35 radial points. The accuracy of the calculated values is seen to be reasonably good.

5. VISCOUS SAMPLE CASES

Viscous calculations were carried out for a non-lifting Joukowsky airfoil with a thickness ratio of 0.118 to permit a comparison with the test results of Reference 15. These test results include detailed surveys of the viscous flow in the boundary layer and in the wake in the neighborhood of the trailing edge suitable for evaluating a viscous calculation method. The test conditions were essentially incompressible ($M_\infty = 0.036$) with measurements recorded for both a smooth surface airfoil and the airfoil with a boundary layer transition strip. The Reynolds number was relatively small (Re = 420,000) having the advantage of increasing the viscous displacement effects but adding the complication of partly turbulent flow. The data for the smooth airfoil were selected for comparison purposes because the TDC program has no provision for representing boundary layer thickening due to a transition strip.

Inviscid flow and boundary layer calculations were also performed for comparison with the test data. Figure 34 compares the experimental pressure distribution with the inviscid flow solutions obtained by the Catherall-Sells method and the TDC program with the 70x50 grid discussed previously in Section 4.4. The inviscid calculations were carried out for $M_\infty = 0.2$ because of the more rapid convergence of the TDC program to the local steady state condition at the higher Mach number. The compressibility effects resulting from the difference from the test Mach number are not large enough to affect the comparison (see Figures 27 and 28). The test data match the inviscid calculations very well over the forward portion of the airfoil (% chord < 40), indicating good quality measurements and small viscous effects. The viscous effects are evident as a rounding of the pressure peak at the trailing edge with a trailing edge C_p about half the inviscid value and with C_p values in the wake somewhat smaller than the inviscid values. The close agreement of the TDC and Catherall-Sells calculations near the trailing edge indicates that viscous effects of this magnitude should be predictable by the time dependent method of computation.

Results of boundary layer surveys aft of mid-chord are given in Reference 15. These are compared with results of the Cebeci finite-difference boundary layer method (Reference 5) in Figures 35 through 38. The boundary layer calculation was carried out with the inviscid pressure distribution from the Catherall-Sells method and also with the measured pressure distribution aft of 21.2% chord. Reference 15 also gives measurements of transition location

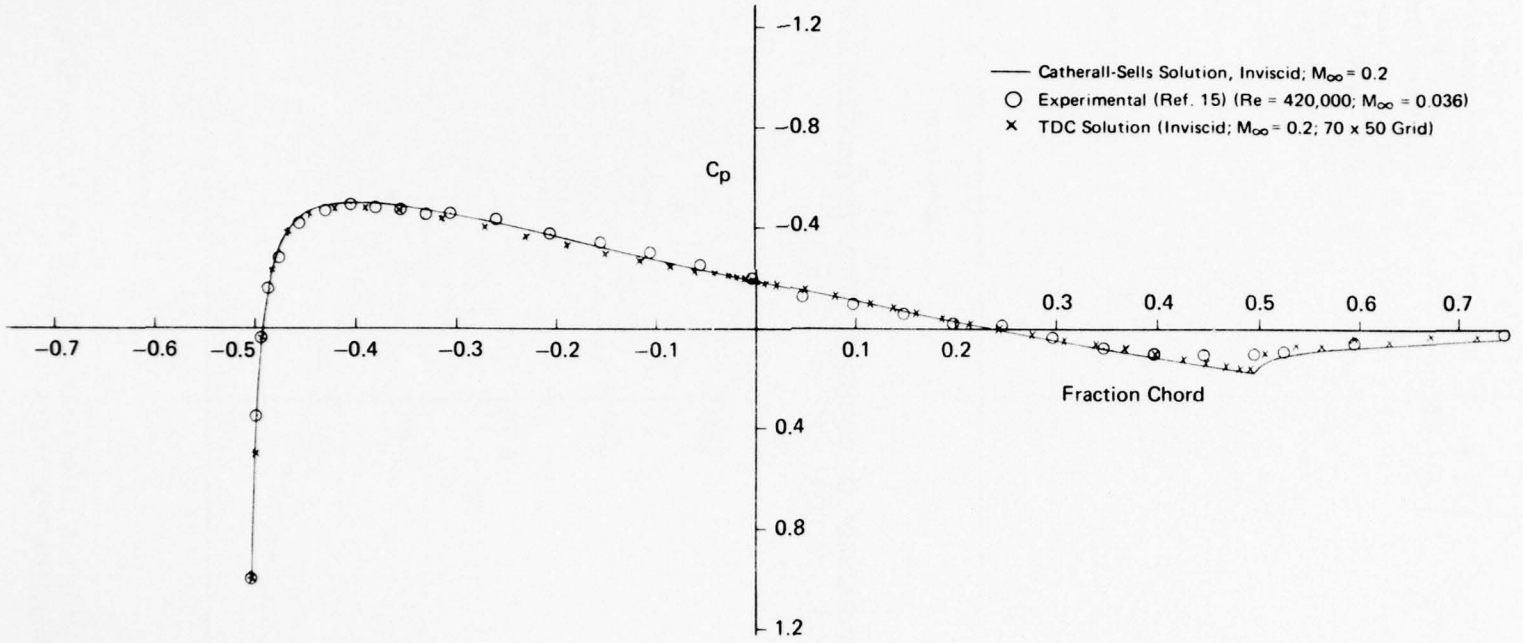


FIGURE 34. VISCOUS EFFECT ON PRESSURE DISTRIBUTION: 11.8% JOUKOWSKY AIRFOIL

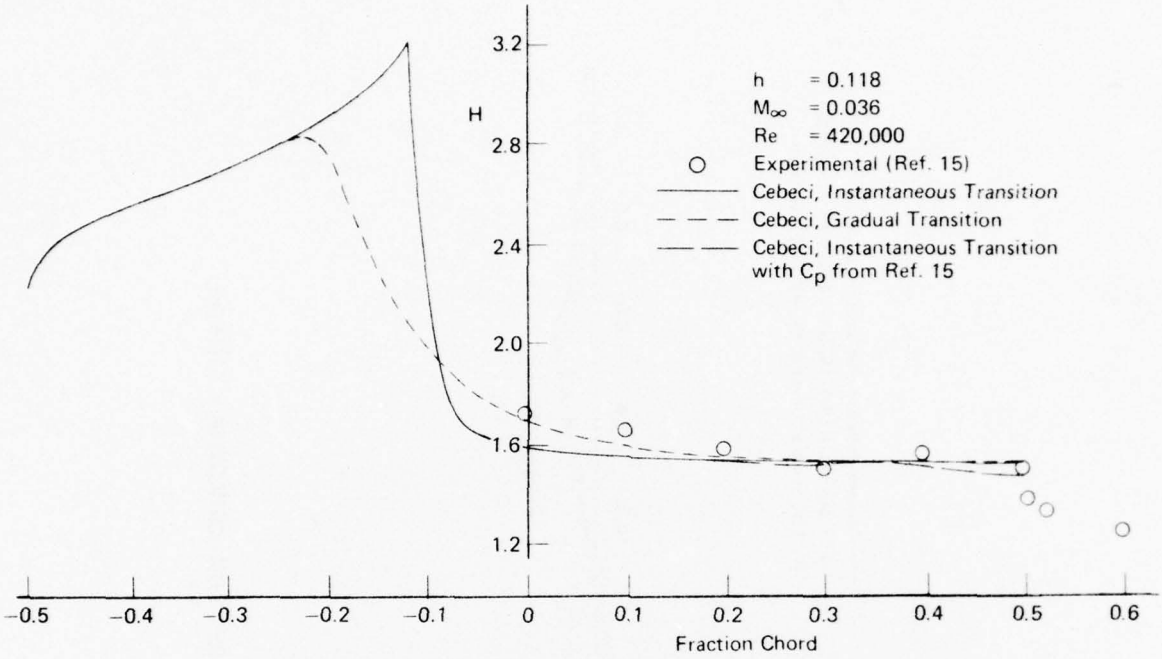


FIGURE 35. COMPARISON OF BOUNDARY LAYERS ON JOUKOWSKY AIRFOIL: SHAPE FACTOR

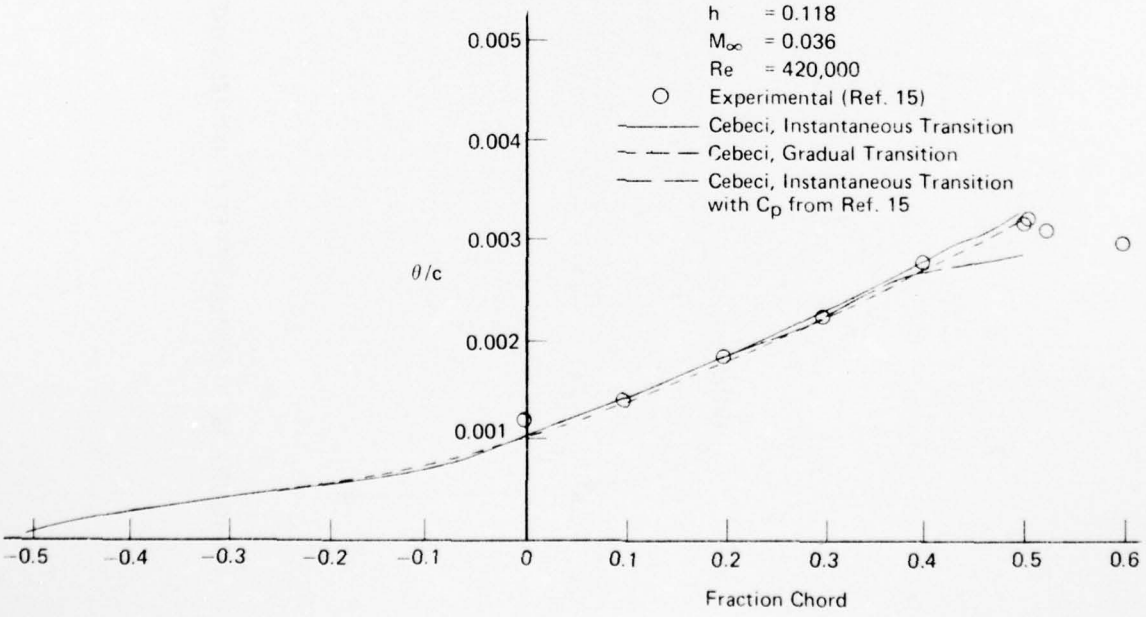


FIGURE 36. COMPARISON OF BOUNDARY LAYERS ON JOUKOWSKY AIRFOIL: MOMENTUM THICKNESS

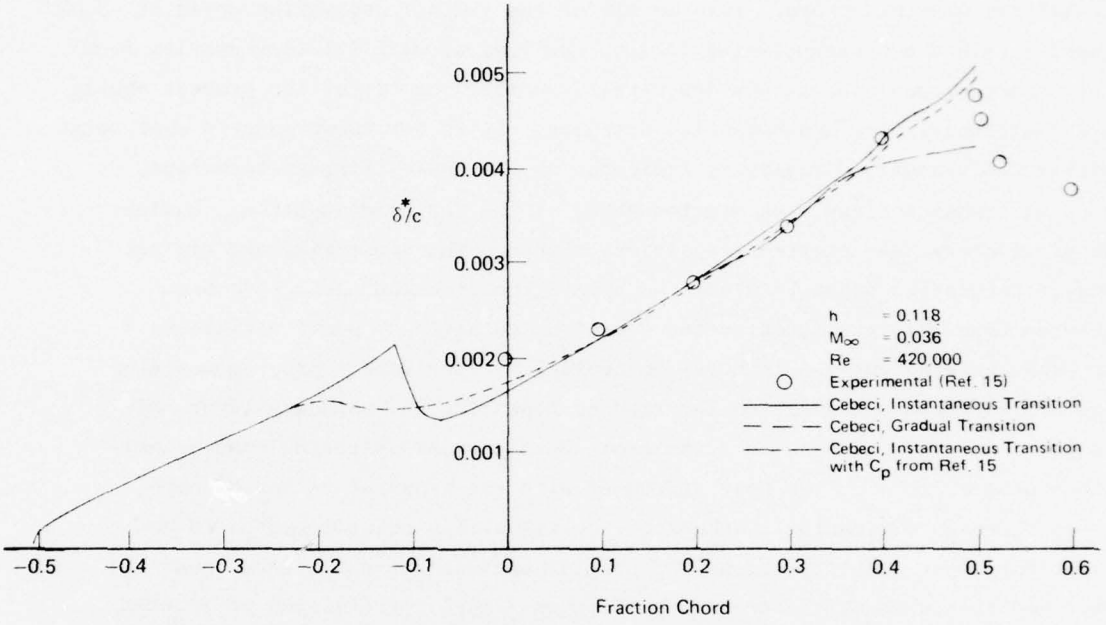


FIGURE 37. COMPARISON OF BOUNDARY LAYERS ON JOUKOWSKY AIRFOIL: DISPLACEMENT THICKNESS

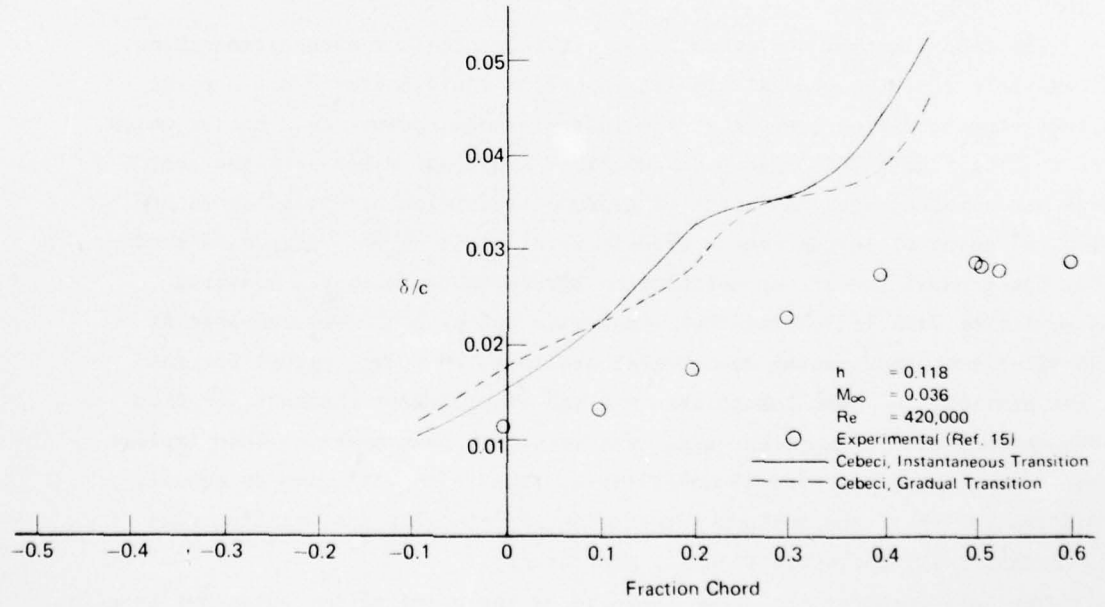


FIGURE 38. COMPARISON OF BOUNDARY LAYERS ON JOUKOWSKY AIRFOIL: BOUNDARY LAYER THICKNESS

for the smooth airfoil obtained by a smoke filament technique which indicate transition near mid-chord. This is aft of the laminar separation point at -8.0% chord obtained by extrapolating to zero the laminar skin friction results from the Cebeci method. At such a low Reynolds number the transition process should occur gradually over a substantial distance. It is not known exactly what point within the transition region is indicated by the smoke filament technique, so that transition may have started ahead of the measured location. Laminar separation may have started transition, although the smoke filament did not show a separation bubble. Also, the separation location could have been changed from that predicted by the Cebeci calculation by small variations in pressure gradient due to model inaccuracies. The Cebeci program was also used to estimate a transition location by repeating the boundary layer calculation for several assumed transition locations and selecting that transition point which gave the best agreement with the measured values of both shape factor and momentum thickness. The transition point location is an important input quantity to the TDC program because the turbulence equations employed do not model the transition process. Abrupt transition is assumed with only the laminar terms in the mean-flow equations entering the calculations upstream of some preselected boundary in the computational space, while the additional turbulence terms and turbulence equations are employed beyond this boundary.

The Cebeci method has options for either gradual or abrupt transition. It was felt that the gradual transition option would better represent the actual flow conditions, but that the instantaneous option would better match the results from a TDC program calculation. The best match with the test data was obtained with the start of gradual transition at -23.9% chord and with the point of instantaneous transition at -9.6% chord. Figure 35 shows that the gradual transition calculation agrees better with the measured shape factor data indicating that transition was probably not complete at the first two experimental measurement stations. However, except for the first station, the momentum thickness θ and displacement thickness δ^* from both options are in excellent agreement with the measurements. This implies that either abrupt or gradual modelling of transition will give an equally good prediction of the viscous interaction effects near the trailing edge if the transition location is adjusted accordingly.

The rapid drop of the shape factor H at the point of instantaneous transition is notable. In response to the sudden application of turbulent eddy viscosity, the value of H at this point has completed most of the change to an equilibrium turbulent level of 1.6 from the laminar value of 3.2 at the

previous station. Combination with the smooth variation of momentum thickness shown in Figure 36 results in a sharp peak in the displacement thickness at the transition point (see Figure 37). This might be expected to produce larger viscous effects on the pressure distribution than the smoother displacement shape obtained from the gradual transition calculation. However, this difference in displacement thickness would be reduced by a fully coupled viscous-inviscid solution.

The momentum thickness and displacement thickness which were calculated from the inviscid pressure distribution are in close agreement with the measured values near the trailing edge. However, the good agreement seems to be coincidental, as the thicknesses calculated from the experimental pressure distribution are significantly lower than the measured values. The experimental flow field data show a drop in pressure outward across the boundary layer at the trailing edge so that the disagreement with the measured thicknesses would be even larger if the pressure at the boundary layer edge were used in the calculation. It seems apparent that this test case has viscous-inviscid interaction effects near the trailing edge which are not calculated correctly by the boundary layer approximation, but should be calculated correctly by solving the turbulent Navier-Stokes equations by the TDC method.

The boundary layer calculations were used as a guide in selecting the grid geometry shown in Figure 39 for the TDC viscous calculations. A grid with 70 points along the body gave good accuracy for the inviscid calculations (see Figure 34); this surface point distribution was therefore used for the viscous calculations. A total of 60 points in the direction normal to the body was used to provide closer spacing in the viscous region. The outer boundary for the viscous calculations was chosen to lie well outside the boundary layer and wake so that the viscous terms in the flow equations would be negligible at the boundary. The edge of the viscous flow region is not a well defined boundary. Several estimates of the boundary layer and wake thickness δ for the selected test case are shown in Figure 38. The experimental values are based on a visual inspection of the measured velocity profiles, and probably correspond to a velocity defect of one-half or one percent of the inviscid edge velocity. The values from the Cebeci boundary layer calculations are considerably larger. They correspond to a numerical test which selects the outer edge of the boundary layer as that point where the normal velocity gradient is about 10^{-6} of the surface value. The selection of the fifteenth grid line out from the airfoil (labeled J = 15 in Figure 39) gave a viscous

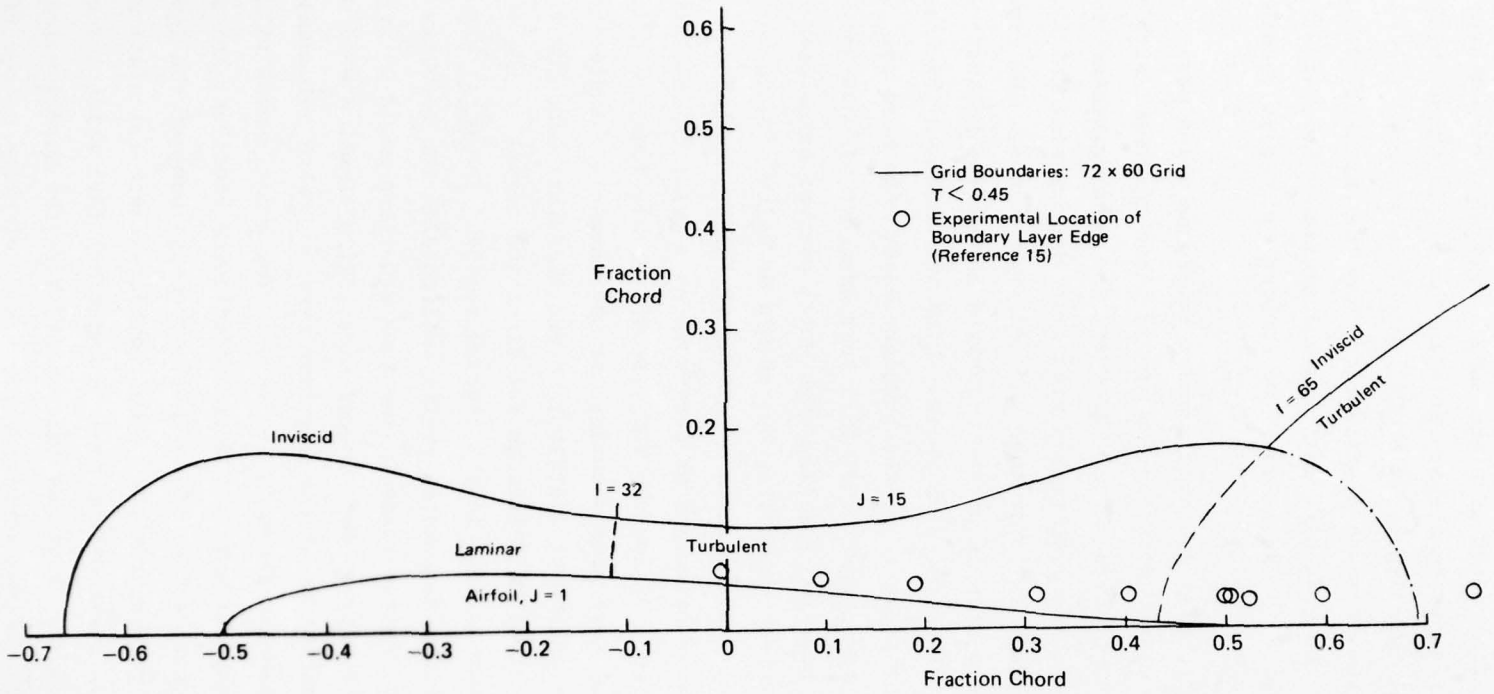


FIGURE 39. JOUKOWSKY AIRFOIL: GRID BOUNDARY OF VISCOUS CALCULATIONS

AD-A036 213 MCDONNELL AIRCRAFT CO ST LOUIS MO F/G 20/4
NUMERICAL SOLUTION OF SUBSONIC VISCOUS-INVISCID INTERACTING FLO--ETC(U)
JUL 76 A VERHOFF F33615-73-C-4062
UNCLASSIFIED AFFDL-TR-76-64 NL

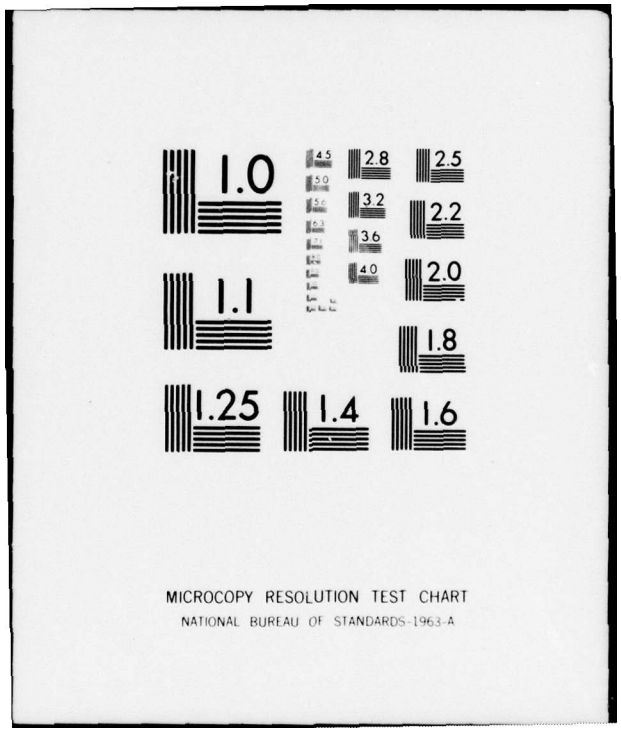
2 OF 2
AD
A036213





END

DATE
FILMED
3-77


1.0
1.1
1.25
1.4
1.6
1.8
2.0
2.2
2.5
2.8
3.2
3.6
4.0
4.5
5.0
MICROCOPY RESOLUTION TEST CHART
NATIONAL BUREAU OF STANDARDS-1963-A

region about three times as thick as the Cebeci limit. The grid line labeled I = 65 in Figure 39 was selected as the outer viscous boundary in the wake region.

The grid line labeled I = 32 in Figure 39 was selected as the upstream boundary for the turbulent calculations. This is the first grid line upstream of the surface point corresponding to the transition location determined from the Cebeci instantaneous transition calculations. Based on the results of the turbulent sample case presented later, this may not have been the right choice. The Cebeci method uses an empirical mixing length formula for eddy viscosity; the large increase in eddy viscosity at the instantaneous transition point causes a rapid change in the boundary layer parameters, as was shown. Because of the zero upstream boundary condition on K and E in the TDC flow equations, it takes some distance for turbulence to be produced and diffuse through the boundary layer to develop an eddy viscosity corresponding to that used in the Cebeci method. The boundary of the turbulent region could possibly be moved a short distance upstream to allow for this. In the test case that was calculated, this eddy viscosity difference is important, because without fully developed turbulence the boundary layer may separate near the laminar separation point a short distance downstream of the selected turbulence boundary.

More testing of the program will be required to select a method for properly simulating transition. One possibility is to use an "equilibrium" value of K on the upstream boundary rather than K = 0, although some analysis would be required to determine what value to use in a time dependent calculation. Another possibility would be to multiply the eddy viscosity μ_t by an intermittency factor to simulate the gradual transition process as the Cebeci program does. Neither of these approaches has been tested.

The "law-of-the-wall" boundary condition for turbulent flow developed in Section 3.3 requires that the first grid point out from the surface be in the "law-of-the-wall" region of the boundary layer, where the "law-of-the-wall" velocity profile is valid and the turbulent shear is approximately equal to the wall shear. Transformation parameters were selected to meet this requirement near mid-chord where the normal spacing of the grid lines is controlled. The velocity profiles from the Cebeci boundary layer calculation with instantaneous transition were used as a guide and are shown in Figure 40. The turbulent profile at mid-chord shows an approximate "law-of-the-wall" region between $y^+ = 20$ and $y^+ = 80$. The selected transformation parameters gave the grid point

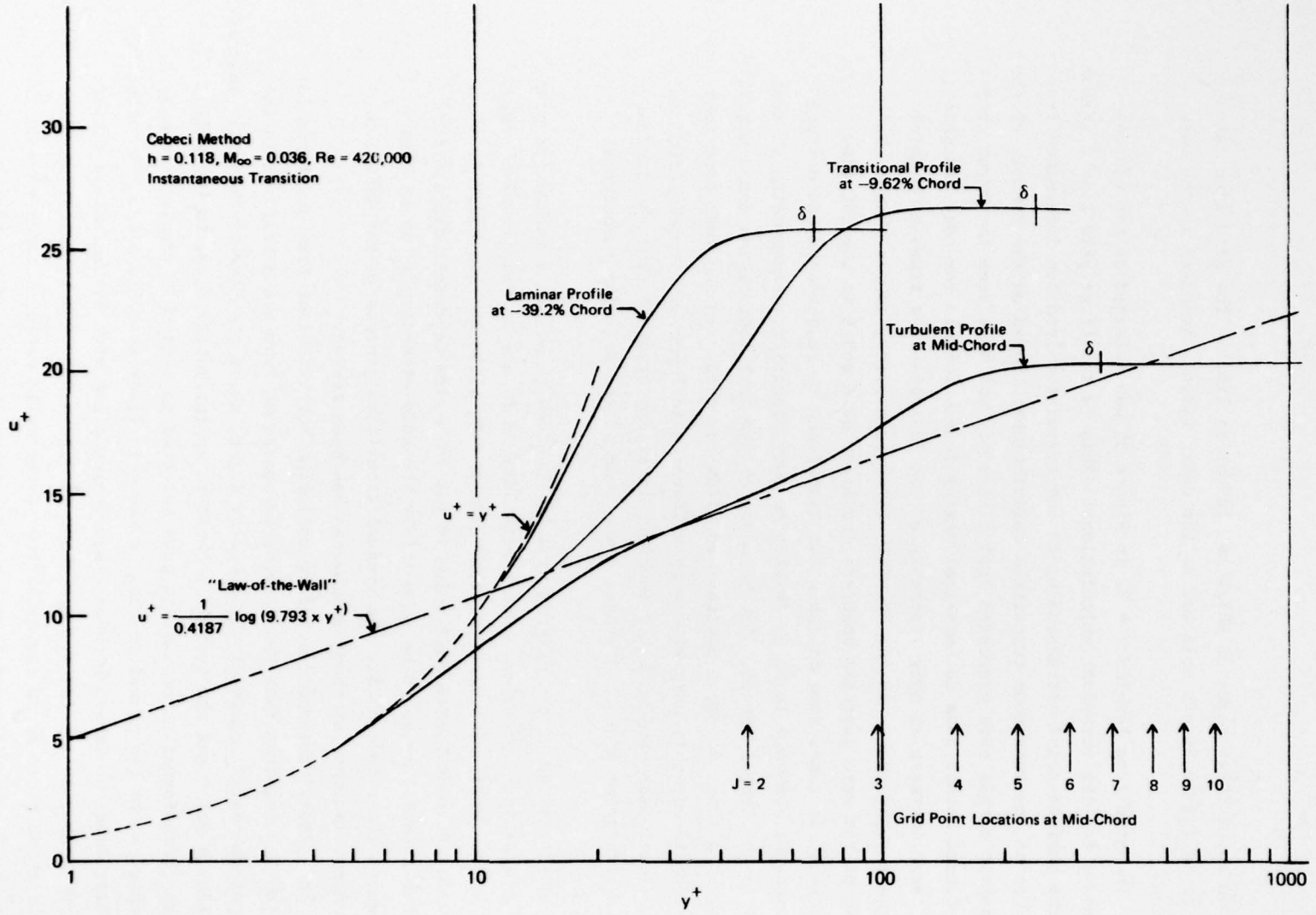


FIGURE 40. JOUKOWSKY AIRFOIL: BOUNDARY LAYER VELOCITY PROFILES IN "LAW-OF-THE-WALL" COORDINATES

locations shown. The first grid point out from the wall (J = 2) is at a distance y/c = 0.002 while the value of y^+ is 47, well within the "law-of-the-wall" region. Farther back on the airfoil, the upper y^+ limit of the "law-of-the-wall" region is even larger. The laminar profile at -39% chord is located near the pressure peak and approximates a flat plate or Blasius profile having a nearly linear variation ($u^+ = y^+$) out to about one-third of the boundary layer thickness. The transitional profile at -9.6% chord does not have a "law-of-the-wall" region so that the slip velocity u_w^+ derived from the "law-of-the-wall" boundary condition will be less accurate in the short distance during which a "law-of-the-wall" region is developing.

The assumption that the shear at the first point outward from the surface equals the wall shear used to determine the wall boundary conditions given by Equations 122 is examined in Figure 41. The shear variation at mid-chord obtained from the Cebeci calculation is shown and the approximation is seen to be valid out to approximately $y^+ = 80$. The first grid point (J = 2) lies well within this region. For the transitional profile, the shear near the first grid point is larger than the wall value due to the larger velocity gradients shown in Figure 40. This will tend to increase the wall values of K and E predicted by Equations 122 in the transitional region. However, the lag in production of turbulent energy in this region inherent in the TDC calculations will have an opposite effect.

The analysis of the boundary layer calculations indicates that the selected grid geometry gives an inner grid point within the "law-of-the-wall" region at mid-chord. For larger Reynolds numbers or locations farther downstream, the outer boundary of the "law-of-the-wall" region becomes larger in "law-of-the-wall" coordinates but approaches a nearly constant ratio to the momentum thickness. Figure 42 shows an estimate of the outer limit y_D of the "law-of-the-wall" region from a correlation of experimental velocity profiles with shape factor H (Reference 16). For near flat-plate shape factors ($1.3 < H < 1.5$) the outer limit is approximately the same as the momentum thickness. For boundary layers approaching separation ($H > 2.0$), the limit is reduced to $y_D/\theta \simeq 0.4$. This indicates that a grid spacing near the wall of y/c = 0.002 at mid-chord should give an acceptable inner grid point location at larger Reynolds number and at angles of attack approaching trailing edge separation.

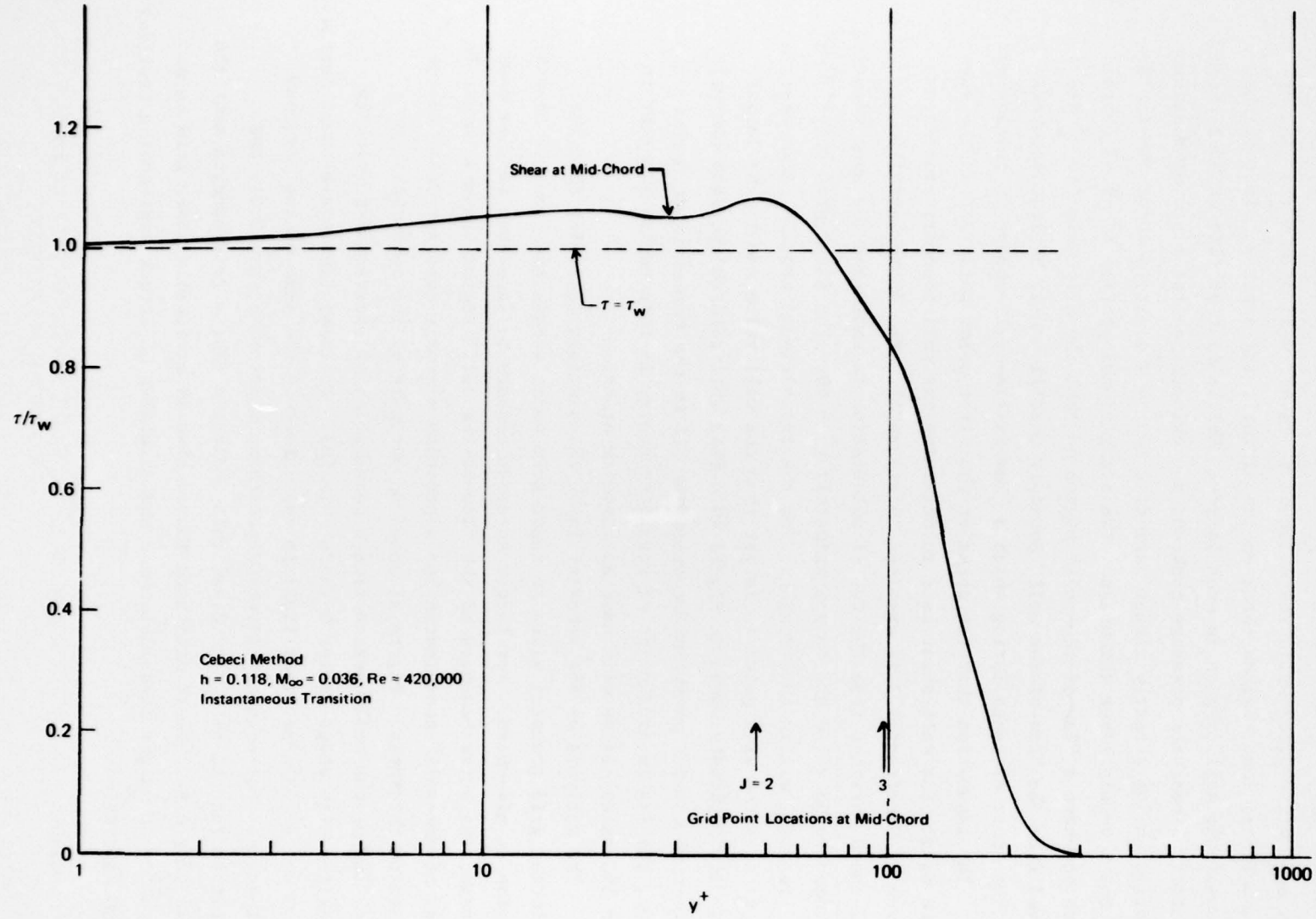


FIGURE 41. JOUKOWSKY AIRFOIL: SHEAR VARIATION ACROSS TURBULENT BOUNDARY LAYER

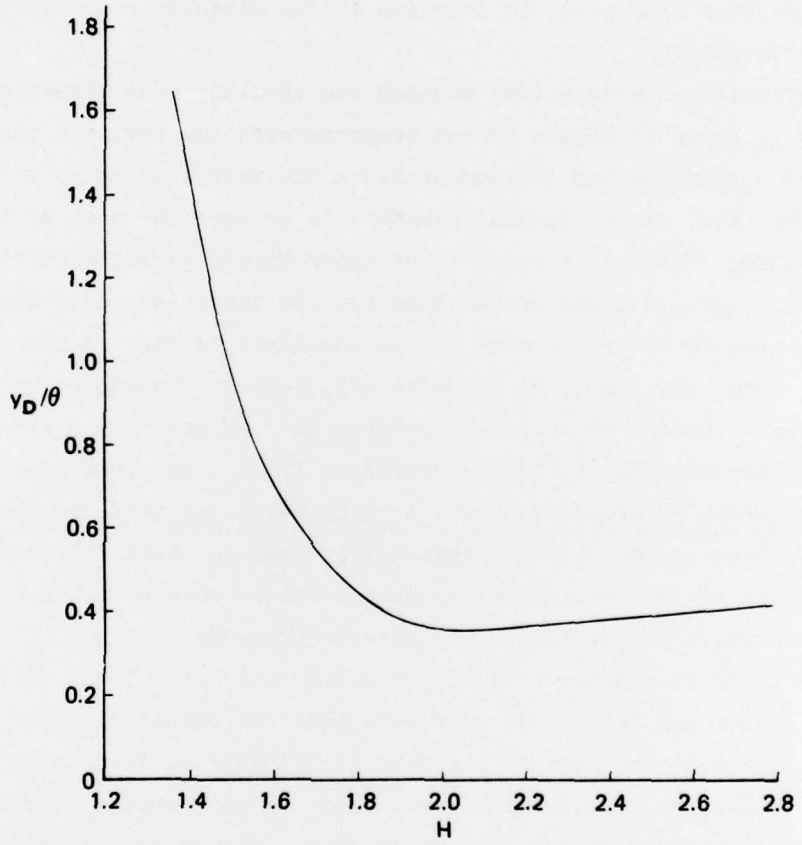


FIGURE 42. JUNCTION BETWEEN "LAW-OF-THE-WALL" AND "VELOCITY DEFECT" REGIONS

5.1 Laminar Flow

The laminar flow calculation was carried out to a non-dimensional time of T = 4.5, at which point the inviscid calculation has essentially reached steady state (see Figure 29). The number of time steps required to reach this time point was about 50 percent larger than for the inviscid calculation because the minimum grid spacing d_{min} was decreased by approximately one third. The allowable time step size given in Equation 103 is directly proportional to the minimum grid spacing.

The time variation of stagnation, minimum and trailing edge pressures for laminar flow is shown in Figure 43 and compared with the inviscid results. The variations of stagnation and minimum pressure are very similar to the inviscid case as expected, as the laminar boundary layer near the nose of the airfoil is very thin. There is a shift in pressure levels giving an error in stagnation pressure several times larger than for the inviscid case. The grid spacing near the nose is about the same as for the inviscid case so that the difference is probably the result of the zero slip velocity boundary condition combined with a grid spacing which places several grid points in the first row outward from the body outside the laminar boundary layer. For time dependent calculations, it is not practical to use a fine grid spacing near the stagnation point with grid points in the constant shear layer near the wall. It would be desirable to develop an improved numerical scheme which would permit a relatively coarse grid while giving reasonably accurate results.

The minimum pressure reaches a nearly constant level near T = 2 similar to the inviscid result and is in fair agreement with the Catherall-Sells steady state value. At T = 4.5, the minimum pressure increases to a less negative value and is no longer steady with time. The cause of this change is related to the surface pressure distributions shown in Figure 44 and the velocity profiles shown in Figure 45. The pressure is less negative over the forward part of the airfoil than the steady state inviscid solution and much more negative over the rear part. The velocity profiles of Figure 45 show a change from a relatively thick boundary layer type profile at T = 1.9 to a very thick shear layer type profile at T = 4.5. The boundary layer type profiles (over the forward part of the airfoil surface) increase gradually in thickness in the early part of the time history. The thickening of the boundary layer profiles may represent the initial stages of laminar separation as predicted by the boundary layer program, but the final shear layer profile is meaningless since the computation near the trailing edge is going unstable.

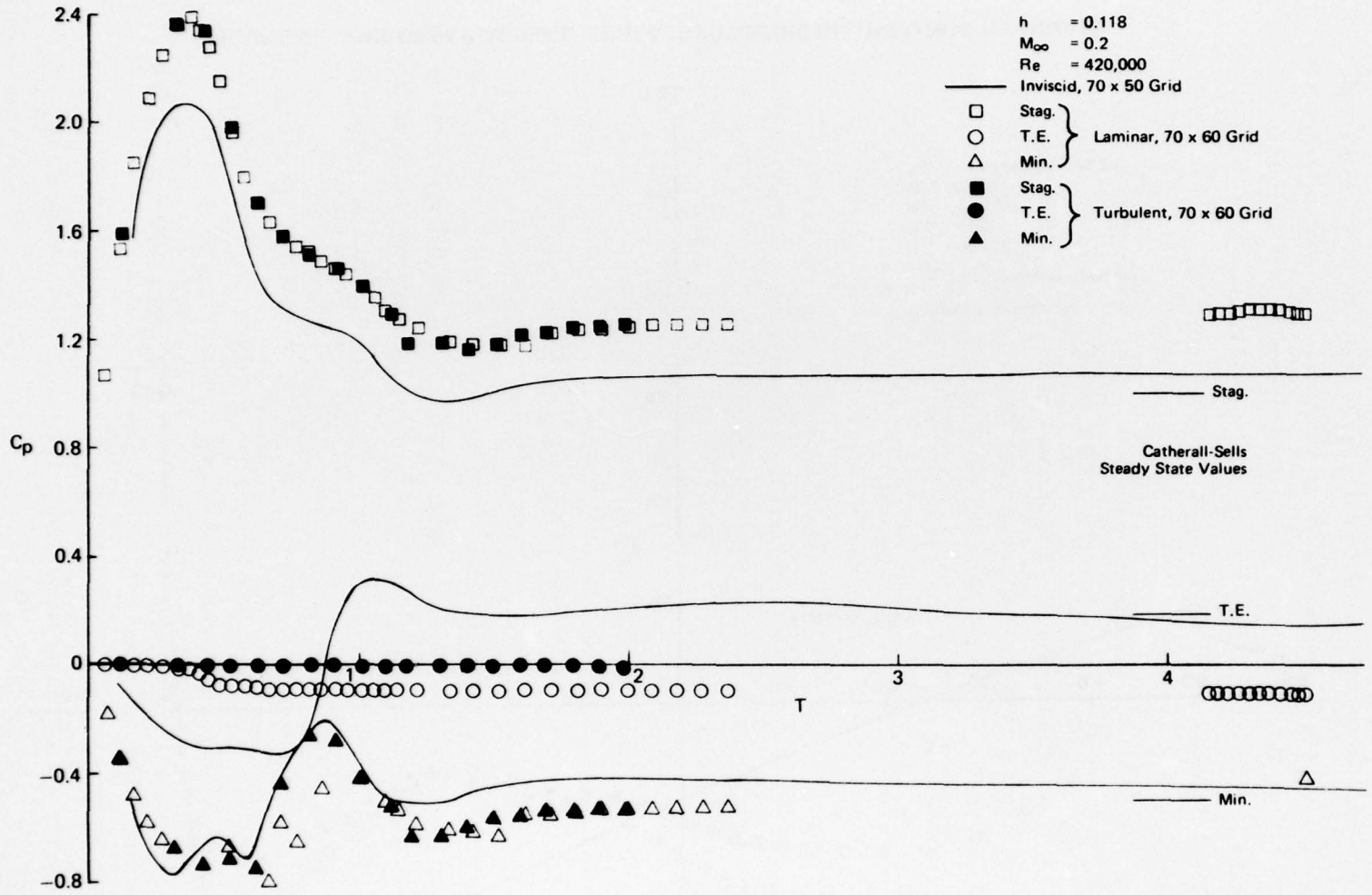


FIGURE 43. JOUKOWSKY AIRFOIL: TIME VARIATION OF STAGNATION, MINIMUM AND TRAILING EDGE PRESSURES (VISCOUS)

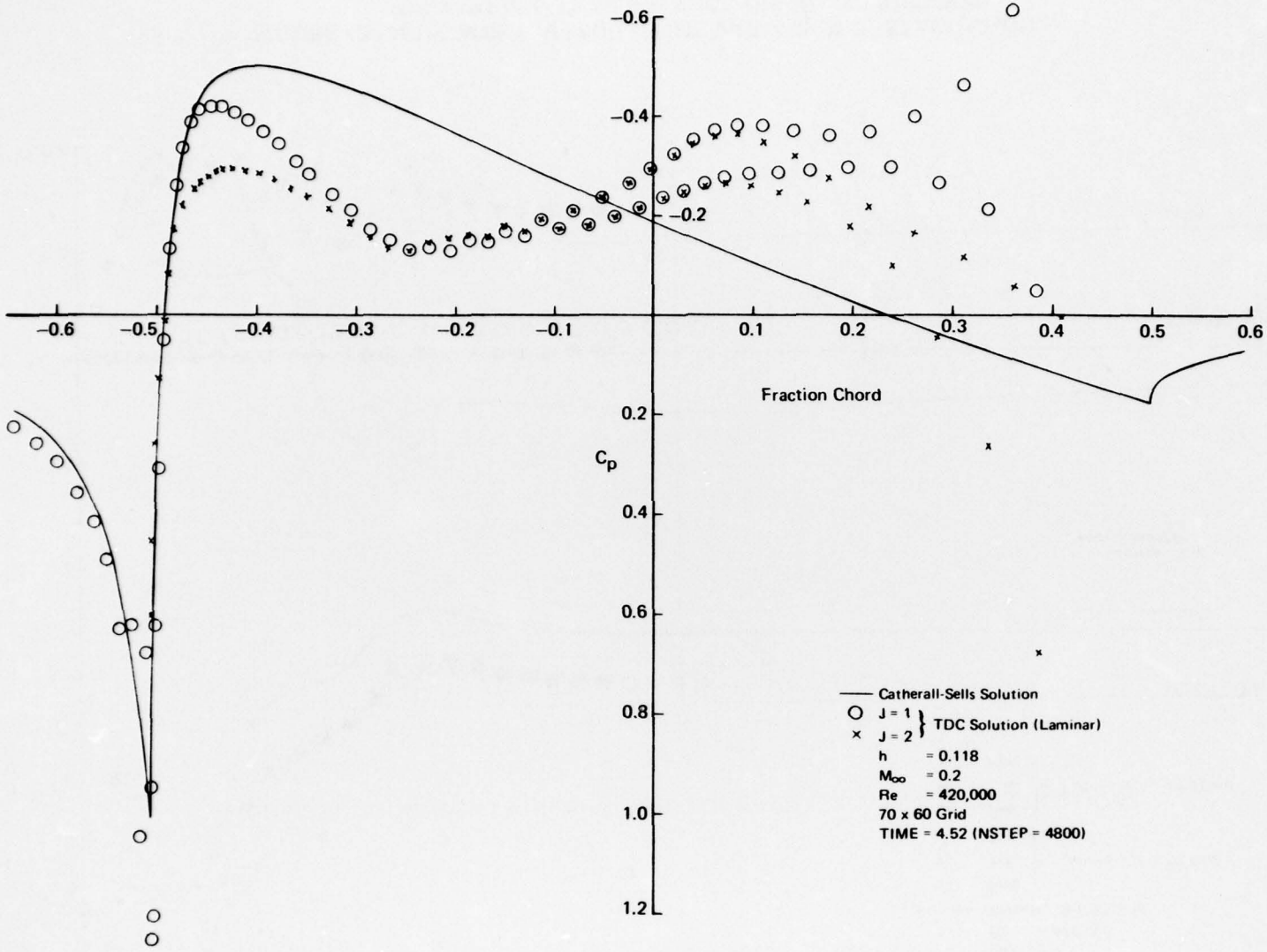


FIGURE 44. JOUKOWSKY AIRFOIL: SURFACE PRESSURE DISTRIBUTION (LAMINAR)

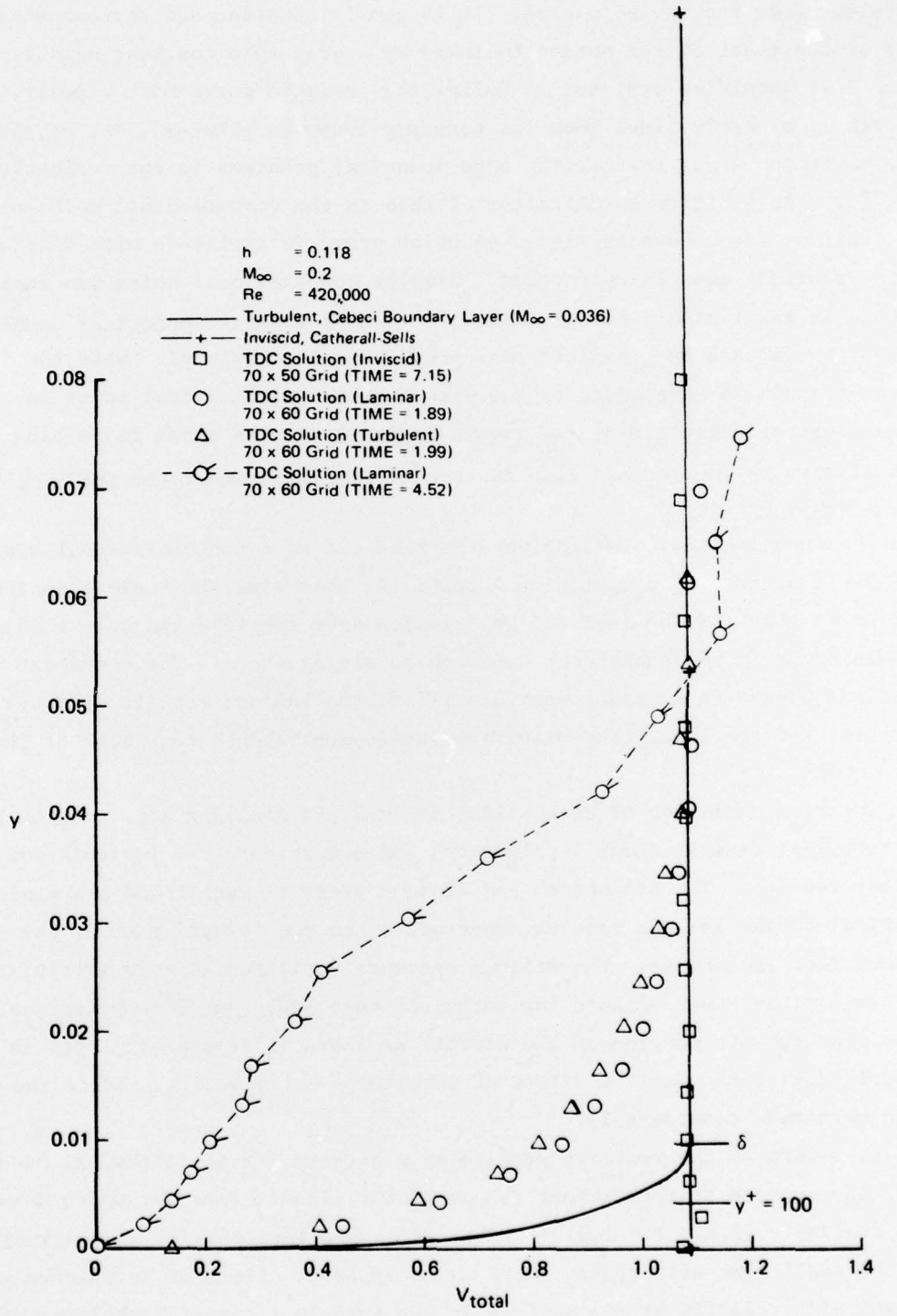


FIGURE 45. JOUKOWSKY AIRFOIL: VELOCITY VARIATION WITH DISTANCE FROM WALL AT MID-CHORD

The time variation of trailing edge pressure shown in Figure 43 is much different from the inviscid case. It is nearly constant and approximately zero at the start of the motion followed by a drop to a constant negative value. It should be expected to follow the inviscid curve more closely, especially at early times when the boundary layer is thinner. The difference seems to be due to trailing edge numerical problems in the evaluation of $\frac{\partial P}{\partial T}$. An additional indication of this is the computational noise near the trailing edge shown in Figure 44 which grows in amplitude with distance as the trailing edge is approached. Similar computational noise was experienced in the inviscid calculations before more accurate numerical techniques to evaluate the trailing edge pressure were developed. When the improved techniques were added to the program, the computational noise decreased dramatically giving the smooth inviscid results shown in Section 4.4. A local mesh refinement may also improve the stability near the trailing edge.

5.2 Turbulent Flow

The turbulent calculations were carried out to a non-dimensional time of only T = 2 because of computational cost. At this time the rapid transients similar to those of the inviscid calculation have subsided and only gradual changes occur in the subsequent approach to steady state. The turbulent calculations behave in a manner very similar to the laminar results in many respects, and the later time-wise flow development should show some of the same trends.

The time variation of stagnation, minimum and trailing edge pressures for turbulent flow is shown in Figure 43 and compared to the inviscid and laminar results. The stagnation and minimum pressure variations are almost identical to the laminar case as expected, since the forward part of the viscous flow is laminar. The minimum pressure variation is more irregular for the laminar case, because the turbulent case has reduced computational noise over the aft portion of the airfoil as shown in Figure 46. This is probably due to the damping effect of turbulence which acts to reduce the noise magnitude considerably.

In Figure 45 the velocity profile at mid-chord for the turbulent case at T = 2 is compared to the laminar result at the closest time for which data were available (i.e., T = 1.9). The profiles are very similar and, allowing for the small time difference, there is no apparent effect of turbulence except for the slip velocity at the surface in the turbulent case. Turbulence might be expected to have a stronger effect on the velocity profile, considering the rapid change in displacement thickness δ^* and shape factor H aft of the

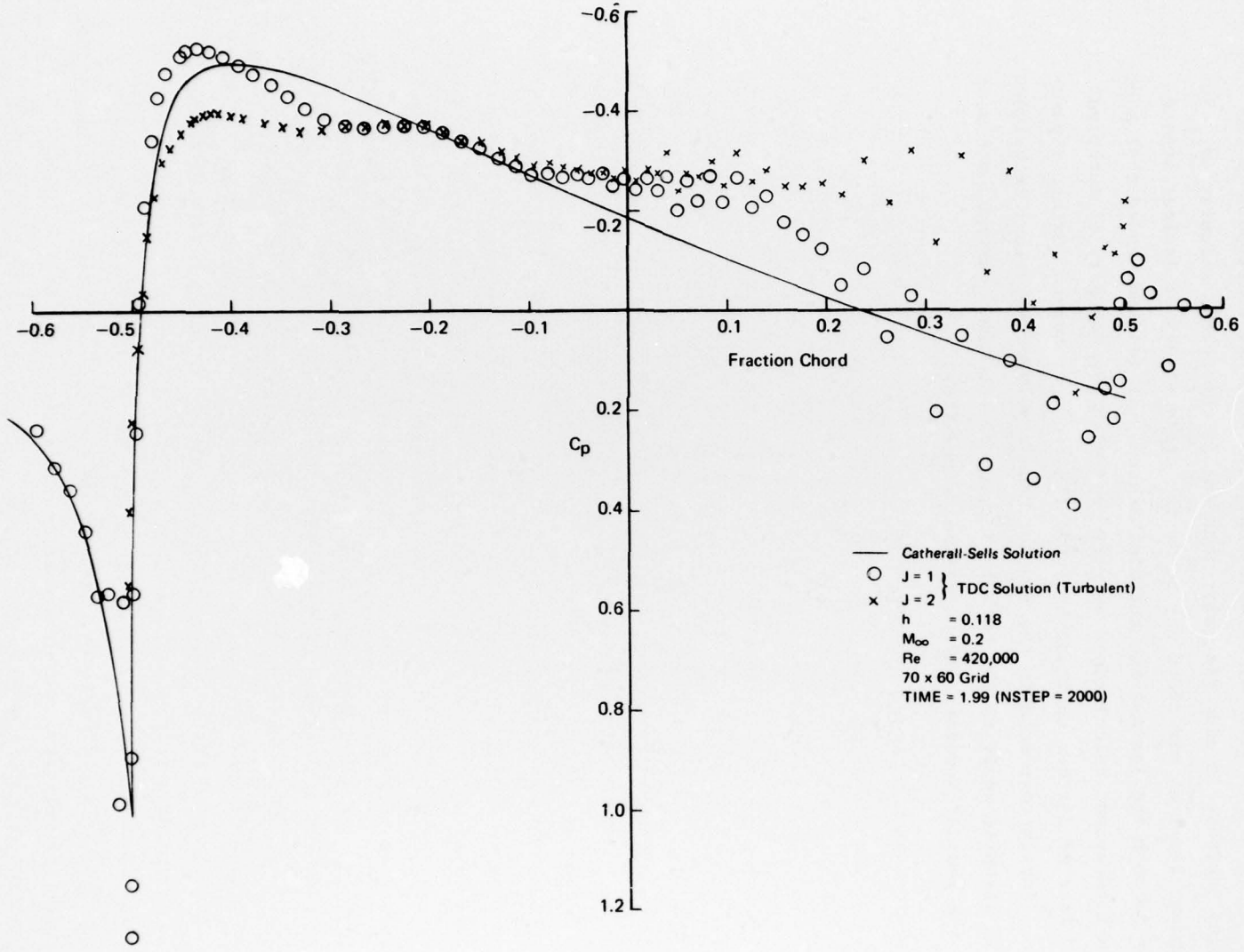


FIGURE 46. JOUKOWSKY AIRFOIL: SURFACE PRESSURE DISTRIBUTION (TURBULENT)

transition point as determined by the Cebeci method. However, it was noted before that the gradual production of turbulence by the TDC flow equations downstream of the boundary of turbulent flow does not correspond to the sudden increase in eddy viscosity inherent in the Cebeci calculation. The boundary layer at mid-chord may be in the early stages of laminar separation in both the laminar and turbulent cases. It is recommended that additional turbulent calculations be performed with the boundary of turbulent flow located farther upstream to avoid the tendency toward laminar separation. Any improvements in the laminar boundary layer numerical techniques would likewise apply to the turbulent case, as the same equations are used for the laminar boundary layer portion of the flow.

6. CONCLUSIONS AND RECOMMENDATIONS

The inviscid version of the Time Dependent Computation (TDC) program has been used to calculate the flow field about various body shapes. For flows with lift, introduction of circulation into the far field has been found to be the physically correct means of generating lift in an inviscid flow. The validity of the method of characteristics approach to correctly predict boundary conditions at a solid surface or moving discontinuity has also been demonstrated. A technique for handling singular boundary points such as cusped trailing edges has been presented and its accuracy verified for the inviscid case of a symmetric Joukowsky airfoil.

A two-equation turbulence model was selected to extend the TDC program formulation to turbulent flow. The additional cost of viscous calculations was reduced by limiting the evaluation of viscous terms to a region encompassing the body and the wake. Additional economy was realized for turbulent flow cases by using a "law-of-the-wall" boundary condition in the turbulent region near the surface to avoid the small grid spacing required to define the steep gradients existing in the viscous sublayer region. Analysis of boundary layer calculations showed that the minimum grid spacing required by the "law-of-the-wall" boundary condition need not be much smaller than that required for an accurate inviscid calculation.

Viscous flow calculations for both completely laminar and partially turbulent boundary layer and wake flow were carried out with the TDC program for a non-lifting, symmetrical Joukowsky airfoil at a low Reynolds number. The calculated pressures near the airfoil nose for the laminar flow case were not as accurate as for the inviscid case, even though the grid point spacing was slightly denser, indicating a need for improvement in the numerical techniques used to evaluate the laminar viscous boundary condition. Boundary layer type velocity profiles increased gradually in thickness in the early part of the time history. At later times, the flow field results developed an instability near the trailing edge, with a large amount of computational noise resulting from the inadequate numerical techniques used at the singular trailing edge point for laminar flow.

The turbulent flow calculation was carried out with the turbulence limited to the region downstream of a "transition" boundary. This boundary was selected as the transition point for which independent boundary layer calculations produced a boundary layer development agreeing with the existing test data of Reference 15. The addition of turbulence effects to the calculation did not significantly alter the thickening of the viscous profile

as observed in the laminar case. The transition boundary may have been located too short a distance upstream of the predicted laminar separation point to produce the expected turbulent boundary layer development. The turbulence considerably reduced the magnitude of the computational noise in the trailing edge region although not sufficiently to give accurate results. This indicates the trailing edge numerical techniques also need improvement for turbulent flow.

It is recommended that improved numerical techniques for the viscous boundary conditions be developed and tested, with special attention given to the trailing edge singularity. A better method of simulating transition should also be developed. These improvements are needed before the capability of the TDC method to predict viscous/inviscid interaction effects can be adequately determined.

REFERENCES

1. Moretti, G., "Transient and Asymptotically Steady Flow of an Inviscid, Compressible Gas Past a Circular Cylinder," Polytechnic Institute of Brooklyn, PIBAL Report No. 70-20, April 1970.
2. MacCormack, R. W., "The Effect of Viscosity in Hypervelocity Impact Cratering," AIAA 7th Aerospace Sciences Meeting, Paper No. 69-354, 1969.
3. Courant, R., Friederichs, K. O., and Lewy, H., "Ueber die Partiellen Differenzgleichungen der Mathematischen Physik," Math. Ann. Vol. 100, pages 32-74, 1928.
4. Moretti, G., and Salas, M. D., "Numerical Analysis of the Viscous Supersonic Blunt Body Problem - Part I," Polytechnic Institute of Brooklyn, PIBAL Report No. 70-48, November 1970.
5. Cebeci, T., "Calculation of Compressible Turbulent Boundary Layers with Heat and Mass Transfer," AIAA Journal, Vol. 9, No. 6, June 1971, pages 1091-1098.
6. Moretti, G., Private Communication.
7. Chiu, P. B., "A Proposed Technique for Discretization of Boundary Conditions in Time-Dependent, Viscous, Compressible Flows," Purdue U. Thesis, December 1972.
8. Launder, B. E., Morse, A., Rodi, W., and Spalding, D. B., "The Prediction of Free Shear Flows - A Comparison of the Performance of Six Turbulence Models," Paper 11 in "Free Turbulent Shear Flows, Volume I - Conference Proceedings," NASA SP-321, 1973.
9. Wilcox, D. C., "Numerical Study of Separated Turbulent Flows," Applied Theory Inc., Report ATR-73-38-1, September 1973.
10. Wilcox, D. C., and Alber, I. E., "A Turbulence Model for High Speed Flows," Proceedings of the 1972 Heat Transfer and Fluid Mechanics Institute, Stanford University Press, pages 231-252, 1972.
11. Hoffman, G. H., "Improved Form of the Low Reynolds Number k-ε Turbulence Model," The Physics of Fluids, Vol. 18, No. 3, pages 309-312, March 1975.
12. Giesing, J. P., "Potential Flow About Two-Dimensional Airfoils," Douglas Aircraft Company Report, LB31946, 1965.
13. Bauer, F., Garabedian, P., and Korn, D., Supercritical Wing Sections, Springer-Verlag, 1972.

14. Sells, C. C. L., "Plane Subcritical Flow Past a Lifting Airfoil," RAE TR67146, 1967.

15. Preston, J. H., and Sweeting, N. E., "The Experimental Determination of the Boundary Layer and Wake Characteristics of a Simple Joukowsky Airfoil, with Particular Reference to the Trailing Edge Region," ARC R&M No. 1998, March 1943.

16. Dvorak, F. A., "Calculation of Turbulent Boundary Layers and Wall Jets Over Curved Surfaces," AIAA Journal, Vol. 11, No. 4, April 1973, pages 517-524.

☆ U. S. GOVERNMENT PRINTING OFFICE: 1976 — 757-001/119